SECOND LAW ANALYSIS OF SOLID OXIDE FUEL CELLS

A THESIS SUBMITTED TO
THE GRADUATE SCHOOL OF NATURAL AND APPLIED SCIENCES
OF
THE MIDDLE EAST TECHNICAL UNIVERSITY

BY

BAŞAR BULUT

IN PARTIAL FULFILLMENT OF THE REQUIREMENTS FOR THE
DEGREE OF
MASTER OF SCIENCE
IN
THE DEPARTMENT OF MECHANICAL ENGINEERING

SEPTEMBER 2003

ABSTRACT

SECOND LAW ANALYSIS OF SOLID OXIDE FUEL CELLS

Bulut, Başar

M.S., Department of Mechanical Engineering

Supervisor : Assoc. Prof. Dr. Cemil Yamalı

Co-Supervisor : Prof. Dr. Hafit Yüncü

September 2003, 111 pages

In this thesis, fuel cell systems are analysed thermodynamically and electrochemically. Thermodynamic relations are applied in order to determine the change of first law and second law efficiencies of the cells, and using the electrochemical relations, the irreversibilities occuring inside the cell are investigated.

Following this general analysis, two simple solid oxide fuel cell systems are examined. The first system consists of a solid oxide unit cell with external reformer. The second law efficiency calculations for the unit cell are carried out at 1273 K and 1073 K, 1 atm and 5 atm, and by assuming different conversion ratios for methane, hydrogen, and oxygen in order to investigate the effects of temperature, pressure and conversion ratios on the second law efficiency. The irreversibilities inside the cell are also calculated and

graphed in order to examine their effects on the actual cell voltage and power density of the cell.

Following the analysis of a solid oxide unit cell, a simple fuel cell system is modeled. Exergy balance is applied at every node and component of the system. First law and second law efficiencies, and exergy loss of the system are calculated.

Keywords: Exergy, Solid oxide fuel cell, Second law efficiency

ÖZ

KATI OKSİT YAKIT HÜCRELERİNİN İKİNCİ KANUN ANALİZİ

Bulut, Başar

Yüksek Lisans, Makina Mühendisliği Bölümü

Tez Yöneticisi : Doç. Dr. Cemil Yamalı

Ortak Tez Yöneticisi : Prof. Dr. Hafit Yüncü

Eylül 2003, 111 sayfa

Bu tez çalışmasında, yakıt hücresi sistemleri termodinamiksel ve elektrokimyasal olarak analiz edilmiştir. Hücrelerin birinci ve ikinci kanun verimlerinin değişiminin incelenmesi için genel termodinamik bağıntılar kullanılmış, elektrokimyasal bağıntılar kullanaran hücre içinde meydana gelen tersinmezlikler incelenmiştir.

Bu genel analizin ardından, iki basit katı oksit yakıt hücresi sistemi incelenmiştir. Birinci sistem dış düzenleyicili bir katı oksit hücresinden oluşmaktadır. İkinci kanun verim hesaplamaları, sıcaklık, basınç ve değişme oranlarının ikinci kanun verimine etkilerini inceleyebilmek amacıyla 1273 K ve 1073 K, 1 atm ve 5 atm, ve de metan, hidrojen ve oksijen için değişik değişme oranları varsayılarak tamamlanmıştır. Hücre içerisindeki

tersinmezlikler de hesaplanmış ve fiili hücre voltajına ve hücrenin güç yoğunluğuna olan etkilerini inceleyebilmek için grafikleri çizilmiştir.

Katı oksit hücre analizini, basit bir katı oksit sisteminin modellenmesi takip etmiştir. Ekserji denklemi, sistem içindeki her parça ve düğüm noktasına uygulanmıştır. Birinci ve ikinci kanun verimleri ve sistemin ekserji kayıpları hesaplanmıştır.

Anahtar Kelimeler: Ekserji, Katı oksit yakıt hücresi, İkinci kanun verimi

To My Parents

ACKNOWLEDGMENTS

I would like to thank to my supervisor Assoc. Prof. Dr. Cemil Yamalı for his guidance and insight throughout the research. I express sincere appretiation to my co-supervisor Prof. Dr. Hafit Yüncü for his guidance, suggestions and comments.

I express sincere thanks to my family for their support and faith in me, and for their understanding in every step of my education.

TABLE OF CONTENTS

LIST OF TABLES

LIST OF FIGURES

FIGURES

LIST OF SYMBOLS

a	Activity
C	Concentration (mole / m^3)
D	Diffusion coefficient (m^2 / s)
e	Energy of molecular interaction (ergs)
E	Cell voltage
F	Faraday constant (= 96487 kJ / V.kmole electrons)
G	Gibbs free energy (jJ)
i	Current density (A / m^2)
i_o	Exchange current density (A / m^2)
I	Current density (A / m^2)
I_L	Limiting current density (A / m^2)
İ	Irreversibility (kJ / s)
J	Mass flux (kg / s)
K	Equilibrium constant
n	Number of moles
n_e	Electrons transferred per reaction
M	Molecular mass
p	Partial pressure (atm)
P	Pressure (atm)
Q	Heat (kJ)
R	Universal gas constant (= 8.3145 kJ / kmole K)
R_e	Area specific resistance (Ω / m^2)
T	Temperature (K)
w	Thickness (μm)
W	Work (kJ)
W_e	Electrical work (kJ)
X	Mole fraction

Greek Letters

α	Transfer coefficient
δ	Thickness of the diffusion layer (m)
ε	Porosity
η	Polarization (V)
η_I	First law efficiency
η_{II}	Second law efficiency
μ	Chemical potential (kJ / mole)
ρ	Resistivity (Ω cm)
ξ	Tortuosity
σ	Collision diameter (Å)
Ω_D	Collision integral nased on the Lennard-Jones potential

Subscripts

a	Anode
A	A specie
B	B specie
c	Cathode
k	Knudsen diffusion
P	Products
R	Reactants
rev	Reversible
(eff)	Effective

Superscripts

I	Inlet condition

CHAPTER 1

INTRODUCTION

1.1 Definition of a Fuel Cell

A fuel cell is an electrochemical device which can continuously convert the free energy of the reactants (i.e. the fuel and the oxidant), which are stored outside the cell itself, directly to electrical energy. The basic physical structure or building block of a fuel cell consists of an electrolyte layer in contact with two porous electrodes; the anode or the fuel electrode, where the fuel that feeds the cell is oxidised, and the cathode or the oxygen (or air) electrode, where the reduction of molecular oxygen occurs, on either side. A schematic representation of a fuel cell with the reactant / product gases and the ion conduction flow directions through the cell is shown in Figure 1.1 [1].

In a fuel cell, gaseous fuels are fed continuously to the anode (negative electrode) and an oxidant (i.e. oxygen from air) is fed continuously to the cathode (positive electrode). The electrochemical reactions take place at the electrodes, where an electric current is produced. The ion species and its transport direction can differ. The ion can either be negative or positive, which means that the ion carries either a negative or a positive charge.

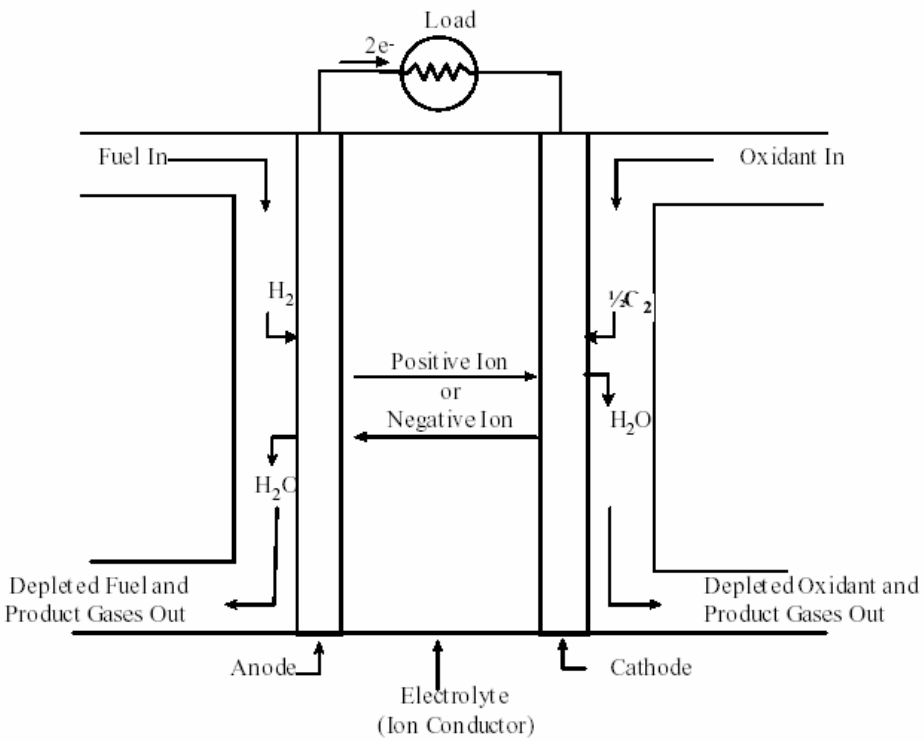

Figure 1.1: Schematic of an individual fuel cell [1].

The basic principles of a fuel cell are similar to the electrochemical batteries, which are involved in many activities of dailylife. The main difference between the batteries and the fuel cells is that, in the case of batteries, the chemical energy is stored in substances located inside them. When this energy has been converted to electrical energy, the battery must be thrown away (primary batteries) or recharged appropriately (secondary batteries). In a fuel cell, on the other hand, since the chemical energy is provided by a fuel and an oxidant stored outside the cell in which the chemical reaction takes place, the electrical energy is produced for as long as the fuel and oxidant are supplied to the electrodes. Figure 1.2 shows the comparison of direct energy conversion with fuel cells to indirect conversion.

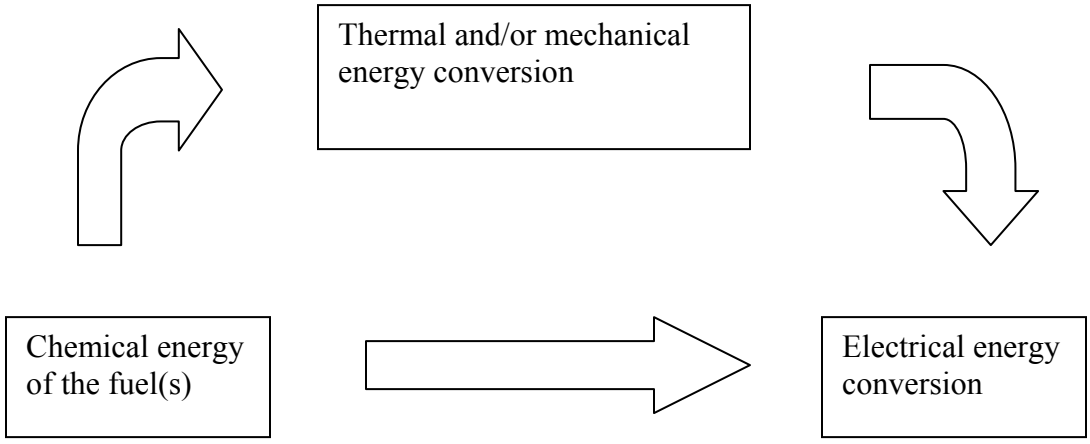

Figure 1.2: Direct energy conversion with fuel cells in comparison to indirect energy conversion.

Gaseous hydrogen has become the fuel of choice for most applications, because of its high reactivity when suitable catalysts are used, its ability to be produced from hydrocarbons and its high energy density when stored cryogenically for closed environment applications. Similarly, the most common oxidant is gaseous oxygen, which is readily and economically available from air, and easily stored in a closed environment.

The electrolyte not only transports dissolved reactants to the electrode, but also conducts ionic charge between the electrodes and thereby completes the cell electric circuit. It also provides a pysical barrier to prevent the mixing of the fuel and oxidant gas streams.

The porous electrodes in the fuel cells provide a surface site where gas/liquid ionization or de-ionization reaction can take place. In order to increase the rates of reactions, the electrode material should be catalytic as well as conductive, porous rather

than solid. The catalytic function of electrodes is more important in lower temperature fuel cells and less so in high temperature fuel cells, because ionization reaction rates are directly proportional with temperature (i.e. increase with temperature). The porous electrodes also provide a physical barrier that separates the bulk gas phase and the electrolyte.

1.2 Fuel Cell Plant Description

In the fuel cell, hydrogen produced from the fuel and oxygen from the air are combined to produce dc power, water, and heat. In cases where CO and CH_4 are reacted in the cell to produce H_2, CO_2 is also a product. These reactions must be carried out at a suitable temperature and pressure for fuel cell operation. A system must be built around the fuel cells to supply air and clean fuel, convert the power to a more usable form (i.e. AC power), and remove the depleted reactants and heat that are produced by the reactions in the cells. Figure 1.3 shows a simple rendition of a fuel cell power plant. Beginning with fuel processing, a conventional fuel (natural gas, other gaseous hydrocarbons, methanol, coal, etc.) is cleaned, then converted into a gas containing hydrogen. Energy conversion occurs when dc electricity is generated by means of individual fuel cells combined in stacks or bundles. A varying number of cells or stacks can be matched to a particular power application. Finally, power conditioning converts the electric power from DC into regulated DC or AC for consumer use [1].

1.3 Fuel Cell Stacking

Individual fuel cells are combined in order to produce the required voltage level. The schematic of stacking of individual fuel cells is given in Figure 1.4. [2]

Anode – electrolyte – cathode sections are connected in series by a bipolar plate between the cathode of the cell and the anode of the other cell. The bipolar plate must be impervious to the fuel and oxidant gases, chemically stable under reducing and oxidizing conditions, and an excellent electronic conductor. [2]

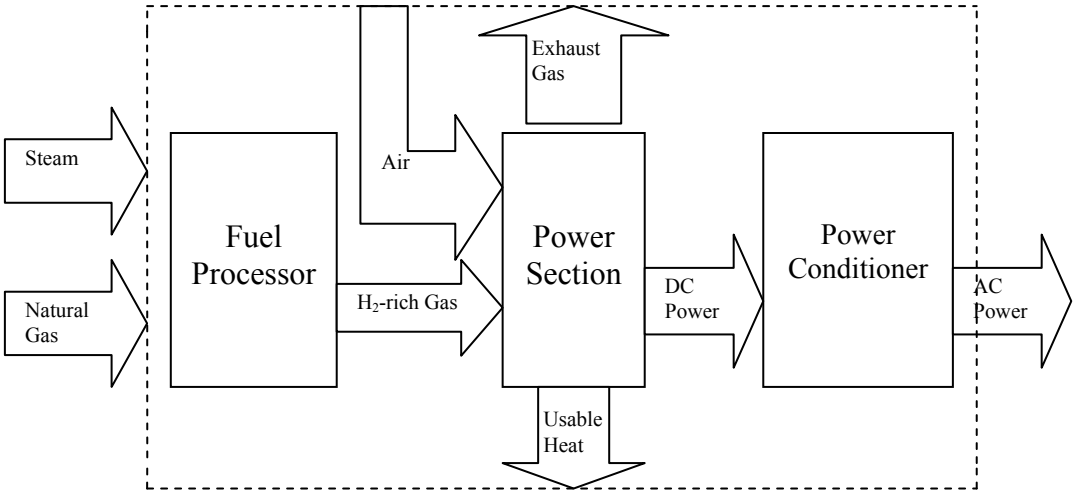

Figure 1.3: Fuel Cell Power Plant Processes

Figure 1.4 is a representation of a flat plate cell. Tubular solid oxide cells are stacked in a different way. There may be other arrangements for stacking as well, provided that the interconnectors are impervious to the gases and are excellent electronic conductors, as explained.

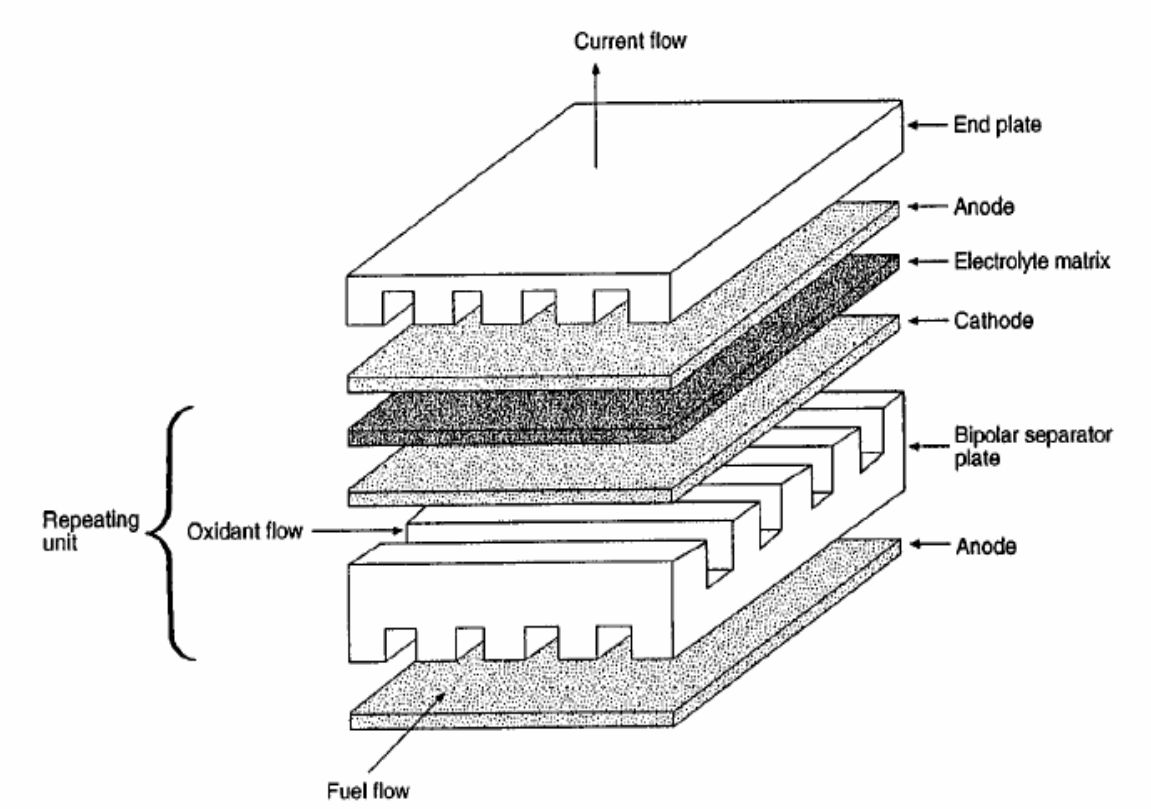

Figure 1.4: Stacking of individual fuel cells. [2]

1.4 Characteristics of Fuel Cells

Fuel cells offer advantages in many fields. These advantages of fuel cells are grouped into categories and are briefly explained in this section.

1.4.1 Efficiency

Chemical energy is converted directly into electrical energy. Since direct energy conversion doesn't require a preliminary conversion into heat, this conversion is not subject to the limitations of Carnot cycle, and thermal efficiencies of as high as 90% are theoretically possible. This direct energy conversion from chemical energy to electrical

energy does not require any mechanical conversion, such as boiler-to-turbine and turbine-to-generator systems. The efficiency of a cell is not dependent upon the size of the cell. A small cell operates with an efficiency equivalent to a larger one, consequently can be just as efficient as large ones. This is very important in the case of the small local power generating systems needed for combined heat and power systems.

1.4.2 Flexibility in Power Plant Design

In order to obtain a desired voltage, due to low voltage level of an individual cell, it is necessary to connect a number of cells in series. The current delivered by an individual cell is proportional to the geometrical area of the electrode. The electrode may be increased in size, or alternatively, several cells may be connected in parallel to increase the current. These cell groups may also be connected in series or parallel to yield high currents at high voltages. The cells need not be localized in one place, thus providing flexibility in weight distribution and space utilization. This characteristics is most convenient from a design viewpoint.

1.4.3 Manufacturing and Maintenance

The manufacturing cost of fuel cells is as low as engines. The whole system of the fuel cells can be manufactured by mass production methods. There are no moving parts in a cell, hence sealing problems are minimum and no bearing problems exist. Because of these, fuel cells require little or no maintenance. Corrosion, on the other hand, is a serious problem, especially for high temperature cells.

1.4.4 Noise

A fuel cell has no moving parts. It runs quietly, does not vibrate, does not generate gaseous pollutants [2]. This characteristics is very important in military and communication applications.

1.4.5 Heat

The electrical inefficiencies in a fuel cell may manifest themselves as heat. With proper design of a cell, efficiency can be maximized and heat can be minimized [3].

1.4.6 Low Emissions

The by-product of the main fuel cell reaction, when hydrogen is the fuel, is water, instead of carbon dioxide, nitrogen oxides, sulfur oxides, and particulate matter inherent to fossil fuel combustion, which means a fuel cell can be essentially a "zero emission" device. This is fuel cells' main advantage when used in vehicles, as there is a requirement to reduce vehicle emissions, and even eliminate them within cities. However, it should be noted that, at present, emissions of CO_2 are nearly always involved in the production of the hydrogen needed as the fuel [4].

Some other characteristics that fuel cells and fuel cell plants offer can be listed as follows :

- Fuel flexibility
- Cleanliness
- Size flexibility
- Cogeneration capability
- Site flexibility

General negative features of fuel cells and fuel cell plants can be listed as follows :

- Cost
- Unfamiliar technology to the power industry

1.5 Types of Fuel Cells and Their Fields of Applications

Fuel cells are usually classified, according to their operating temperatures, into low, medium, and high temperature fuel cells. Table 1.1 gives an overview of the fuel cell technologies presently under development [5].

Table 1.1: Classification of fuel cells. [5]

Fuel Cell Type	**Operating Temperature [^{o}C]**	**Fuel**	**Oxidation Media**	**Typical Unit Sizes [kW_e]**
Alkaline	70 - 100	H_2	Oxygen	<< 100
Protone Exchange Membrane	50 - 100	H_2 and reformed H_2	Oxygen from air	0,1 - 500
Phosphoric Acid	160 - 210	H_2 reformed from natural gas	Oxygen from air	5 - 200 (plants up to 5,000)
Molten Carbonate	650	H_2 and CO from internal reforming of natural/coal gas	Oxygen from air	800 - 2,000 (plants up to 100,000)
Solid Oxide	800 - 1000	H_2 and CO from internal reforming of natural/coal gas	Oxygen from air	2.5 - 100,000

The most probable application fields for the different types of fuel cells are presented in Table 1.2.

Table 1.2: Application fields of fuel cells.

Fuel Cell Type	**Fields of Application**
Alkaline	Space applications and special military applications
Protone Exchange Membrane	Stationary applications for direct hydrogen use Stationary applications for power and heat production Mobile applications for buses, service vehicles Mobile applications for railroad systems Mobile applications for passenger cars
Phosphoric Acid	Stationary applications for power and heat production Mobile applications for railroad systems
Molten Carbonate	Stationary applications for combined power and vapor production Stationary applications for utility use
Solid Oxide	Stationary applications for power and heat production Stationary applications for utility use Mobile applications for railroad systems

CHAPTER 2

THERMODYNAMICS OF FUEL CELLS

2.1 Some Fundamental Relations

2.1.1 TdS Equations and Maxwell Relations

Consider a simple compressible system undergoing an internally reversible process. An energy balance for this simple compressible system, in the absence of overall system motion and gravity effect, can be written in differential form as follows;

$$\delta Q_{\text{int}.rev.} = dU + \delta W_{\text{int}.rev.} \qquad (2.1)$$

The only mode of energy transfer by work that can occur as a simple compressible system undergoes quasiequilibrium processes is associated with volume change and is given by $\int pdV$ [6]. Therefore, the work is given by

$$\delta W_{\text{int}.rev.} = pdV \qquad (2.2)$$

The equation for entropy change on a differential basis is given by

$$dS = \frac{\delta Q}{T}_{\text{int}.rev.} \qquad (2.3)$$

By rearrangement,

$$\delta Q_{\text{int}.rev.} = TdS \qquad (2.4)$$

Substituting Eqs.2.2 and 2.4 into Eq.2.1 and rearranging the terms gives the first TdS equation;

$$dU = TdS - pdV \qquad (2.5)$$

Enthalpy is, by definition,

$$H = U + pV \qquad (2.6)$$

On a differential basis,

$$dH = dU + d(pV) = dU + pdV + Vdp \qquad (2.7)$$

Rearranging the terms results,

$$dU + pdV = dH - Vdp \qquad (2.8)$$

Substituting Eq.2.8 into Eq.2.5 and rearranging the terms gives the second TdS equation;

$$dH = TdS + Vdp \qquad (2.9)$$

The TdS equations on a unit mass basis can be written as

$$du = Tds - pdv \qquad (2.10)$$

$$dh = Tds + vdp \qquad (2.11)$$

or on a per mole basis as

$$d\bar{u} = Td\bar{s} - pd\bar{v} \qquad (2.12)$$

$$d\bar{h} = Td\bar{s} + vd\bar{p} \qquad (2.13)$$

From these two fundamental relations, two additional equations may be formed by defining two other properties of matter.

The Helmholtz function ψ is defined by the equation

$$\Psi = u - Ts \qquad (2.14)$$

Forming the differential $d\psi$ results,

$$d\Psi = du - d(Ts) = du - Tds - sdT \tag{2.15}$$

Substituting Eq.2.10 into Eq.2.15 gives

$$d\Psi = -pdV - sdT \tag{2.16}$$

The Gibbs function is defined by the equation

$$g = h - Ts \tag{2.17}$$

Forming the differential dg results,

$$dg = dh - d(Ts) = dh - Tds - sdT \tag{2.18}$$

Substituting Eq. 2.1 into Eq. 2.8 gives

$$dg = vdp - sdT \tag{2.19}$$

From the comparison of Eq.2.16 and Eq.2.19, one can conclude that Gibbs function carries out reactions at constant pressure and temperature, while Helmholtz function does at constant volume and temperature. Since it is more practical to carry out reactions at constant pressure and temperature, Gibbs function is more useful and is preferred in calculations.

As a result, the summary of these four important relationships among properties of simple compressible systems are collected and presented below:

$$du = Tds - pdv \tag{2.10}$$

$$dh = Tds + vdp \tag{2.11}$$

$$d\Psi = -pdV - sdT \tag{2.16}$$

$$dg = vdp - sdT \tag{2.19}$$

These equations are referred to as TdS (or Gibbsian) equations. Note that the variables on the right-hand sides of these equations include only T, s, p, and v.

Consider three thermodynamic variables represented by x, y, and z. Their functional relationship may be expressed in the form x = x (y, z). The total differential of the dependent variable x is given by the equation

$$dx = \left(\frac{\partial x}{\partial y}\right)_z dy + \left(\frac{\partial x}{\partial z}\right)_y dz \tag{2.20a}$$

If in Eq.2.20a we denote the coefficient of *dy* by *M* and the coefficient of *dz* by *N*, Eq.2.20a becomes

$$dx = Mdy + Ndz \tag{2.20b}$$

Partial differentiation of M and N with resprect to z and y, respectively, leads to

$$\frac{\partial M}{\partial z}\Big)_y = \frac{\partial^2 x}{\partial y \partial z} \tag{2.21a}$$

and

$$\frac{\partial N}{\partial y}\Big)_z = \frac{\partial^2 x}{\partial z \partial y} \tag{2.21b}$$

If these partial derivatives exist, it is known from the calculus that the order of differentiation is immaterial, so that

$$\frac{\partial M}{\partial z}\Big)_y = \frac{\partial N}{\partial y}\Big)_z \tag{2.21c}$$

When Eq.2.21c is satisfied for any function x, then dx is an exact differential. Eq.2.21c is known as the test for exactness. [7]

Since only properties are involved, each TdS equation is an exact differential exhibiting the general form of Eq.2.20a. Underlying these exact differentials are functions of the form u (s, v), h (s, p), ψ (v, T), and g (T, p), respectively.

The differential of the function u (s, v) is

$$du = \left(\frac{\partial u}{\partial s}\right)_v ds + \left(\frac{\partial u}{\partial v}\right)_s dv \tag{2.22}$$

Comparing Eq.2.22 to Eq.2.10 results,

$$T = \left(\frac{\partial u}{\partial s} \right)_v \tag{2.23a}$$

$$-p = \left(\frac{\partial u}{\partial v} \right)_s \tag{2.23b}$$

The differential of the function h (s, p) is

$$dh = \left(\frac{\partial h}{\partial s} \right)_p ds + \left(\frac{\partial h}{\partial p} \right)_s dp \tag{2.24}$$

Comparing Eq.2.24 to Eq.2.11 results,

$$T = \left(\frac{\partial h}{\partial s} \right)_p \tag{2.25a}$$

$$v = \left(\frac{\partial h}{\partial p} \right)_s \tag{2.25b}$$

The differential of the function ψ (v, T) is

$$d\Psi = \left(\frac{\partial \Psi}{\partial v} \right)_T dv + \left(\frac{\alpha \Psi}{\partial T} \right)_v dT \tag{2.26}$$

Comparing Eq.2.26 to Eq.2.16 results,

$$-p = \left(\frac{\partial \Psi}{\partial v} \right)_T \tag{2.27a}$$

$$-s = \left(\frac{\partial \Psi}{\partial T} \right)_v \tag{2.27b}$$

The differential of the function g (T, p) is

$$dg = \left(\frac{\partial g}{\partial p} \right)_T dp + \left(\frac{\partial g}{\partial T} \right)_p dT \tag{2.28}$$

Comparing Eq.2.28 to Eq.2.19 results,

$$v = \left(\frac{\partial g}{\partial p}\right)_T \tag{2.29a}$$

$$-s = \left(\frac{\partial g}{\partial T}\right)_p \tag{2.29b}$$

Since each of the four differentials is exact and similar to Eq.2.20a, referring to Eq.2.21c, the following relations can be written:

$$\left(\frac{\partial T}{\partial v}\right)_s = -\left(\frac{\partial p}{\partial s}\right)_v \tag{2.30}$$

$$\left(\frac{\partial T}{\partial p}\right)_s = \left(\frac{\partial v}{\partial s}\right)_p \tag{2.31}$$

$$\left(\frac{\partial p}{\partial T}\right)_v = \left(\frac{\partial s}{\partial v}\right)_T \tag{2.32}$$

$$\left(\frac{\partial v}{\partial T}\right)_p = -\left(\frac{\partial s}{\partial p}\right)_T \tag{2.33}$$

This set of equations is referred to as the Maxwell relations.

2.1.2 Partial Molal Properties

In general, the change in any extensive thermodynamic property X of a multicomponent system can be expressed as a function of two independent intensive properties and size of the system. Selecting temperature and pressure as the independent properties and the number of moles n as the measure of size, this change in any extensive thermodynamic property X can be expressed as follows:

$$dX = \left(\frac{\partial X}{\partial T}\right)_{p,n} dT + \left(\frac{\partial X}{\partial p}\right)_{T,n} dp + \sum_i \left(\frac{\partial X}{\partial n_i}\right)_{T,p,n_j} dn_i \tag{2.34}$$

where the subscript n_j denotes that all n's except n_i are held fixed during differentiation. The last term on the right-hand side of the Eq.2.34 is defined as the partial molal property $\overline{X}_i$ of the *i*th component in a mixture. Therefore, the partial molal property $\overline{X}_i$ is, by definition

$$\overline{X}_i = \frac{\partial X}{\partial n_i}\Bigg)_{T,p,n_j} \tag{2.35}$$

The extensive thermodynamic property X, can be expressed in terms of the partial molal property $\overline{X}_i$ as

$$X = \sum_{1}^{j} n_i \overline{X}_i \tag{2.36}$$

Eq.2.36 can be referred in order to evaluate the change in volume on mixing of pure components which are at the same temperature and pressure. Selecting V as the extensive property X in Eq.2.36 the total volume of the pure components before mixing is

$$V_{comp.} = \sum_{i=1}^{j} n_i \overline{v}_{0,i} \tag{2.37}$$

where $\overline{v}_{0,i}$ is the molar specific volume of pure component *i*. The volume of the mixture, using Eq.2.36, is

$$V_{mix.} = \sum_{i=1}^{j} n_i \overline{v}_i \tag{2.38}$$

where $\overline{v}_i$ is the partial molal volume of component *i* in the mixture. Hence, the volume change on mixing is given by

$$\Delta V_{mixing} = V_{mix.} - V_{comp.} = \sum_{i=1}^{j} n_i \overline{v}_i - \sum_{i=1}^{j} n_i \overline{v}_{0,i} \tag{2.39a}$$

or

$$\Delta V_{mixing} = \sum_{i=1}^{j} n_i \left(\overline{v}_i - \overline{v}_{0,i} \right) \tag{2.39b}$$

Selecting U, H, and S as the extensive properties, the similar results can be obtained as follows:

$$\Delta U_{mixing} = \sum_{i=1}^{j} n_i \left(\overline{u}_i - \overline{u}_{0,i} \right) \tag{2.40a}$$

$$\Delta H_{mixing} = \sum_{i=1}^{j} n_i \left(\overline{h}_i - \overline{h}_{0,i} \right) \tag{2.40b}$$

$$\Delta S_{mixing} = \sum_{i=1}^{j} n_i \left(\overline{s}_i - \overline{s}_{0,i} \right) \tag{2.40c}$$

In Eqs.2.40a – c, $\overline{u}_{0,i}$, $\overline{h}_{0,i}$, and $\overline{s}_{0,i}$ denote molar internal energy, enthalpy, and entropy of pure component *i*; $\overline{u}_i$, $\overline{h}_i$, and $\overline{s}_i$ denote respective partial molal properties.

2.1.3 Chemical Potential

Of the partial molal properties, the partial molal Gibbs function is particularly useful in describing the behaviour of mixtures and solutions. This quantity plays a central role in the criteria of both chemical and phase equilibrium. Because of its importance in study of multicomponent systems, the partial molal Gibbs function of component *i* is given a special name and symbol. It is called the chemical potential of component *i* and symbolized by μ_i. [6]

$$\mu_i = \overline{G}_i = \left. \frac{\partial G}{\partial n_i} \right)_{T,p,n_j} \tag{2.41}$$

Gibbs function can be expressed in terms of chemical potential as

$$G = \sum_{1}^{j} n_i \mu_i \tag{2.42}$$

The differential of G (T, p, n_1, n_2, ... , n_j) can be formed as

$$dG = \left(\frac{\partial G}{\partial p}\right)_{T,n} dp + \left(\frac{\partial G}{\partial T}\right)_{p,n} dT + \sum_i \left(\frac{\partial G}{\partial n_i}\right)_{T,p,n_j} dn_i \tag{2.43}$$

Substituting Eqs.2.29a – b into Eq.2.43 yields,

$$dG = Vdp - SdT + \sum_{i=1}^{j} \mu_i dn_i \tag{2.44}$$

2.2 Thermodynamics of Chemical Reactions

2.2.1 Free Energy Change of Chemical Reactions

Consider the chemical reaction below;

$$aA + bB \rightarrow cC + dD \tag{2.45}$$

The change in Gibbs function of reaction, or Gibbs free energy of the reaction, under constant temperature and pressure, is given by the equation

$$\Delta G = c\mu_C + d\mu_D - a\mu_A - b\mu_B \tag{2.46}$$

where μ is the chemical potential of the species.

The maximum net work obtainable from a chemical reaction can be calculated by the free energy change of the chemical reaction. Referring to Eq.2.17, the free energy change of a chemical reaction is given by,

$$\Delta G = \Delta H - T\Delta S \tag{2.47}$$

2.2.2 Standard Free Energy Change of a Chemical Reaction

The chemical potential of any substance may be expressed by an equation of the form

$$\mu = \mu^o + RT \ln a \tag{2.48}$$

where a is the activity of the substance and μ has the value μ° when a is unity. The standard free energy change ΔG° of the reaction 2.43 is given by

$$\Delta G^o = c\mu_{C^o} + d\mu_{D^o} - a\mu_{A^o} - b\mu_{B^o} \tag{2.49}$$

where μ_C° indicates the standard chemical potential of product C, and so on. Substituting Eqs.2.48 and 2.49 into Eq.2.46 yields

$$\Delta G = \Delta G^o + RT \ln \frac{a_C^c a_D^d}{a_A^a a_B^b} \tag{2.50}$$

Hence, the standard free energy change of a chemical reaction is

$$\Delta G^o = \Delta G - RT \ln \frac{a_C^c a_D^d}{a_A^a a_B^b} \tag{2.51}$$

Assuming a process at constant temperature and pressure at equilibrium, since the free energy change for this process is zero, Eq.2.51 becomes

$$\Delta G^o = -RT \ln \frac{a_{C,eq}^c a_{D,eq}^d}{a_{A,eq}^a a_{B,eq}^b} = -RT \ln K \tag{2.52}$$

where the suffixes *eq* in the activity terms indicate the values of the activities at equilibrium, and K is the equilibrium constant for the reaction.

The importance of the knowledge of ΔG° is that it allows ΔG to be calculated for any composition of a reaction mixture. Knowledge of ΔG indicates whether a reaction will occur or not. If ΔG is positive, a reaction cannot occur for the assumed composition of reactants and products. If ΔG is negative, a reaction can occur. [8]

2.2.3 Relation Between Free Energy Change in a Cell Reaction and Cell Potential

The enthalpy change of any reaction, assuming constant temperature and pressure, can be showed as follows :

$$\Delta H = \Delta E + P\Delta V = Q - W + P\Delta V \tag{2.53}$$

If the reaction is carried out in a heat engine, then the only work done by the system would be the expansion work,

$$W = P\Delta V \tag{2.54}$$

Hence Eq.2.51 becomes;

$$\Delta H = Q \tag{2.55}$$

If the same reaction, which is under consideration is carried out electrochemically, the only work done by the system will not be the expansion work of the gases produced, but will also be the electrical work due to the charges being transported around the circuit between the electrodes. The maximum electrical work that can be done by the overall reaction carried out in a cell, where $V_{rev,c}$ and $V_{rev,a}$ are the reversible potentials at the cathode and anode respectively, is given by

$$W_{e,\max} = ne\left(V_{rev,c} - V_{rev,a}\right) \tag{2.56}$$

In the cell, n electrons are involved and the cell is assumed to be reversible (i.e., overpotential losses are assumed to be zero). Multiplying Eq.2.56 by the Avogadro number, N, in order to have molar quantities gives;

$$W_{e,\max} = nF\Delta V_{rev} \tag{2.57}$$

where F is the Faraday number, and ΔV_{rev} is the difference between reversible electrode potentials.

The only work forms assumed are the expansion work and electrical work.

$$W = W_{e,\max} + P\Delta V \tag{2.58}$$

In addition to these, assuming the process is reversible

$$Q = T\Delta S \tag{2.59}$$

Substituting Eqs.2.57 – 2.59 into Eq.2.53, the enthalpy change will be

$$\Delta H = T\Delta S - nF\Delta V_{rev} \tag{2.60}$$

Eq.2.60 can be rearranged as follows,

$$\Delta H - T\Delta S = -nF\Delta V_{rev} \tag{2.61}$$

where

$$\Delta G = \Delta H - T\Delta S \tag{2.47}$$

and

$$E = \Delta V_{rev} \tag{2.62}$$

Substituting Eqs.2.47 and 2.62 into Eq.2.61 gives

$$\Delta G = -nFE \tag{2.63}$$

E, which is defined as the difference in potentials between the electrodes is called as the electromotive force of the cell (i.e, the reversible potential of the cell, E_{rev}). If both the reactants and the products are in their standard states, Eq.2.63 can be written as,

$$\Delta G^{o} = -nFE^{o} \tag{2.64}$$

where E° is the standard electromotive force, or – as most commonly referred to – is the standard reversible potential of the cell.

2.3 Nernst Equation

Let us consider the following reaction,

$$kK + lL \rightarrow mM \tag{2.65}$$

where k moles of K react with l moles of L to produce m moles of M. Each of the reactants and the products have an associated activity; a_K , and a_L being the activity of the reactants, a_M being the activity of the product. For ideal gases, activity term can be written as

$$a = \frac{p}{p_0} \tag{2.66}$$

p is the partial pressure of the gas, and p_0 is the pressure of the cell. Eq.2.50 can be rearranged for the the reaction given in Eq.2.65, as follows.

$$\Delta\overline{G} = \Delta\overline{G}^{o} + RT \ln\left(\frac{a_M^m}{a_K^k a_L^l}\right) \tag{2.67}$$

In the Eq.2.67, $\Delta\overline{G}$ and $\Delta\overline{G}^{o}$ show the change in molar Gibbs free energy of formation, and the change in standard molar Gibbs free energy of formation.

From Eq.2.63, the following relation can be written,

$$E = -\frac{\Delta G}{nF} \tag{2.68}$$

Substituting Eq.2.68 into Eq.2.67 gives the effect on voltage as follows,

$$E = -\frac{\Delta\overline{G}^{o}}{nF} - \frac{RT}{nF}\ln\left(\frac{a_M^m}{a_K^k a_L^l}\right) \tag{2.69}$$

Substituting Eq. 2.64 into Eq 2.69 yields,

$$E_o = E^{o} - \frac{RT}{nF}\ln\left(\frac{a_M^m}{a_K^k a_L^l}\right) \tag{2.70a}$$

where E° is the standard electromotive force, and E_o is defined to indicate the reversible electric voltage. Eq.2.70a can be rewritten by substituting Eq.2.52 and Eq.2.66, as follows.

$$E_o = \frac{RT}{nF}\ln K - \frac{RT}{nF}\ln\left(\frac{\left(\frac{p_M}{p_o}\right)^m}{\left(\frac{p_K}{p_o}\right)^k\left(\frac{p_L}{p_o}\right)^l}\right) \tag{2.70b}$$

Eq. 2.70a and 2.70b give the electromotive force in terms of product or/and reactant activity, and is called Nernst equation. The electromotive force calculated using this equation is known as the Nernst voltage, and is the reversible cell voltage that would exist at a given temperature and pressure.

2.4 Exergy Concept

2.4.1 Exergy Balance

Exergy is defined as the maximum amount of work obtainable a substance can yield when it is brought reversibly to equilibrium with the environment [9]. The exergy analysis of a system is based on the second law of thermodynamics and the concept of entropy production. In order to describe the exergy concept, a fuel cell can be modeled as a control volume of a thermodynamic system with a single inlet and outlet, as shown in Figure 2.1.

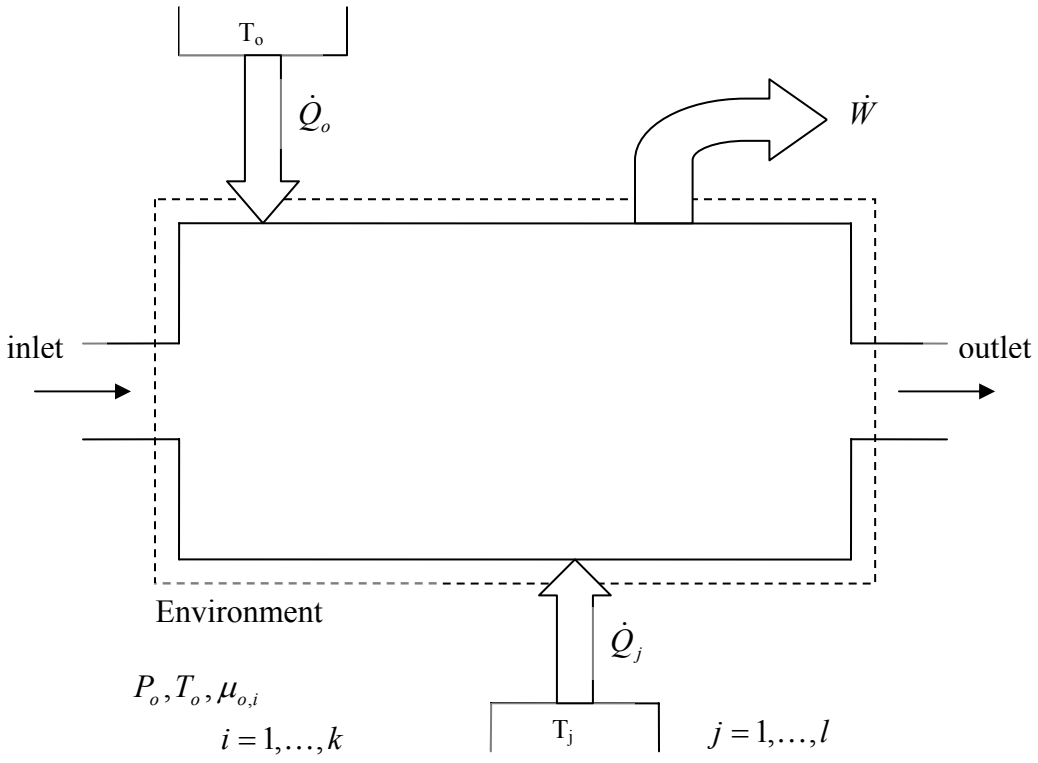

Figure 2.1 : An open thermodynamic system with single inlet and outlet.

The goal in power producing systems is to maximize net work and efficiency. A power plant operates according to the first and second laws of thermodynamics [10]. To calculate the maximum work that can be produced, let us consider the system in Figure 2.1. The streams in and out of the system consist of n species with molar flow rates $\dot{n}_{i,in}, \dot{n}_{i,out}$, where i = 1… k. The heat transfer interactions $\dot{Q}_1 \ldots \dot{Q}_l$ and properties at the inlet and outlet are assumed to be fixed. [11] The first law for the system in Figure 2.1 can be written as;

$$\frac{dE}{dt} = \dot{Q}_0 + \sum_{j=1}^{l} \dot{Q}_j - \dot{W} + \sum_{i=1}^{k} \left(\overline{h}_{t,i} - \overline{h}_{0,i}\right)_{in} \dot{n}_{i,in} - \sum_{i=1}^{k} \left(\overline{h}_{t,i} - \overline{h}_{0,i}\right)_{out} \dot{n}_{i,out} \tag{2.71}$$

The second law for the same system can be written as;

$$\frac{dS}{dt} = \left(\frac{\dot{Q}_0}{T_0}\right) + \sum_{j=1}^{l} \left(\frac{\dot{Q}_j}{T_j}\right) + \sum_{i=1}^{k} \left(\overline{s}_i - \overline{s}_{0,i}\right)_{in} \dot{n}_{i,in} - \sum_{i=1}^{k} \left(\overline{s}_i - \overline{s}_{0,i}\right)_{out} \dot{n}_{i,out} + \dot{S}_{gen} \tag{2.72}$$

In the equations above, $h_{t,i}$ is the total specific enthalpy and is

$$h_{t,i} = \left(h + \frac{1}{2}V^2 + gz\right)_i \tag{2.73}$$

$\frac{1}{2}V^2$ is the kinetic energy, gz is the potential energy of the mass flow, and these kinetic and potential energies may be neglected so that $h_{t,i} = h_i$. E is the total energy of the system, and S is the entropy of the system. In order to make time derivatives zero, system is assumed to be steady state, steady flow. By eliminating $\dot{Q}_0$ between Eqs.2.71 and 2.72, the exergy balance can be obtained. Therefore, the exergy balance is given by the following equation.

$$\begin{aligned} \sum_{j=1}^{l} \left(1 - \frac{T_0}{T_j}\right) \dot{Q}_j + \sum_{i=1}^{k} \left[\left(\overline{h}_i - T_0 \overline{s}_i\right)_{in} - \mu_{0,i}\right] \cdot \dot{n}_{i,in} \\ = \dot{W} + \sum_{i=1}^{k} \left[\left(\overline{h}_i - T_0 \overline{s}_i\right)_{out} - \mu_{0,i}\right] \cdot \dot{n}_{i,out} + T_0 \dot{S}_{gen} \end{aligned} \tag{2.74}$$

$\dot{W}$ is the actual work of the system. It can be noted that entropy generation reduces the available work, as is expected. The exergy balance for an open system in Eq.2.74 shows that the exergies in heat flows (the first term on the left hand side of the equation) and mass flows (the second term on the left hand side of the equation) supplied to the system are equal to the work produced (the first term on the right hand side of the equation), exergy in the outlet mass flow (the second term on the right hand side of the equation), and exergy destroyed through irreversible processes (the third term on the right hand side of the equation) [11]. For the steady state, steady flow system, energy input is equal to the energy output. Due to irreversible processes, outlet exergy is always less than the inlet exergy. Exergy destruction is a result of chemical and physical processes that take place in the system.

Irreversibility, for a system can be described as the difference between the reversible work (maximum work that can be obtained) and the actual work. Hence, from the definition

$$\dot{I} = \dot{W}_{rev} - \dot{W}_{act} = T_0 \dot{S}_{gen} \tag{2.75}$$

The exergy balance (Eq.2.74) can be used to calculate the irreversibility.

Exergy analysis requires that the environment is defined. For a general case, environment can be assumed to be at standard temperature and pressure conditions (i.e., T = 298 K, P = 1 atm), but this assumption is not always the case. Environment definition can differ from system to system.

2.4.2 Chemical Exergy

Chemical exergy is equal to the maximum amount of work obtainable when the substance under consideration is brought from the environmental state to the dead state by processes involving heat transfer and exchange of substances only with the environment. [9]

Chemical exergy of a mixture is given by the following equation.

$$Ex_{mix} = \sum_i x_i \tilde{\varepsilon}_i^{\,o} + RT_o \sum_i x_i \ln x_i \tag{2.76}$$

$\tilde{\varepsilon}_i^{\,o}$ is the standard chemical exergy of substance i. [9] The exergy of the mixture is always less than the sum of the exergies of its components at the temperature and pressure of the mixture, since the second term on the right hand side is always negative.

2.4.3 Physical Exergy

Physical exergy is equal to the maximum amount of work obtainable when the stream of substance is brought from its initial state to the environmental state defined by P_o and T_o by physical processes involving only thermal interaction with the environment. [9]

Defining the environment state at P_o, T_o, assuming the kinetic and potential energies are negligible, the physical exergy of a substance at state P_1, T_1 is calculated by the following equation.

$$Ex_{ph,1} = (h_1 - T_o s_1) - (h_o - T_o s_o) \tag{2.77}$$

2.5 Efficiency of Fuel Cells

2.5.1 Thermodynamic (First and Second Law) Efficiencies

In order to define the efficiency of fuel cells, let us consider a simple H_2/O_2 fuel cell, operating at T = 25°C. and P = 1 atm. as shown in Figure 2.2. The inlet and outlet conditions are assumed to be the same for simplicity.

The energy balance for the fuel cell is,

$$\dot{Q} + \overline{h}_{H_2}(T) + \frac{1}{2}\overline{h}_{O_2}(T) = -\dot{W} + \overline{h}_{H_2O}(T) \tag{2.78a}$$

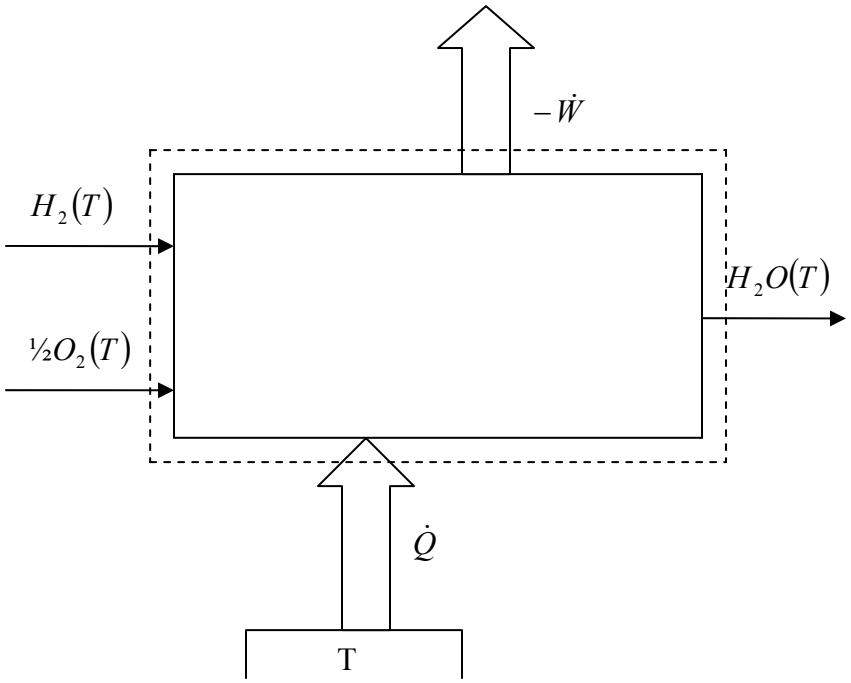

Figure 2.2 : Simple H_2/O_2 fuel cell system, T = 25°C.

The entropy balance for the fuel cell is,

$$\frac{\dot{Q}}{T} + \bar{s}_{H_2}(T) + \frac{1}{2}\bar{s}_{O_2}(T) = \bar{s}_{H_2O} \tag{2.78b}$$

The energy and entropy balance can be rewritten respectively, as follows,

$$\dot{Q} = \Delta\overline{H} - \dot{W} \tag{2.79a}$$

$$\dot{Q} = T\Delta\overline{S} \tag{2.79b}$$

Combining energy and entropy balances yields,

$$T\Delta\overline{S} = \Delta\overline{H} - \dot{W} \tag{2.80}$$

Hence, work output of the system is,

$$\dot{W} = \Delta\overline{H} - T\Delta\overline{S} \tag{2.81}$$

The first law efficiency is defined as the ratio of the work output of the system to energy input to the system. The work output of the system is equal to the free energy change (i.e., Gibbs function). The energy input to the system, is the chemical energy of the fuel. Therefore the energy input is,

$$\dot{Q} = \Delta\overline{H} \tag{2.82}$$

Hence, the first law efficiency is given by,

$$\eta_I = \frac{\dot{W}}{\dot{Q}} = \frac{\Delta\overline{H} - T\Delta\overline{S}}{\Delta\overline{H}} = 1 - \frac{T\Delta\overline{S}}{\Delta\overline{H}} \tag{2.83}$$

The second law efficiency is defined as the ratio of the work output of the system to the maximum work output (i.e., reversible work) of the system. To determine the second law efficiency, let us assume that the fuel cell is adiabatic, and no work interactions occur inside the cell. Hence, the energy input to the system is unchanged at the outlet of the fuel cell. If we can consume all of this energy and change it to work, then we can determine the reversible work output of the system. A model for this study is shown in Figure 2.3.

The reversible heat exchanger, added to the exit of the fuel cell, operates between the fuel cell outlet temperature and the environment temperature T_o (which usually is 25°C). The heat consumed is sent to a reversible heat engine, operating between the heat exchanger and the environment. The work obtained by the heat engine is the reversible work output of the system.

The subscripts “R” and “P” are used in order to indicate the reactants, and the products respectively.

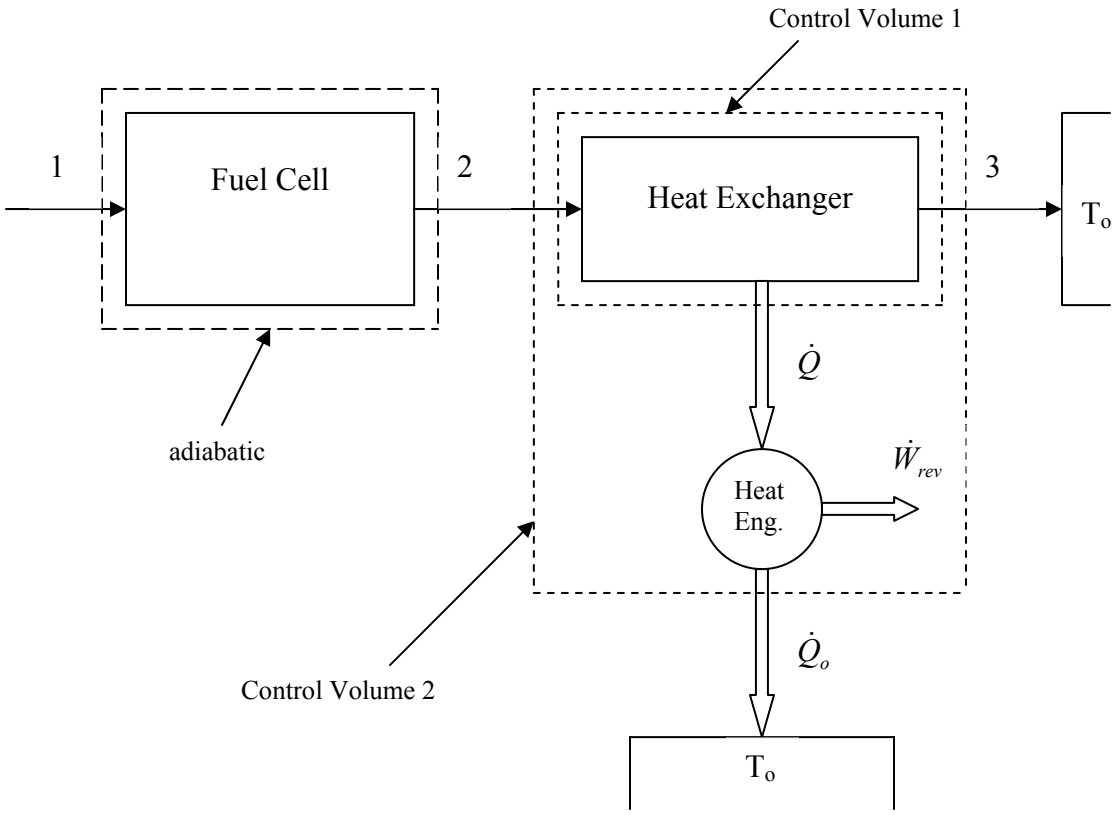

Figure 2.3 : Schematic of the system used to calculate the second law efficiency of the simple fuel cell.

Now, let us apply energy balance to the control volume 1.

$$\overline{H}_P(T_2) = \dot{Q} + \overline{H}_P(T_3) \tag{2.84}$$

Applying the entropy balance to the control volume 2 gives,

$$\overline{S}_P(T_2) = \frac{\dot{Q}_o}{T_o} + \overline{S}_P(T_3) \tag{2.85}$$

The energy balance for the heat engine can be written as,

$$\dot{Q} = \dot{W}_{rev} + \dot{Q}_o \tag{2.86}$$

Therefore, substituting Eqs.2.84 and 2.85 into Eq.2.86, the reversible work output can be obtained.

$$\dot{W}_{rev} = \left(\overline{H}_P(T_2) - \overline{H}_P(T_3)\right) - T_o\left(\overline{S}_P(T_2) - \overline{S}_P(T_3)\right) \tag{2.87a}$$

$$\dot{W}_{rev} = \Delta\overline{H} - T_o\Delta\overline{S} \tag{2.87b}$$

The work output of the system was found by Eq.2.81 as

$$\dot{W} = \Delta\overline{H} - T\Delta\overline{S} \tag{2.81}$$

Therefore, the second law efficiency for the fuel cell can be written as follows.

$$\eta_{II} = \frac{\dot{W}}{\dot{W}_{rev}} = \frac{\Delta\overline{H} - T\Delta\overline{S}}{\Delta\overline{H} - T_o\Delta\overline{S}} \tag{2.88}$$

One of the advantages of the fuel cells is their high efficiency, as mentioned before. Using Eq.2.83 and 2.88, the change of first and second law efficiencies with temperature is graphed and is given in Figure 2.4. Referencing Figure 2.4, we can conclude that fuel cell has higher efficiency at lower temperatures. As the temperature increases, the efficiency decreases. This is the main difference between fuel cell efficiency and the Carnot efficiency. The Carnot efficiency, by which thermal engines are compared in their efficiency, for a thermal engine operating at temperature T, is given by,

$$\eta_C = 1 - \frac{T_o}{T} \tag{2.89}$$

T_o is the environment temperature where thermal engine is working. As the working temperature of thermal engine increases, since the second term of the Carnot efficiency will approach zero, the Carnot efficiency increases as well. The comparison of fuel cell efficiencies and the Carnot efficiency with temperature is shown in Figure 2.4.

Fuel cell efficiency decreases with increasing temperature, while the Carnot efficiency increases with increasing temperature. Investigating this graph only, gives the low

temperature fuel cells have high efficiencies than the high temperature ones. But, although the graph suggests that lower temperature fuel cells are better, the voltage losses are usually less at high temperatures.* So, in general, fuel cell voltages are usually higher at high temperatures. On the other hand, the waste heat from the high temperature fuel cells is more useful than the waste heat from the low temperature fuel cells. Therefore, only this graph itself cannot be referenced to make a decision on fuel cells working at different conditions.

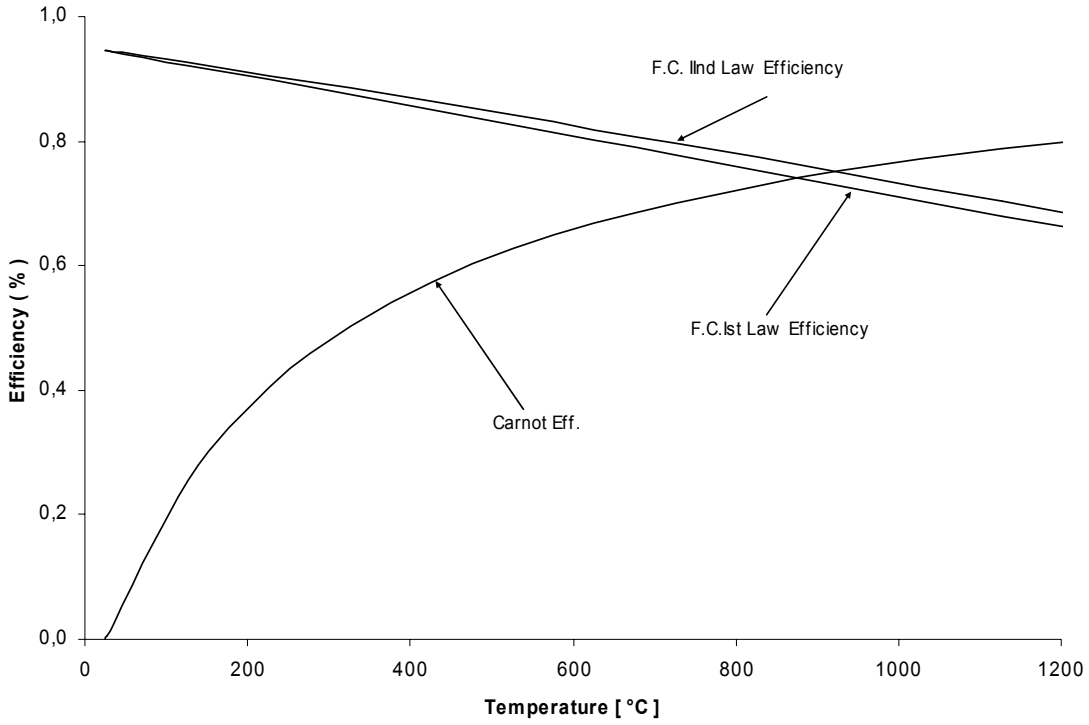

Figure 2.4: Comparison between fuel cell first law and second law efficiency changes with temperature and Carnot efficiency change with temperature.

* Voltage losses and causes of voltage drops are discussed in Chapter 3.

2.5.2 Electrochemical Efficiencies

The efficiency term for fuel cells, given by the Eq. 2.81, can be written in terms of the reversible electrode potentials, using Eq. 2.63, the ideal efficiency is given as follows,

$$\eta_i = \frac{-nFV_{rev}}{\Delta H} \tag{2.90}$$

V_{rev} is the reversible potential of the cell, which is the ideal case. When the fuel cell is under load, the actual potential of the cell, V_{act}, will fall below the reversible potential, due to the irreversibilities. Hence, the actual efficiency will be,

$$\eta_{ac} = \frac{-nFV_{act}}{\Delta H} \tag{2.91}$$

These irreversibilities are unwanted effects in the cell, since they decrease the reversible potential. As a result, the reversible work of the system will decrease. This difference between the reversible work and the actual work is the heat rejected from the system., and is larger than the reversible heat transfer TΔS.

The ratio of the actual potential of the cell to the reversible potential of the cell is defined as the voltage efficiency, η_v. Hence,

$$\eta_v = \frac{V_{act}}{V_{rev}} \tag{2.92}$$

When the fuel reacts electrochemically in the cell, some fuels may react directly to give heat release in the cell or may react to products other than those required, hence do not take place in the electrochemical reaction. Considering the total number of moles of fuels, being reacted electrochemically, the faradaic efficiency, η_F can be expressed as follows.

$$\eta_F = \frac{i}{nF\dot{N}_f} \tag{2.93}$$

$\dot{N}_f$ is the total number of moles of fuel reacted electrochemically per second. η_F is the fraction of reaction which is occurring electrochemically to give current.

CHAPTER 3

KINETIC EFFECTS

3.1 Introduction

In order for a chemical reaction to be considered as a source of energy in a fuel cell, there are two criteria that must be satisfied. First, at least one of the reactants must be ionizable at the operating conditions. The formation of ions results in the establishment of an oxidation – reduction potential which, when traversed by the ions, ultimately provides the energy that will be used at the terminals. Second, while the ionizable reaction system is the source of energetic electron flow that does work in the external circuit, a high flow rate is required for practical purposes. [3] As a result, rapid rates for the electron supplying and consuming reactions are a second criterion.

This second criterion is the subject of chemical kinetics and is dynamic in nature. On the other hand, the first criterion is associated with a static or equilibrium system and is often the object of thermodynamics inquiry. The equal rates of the forward and backward electrode reactions that occur at static conditions establish the equilibrium. Therefore, this equilibrium may be considered dynamic and it may be helpful to consider it a problem in kinetics.

The open circuit voltage of a fuel cell is given by the following formula,

$$E = -\frac{\Delta G}{nF} \tag{2.66}$$

This is the theoretical value of the open circuit voltage, which is also referred to as the reversible open circuit voltage.

Whenever a load is applied to a cell in which the electrodes are reversible, it causes its electrodes to shift its potential, i.e. polarize in opposite direction. As a result of this polarization, the cathodes become less cathodic and the anodes become less anodic, resulting a decrease in the available cell voltage. Therefore, the operating voltage is less than the reversible voltage and this is because of the losses or irreversibilities.

Figure 3.1 shows the performance of a simple fuel cell operating at about 40°C, at normal air pressure [4].

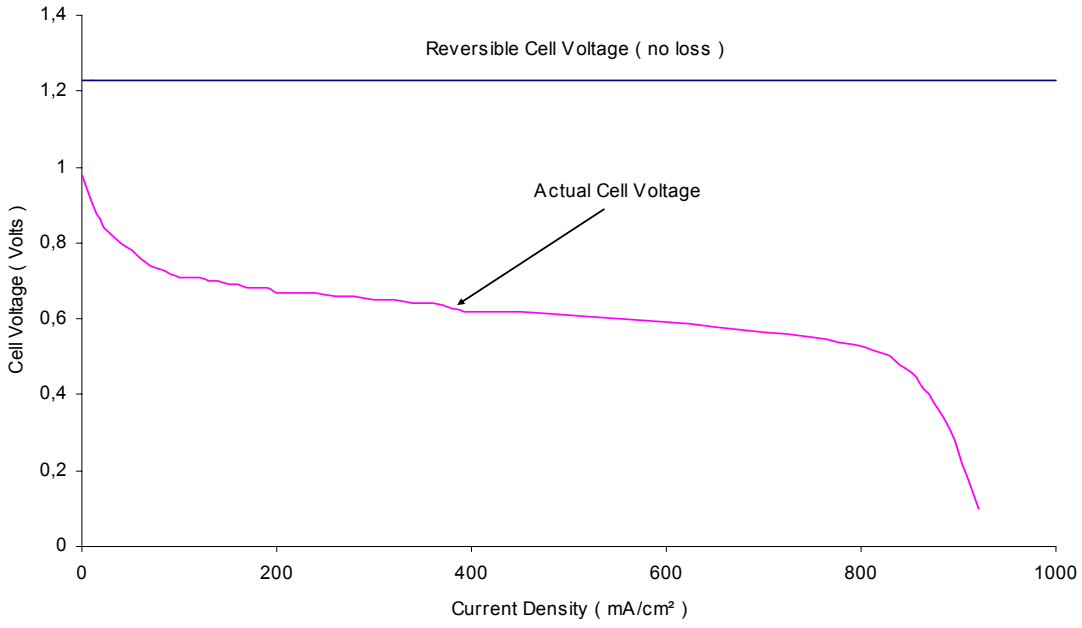

Figure 3.1: Voltage change with current density for a simple fuel cell operating at about 40°C, and at standard pressure. [4]

By examining Figure 3.1, some key points may be listed as follows:

- The open circuit voltage is less the theoretical open circuit voltage.
- There is a rapid initial fall in voltage.
- After this rapid fall, voltage loss is less slowly, and more linearly.
- At some higher current density, voltage falls rapidly.

Another graph showing the voltage change with current density for a fuel cell, which is a solid oxide fuel cell this time, is shown in Figure 3.2, in order to show the effect of high temperature on circuit voltage change. From this graph, the following key points may be listed:

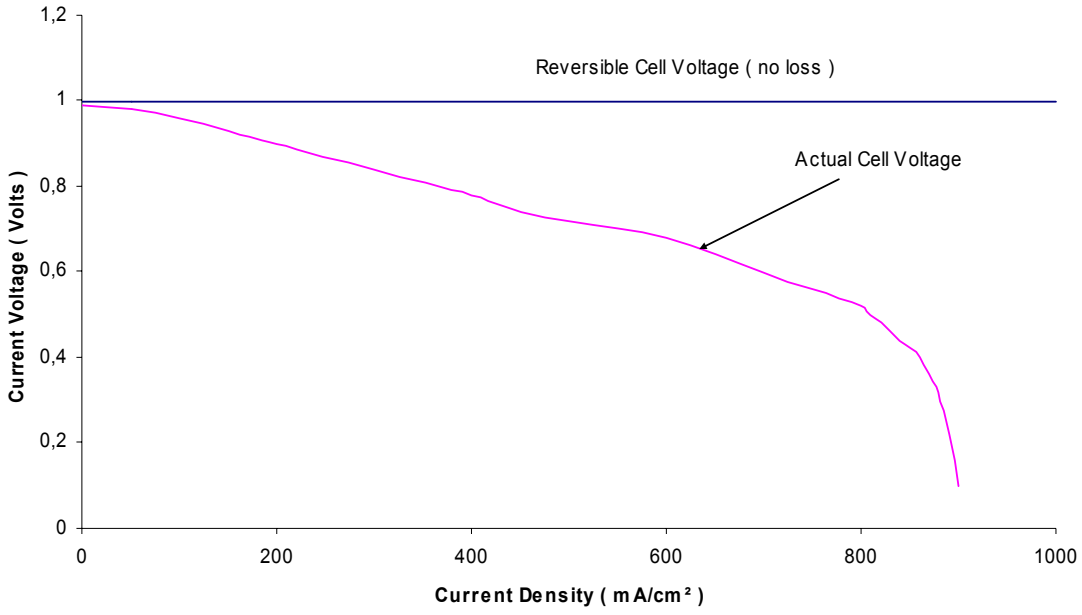

Figure 3.2: Voltage change with current density for a solid oxide fuel cell operating at about 800°C.

- The open circuit voltage is equal to the theoretical open circuit voltage, or there is only a very little difference
- Initial fall of voltage is very small, the graph is much more linear
- At some higher current density, voltage falls rapidly.

Comparison between Figures 3.1 and 3.2, it can be shown that the high temperature fuel cells have lower reversible cell voltage, while they can have high operating voltages since the voltage drop is smaller.

Examining Figures 3.1 and 3.2, the difference between the reversible cell voltage and the actual voltage can be noticed. This difference, which grows as the current density is increased is called the voltage drop. Voltage drop is the result of the irreversibilities in the cell. These irreversibilities are the main subject of this chapter. The effects which cause the actual voltage fall below the reversible voltage will be considered.

3.2 Fuel Cell Irreversibilities

If the cell is reversible, there will not be any voltage drop and the electric voltage will be determined from the Nernst equation. The electric voltage, due to the irreversibilities occuring in the cell decreases from its ideal value (i.e., reversible value). This relation can be shown as follows.

$$E = E_o - \eta \tag{3.1}$$

η is the sum of the irreversibilities in the cell.

The causes of voltage drop in the fuel cell can be the results of three major irreversibilities. These irreversibilities are explained in details in this section.

3.2.1 Activation Polarization

When the forward and backward reactions occur at equal rates and the currents associated with these reactions are equal and are in opposite direction, electrode processes are said to be in a state of reversible equilibrium, in which no net reaction takes place. This state of reversible equilibrium is satisfied unless a current flows in an external circuit connecting the two electrodes of the cell. Due to this reversible state, for a current to flow, a net reaction must occur at each electrode and the forward and backward reaction rates at each electrode cannot be equal.

In many chemical reactions the reacting species have to overcome an energy barrier in order to react. This energy barrier is called the "activation energy" and results in activation polarization.

Consider the elementary electrode reaction below;

$$R + ne \leftrightarrow P \tag{3.2}$$

where R shows the reactants and P shows the products, both of which include the molecules and ions as well. For this reaction, the forward (or the cathodic) and the backward (or the anodic) reaction rates can be written as follows:

$$V_f = k_f \cdot A \cdot a_R \tag{3.3a}$$

$$V_b = k_b \cdot A \cdot a_P \tag{3.3b}$$

where A is the actual electrode surface area, k_f and k_b are the forwanrd anc backward reaction rate constants per unit area, respectively, and a_R and a_P are the activities of the reactants and products, respectively.

The relation between the electron flow (or current) and the reaction rate is given as,

$$i = nFV \tag{3.4}$$

where F is the Faraday's constant. The net current in the forward direction (i.e. cathodic current) will then be the resultant of the forward and backward currents,

$$i_c = nF\left(V_f - V_b\right) = i_f - i_b \tag{3.5a}$$

and the net current in the backward direction (i.e. anodic current) will be,

$$i_a = nF\left(V_b - V_f\right) = i_b - i_f \tag{3.5b}$$

Substituting Eqs.3.3a and 3.3b into Eq.3.5a, the net cathodic current becomes

$$i_c = nFA\left[\left(k_f \cdot a_R\right) - \left(k_b \cdot a_P\right)\right] \tag{3.6}$$

Figures 3.1 and 3.2 show that the electrode potential decreases as the net current increases. From this given fact, it is obvious that either the reactant and product activities are not constant, or that potential and rate constants are interdependent. Assuming that the activities of the reactants and the products can be held constant, the relation of change in potential to current must depend on its relation to the reaction rate constant. Since the reaction rates are functions of the activation energy, activation energy may then be affected by potential.

The relation between reaction rate and activation energy is exponential and it is given as follows:

$$V_f = A\left(\frac{kT}{h}\right)a_R \exp\left(\frac{-\Delta G_f^\circ + \alpha nFE}{RT}\right) \tag{3.7}$$

where ΔG_f° is the standard free energy of activation for the forward reaction, k is Boltzmann constant, h is Planck's constant, and α is a proportionality factor which is usually referred to as the transfer coefficient. Eq.3.7 can be rewritten in terms of reaction rate constants for both forward and backward reactions as follows:

$$k_f = \frac{kT}{h}\exp\left(\frac{-\Delta G_f^\circ + \alpha nFE}{RT}\right) \tag{3.8a}$$

$$k_b = \frac{kT}{h}\exp\left(\frac{-\Delta G_b^\circ - (1-\alpha)nFE}{RT}\right) \tag{3.8b}$$

where ΔG_b° is the standard free energy of activation for the backward reaction, and may also be written as,

$$\Delta G_b^\circ = \Delta G^\circ + \Delta G_f^\circ \tag{3.9}$$

From Eqs.3.6 and 3.8a and b, the rate of the forward reaction, expressed as current density i_c may be written as

$$i_c = nFA\frac{kT}{h}\left\{a_R \exp\left(\frac{-\Delta G_f^\circ + \alpha nFE}{RT}\right) - a_P \exp\left(\frac{-\Delta G^\circ - \Delta G_f^\circ - (1-\alpha)nFE}{RT}\right)\right\} \tag{3.10}$$

Substituting Eq.3.7 into Eq. 3.10 gives

$$i_c = nF\left\{V_f \exp\left(\frac{\alpha nFE}{RT}\right) - V_r \exp\left(\frac{-(1-\alpha)nFE}{RT}\right)\right\} \tag{3.11}$$

Referring from Eq.3.1, polarization, or overpotential, can be written as,

$$\eta = E - E_0 \tag{3.12}$$

where E_0 is the reversible potential. Modifying Eq.3.11 in terms of polarization and the reversible potential yields,

$$i_c = nFV_f \exp\left(\frac{\alpha nFE_0}{RT}\right)\exp\left(\frac{\alpha nF\eta}{RT}\right) - nFV_b \exp\left(\frac{-(1-\alpha)nFE_0}{RT}\right)\exp\left(\frac{-(1-\alpha)nF\eta}{RT}\right) \tag{3.13}$$

At open circuit or reversible potential, the net cathodic and anodic currents are zero, i.e., Eq.3.13 equals zero. The cathodic current i_f and anodic current i_b are equal. This current, which flows with equal intensity anodically and cathodically, at E_o is specifically identified as the exchange current, i_o [3]. Therefore, the net cathodic current can be written as

$$i_c = i_o\left[\exp\frac{\alpha nF\eta}{RT} - \exp\frac{-(1-\alpha)nF\eta}{RT}\right] \tag{3.14a}$$

The transfer coefficient is considered to be the fraction of the change in polarization that leads to a change in the reaction rate constant, and its value is usually 0.5 for the fuel cell applications [12]. Therefore, Eq.3.14a may be written as,

$$i_c = i_o\left[\exp\frac{nF\eta}{2RT} - \exp\frac{-nF\eta}{2RT}\right] \tag{3.14b}$$

From calculus the following relation can be written.

$$\frac{\exp(b)-\exp(-b)}{2}=\sinh(b) \tag{3.15}$$

where b is any variable. Using this general knowledge, Eq.3.14b can be rearranged in terms of sinh function as follows,

$$i_c = 2i_o \sinh\left(\frac{nF\eta}{2RT}\right) \tag{3.16}$$

In the discussion up to this point, we assumed that the reaction occurs in a single step. But, in reality, this is not the case all the time, the reaction may go through several intermediate steps, each with an associated energy barrier. The step with the highest energy barrier within these intermediate steps is usually assumed to be the rate determining step. Hence the other steps will be in an equilibrium state. The rate determining step, however, may involve fewer electrons than the overall reaction. For this reason, for the Eqs.3.4 – 3.16, the number of electrons term "n" must be replaced with the number of electrons transferred in the rate determining step "n_e" and n_e must be lower than or equal to n [13].

The cathodic current and the anodic current are the same in magnitude but are opposite in sign. This is because of the direction of flowing electrons through the electric current. Therefore, rearranging Eq.3.16, the cathodic and anodic activation polarization can be determined as follows,

$$\eta_{Act,c} = \frac{2RT}{n_e F}\sinh^{-1}\left(\frac{i}{2i_{o,c}}\right) \tag{3.17a}$$

$$\eta_{Act,a} = \frac{2RT}{n_e F}\sinh^{-1}\left(\frac{i}{2i_{o,a}}\right) \tag{3.17b}$$

where $\eta_{Act,c}$ and $\eta_{Act,a}$ are the cathodic activation polarization and the anodic activation polarization respectively, and $i_{o,c}$ and $i_{o,a}$ are the cathodic exchange current density and anodic exchange current density respectively.

3.2.2 Ohmic Polarization

Resistance to the flow of ions through the electrolyte and resistance to the flow of electrons between electrodes via electric circuit cause ohmic losses in the fuel cell. These resistances obey Ohm's law. Therefore, ohmic polarization can be expressed by the equation,

$$\eta_{Ohm} = i \cdot R_e \tag{3.18}$$

R_e is the resistance of each material used in the fuel cell components and can be calculated by the equation,

$$R_e = w \cdot \rho \tag{3.19}$$

where w is the thickness and ρ is the electrical resistivity of each component.

3.2.3 Concentration Polarization

Certain changes in the concentration of the potential determining species (i.e., ions) will occur after current begins to flow in an electrochemical cell. This concentration produces an electromotive force, which reduces the reversible electrical voltage of the cell.

The concentration polarization is the reduction in potential due to a concentration change of the electrolyte during a reaction in the vicinity of an electrode. Assuming that the supply of the potential determining species to the electrode is by diffusion only, Fick's law of diffusion can be used to give the rate of diffusion. If the concentration of species at the electrode is C_e and the bulk concentration is C_o, then the rate of diffusion can be written as [13],

$$J = \frac{D}{\delta}\left(C_o - C_e\right) = \frac{I}{nF} \tag{3.20}$$

J is the mass flux (i.e. mass transfer rate), D is the diffusion coefficient, and δ is the thickness of the diffusion layer. The diffusion layer is represented in Figure 3.3.

From Eq.3.20, it can be examined that when the electrolyte near the electrode is depleted (i.e. $C_e = 0$), the maximum current occurs,

$$I_L = \frac{nFD}{\delta} C_o \tag{3.21}$$

I_L is called the limiting current density. Limiting current is proportional to the bulk concentration of the reactant. Assuming that the diffusion layer thickness is independent of the rate of diffusion, combining Eqs.3.20 and 3.21 gives,

$$\frac{C_e}{C_o} = 1 - \frac{I}{I_L} \tag{3.22}$$

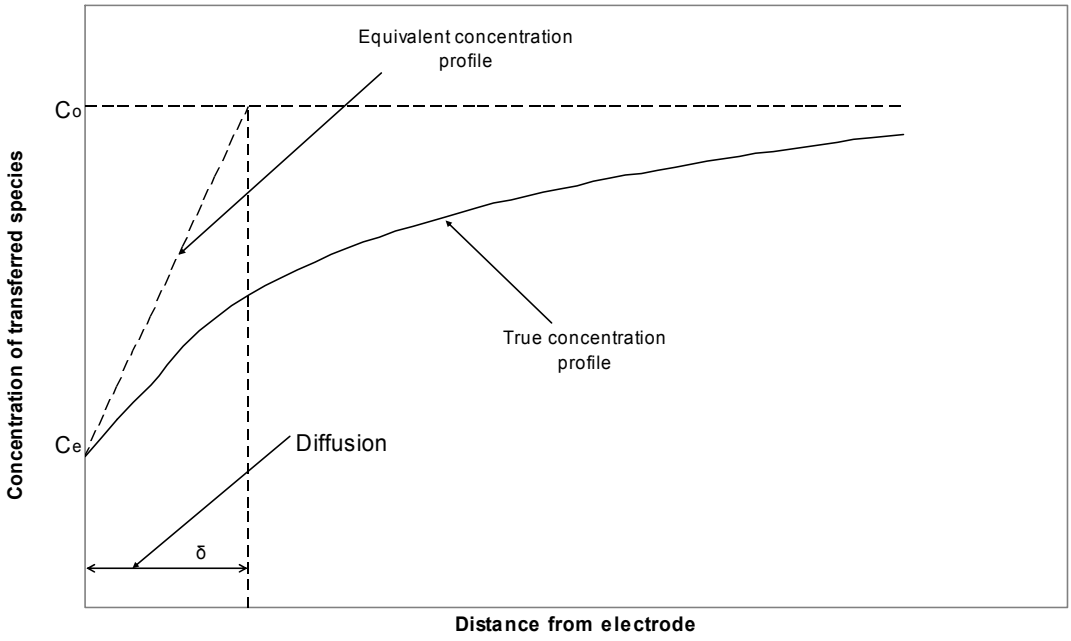

Figure 3.3: The film thickness theory

Assuming that migration of the potential determining ion is negligible and that the ions in the bulk fluid and near the electrode have the same activity coefficients, the concentration polarization can be written as, [14]

$$\eta_{Conc} = \frac{RT}{nF} \ln\left(\frac{C_e}{C_o}\right) \tag{3.23}$$

Concentration polarization can be written in terms of the limiting current density as follows,

$$\eta_{Conc} = \frac{RT}{nF} \ln\left(\frac{I_L - I}{I_L}\right) \tag{3.24}$$

Eq.3.24 refers to the electrode process where species is being removed from the electrolyte. Concentration polarization at the opposite electrode where species is generated and concentration builds up can be written as,

$$\eta_{Conc} = \frac{RT}{nF} \ln\left(\frac{I_L + I}{I_L}\right) \tag{3.25}$$

From Eqs.3.24 and 3.25, it can be noticed that to calculate the concentration polarization, the limiting current density must be calculated. In order to eliminate this difficulty, another calculation method for the concentration polarization analysis may be developed from the same point of view. Since the reactants and products are in gaseous states, and a change in the partial pressure of the potential determining gaseous species at the reaction zone occurs in respect to its partial pressure in the bulk of the gaseous phase, gas side concentration polarization arises.

The relation of the limiting current density to the concentration is given in Eq.3.22 as,

$$\frac{C_e}{C_o} = 1 - \frac{I}{I_L} \tag{3.22}$$

A similar relation may be estimated between the limiting current and the change in the pressure of the fuel gas as follows.

We postulate a limiting current density, I_L, at which the fuel is used up at a rate equal to its maximum supply speed. The current density cannot rise above this value, because the fuel gas cannot be supplied at a greater rate. At this current density the pressure will have just reached zero [4].

If P_1 is the pressure when the current density is zero, and assuming a linear drop of pressure to zero, when the limiting current density is reached, then the pressure ratio of P_2, at any current density to P_1 can be expressed as,

$$\frac{P_2}{P_1} = \left(1 - \frac{I}{I_L}\right) \tag{3.26}$$

Substituting Eq.3.26 into Eq.3.24, the following relation is obtained.

$$\eta_{Conc} = \frac{RT}{nF} \ln\left(\frac{P_2}{P_1}\right) \tag{3.27}$$

Eq.3.26 is named as the gas side concentration polarization.

The gases have to diffuse through the gas filled pores of the electrode in order to reach the reaction sites. Whenever this happens, it is possible for the concentration polarization to be significant, since when the current is being drawn, the gas partial pressure at the reaction sites will be less than that in the bulk of the gas stream. Hence, decrease of gas concentration in the gas filled pores of the electrode may give rise to severe polarization and lead to limiting current. [15]

To determine the concentration polarization, the mass transport effects in the fuel cell is to be investigated. The concentration polarizations at anode and cathode are obtained in the next section.

3.3 Mass Transport Effects

Diffusion through the porous material is described by molecular diffusion, Knudsen diffusion, or transition region diffusion (the case both molecular and Knudsen diffusion occurs). Since the pores of porous solids are usually very small, the diffusion of gases depends on the diameter of the pores. Because of this reason, different diffusion types may occur. To determine which mechanisms of diffusion occur, a mean free path is defined firstly. The mean free path is the average distance a molecule passes through until it collides with another molecule. Mean free path is given as follows [16].

$$\lambda = \frac{3.2\mu}{P}\sqrt{\frac{RT}{2\pi g_c M}} \tag{3.28}$$

In the equation, λ is the mean free path, μ is the viscosity, g_c is the gravitational acceleration, and M is the molecular weight.

After the calculation of the mean free path, from the comparison between the mean free path and the average pore diameter, the diffusion type can be determined. Each diffusion type is shown in Figure 3.4a – c [16].

In the Figures 3.4a - c, N_A indicates the flux of the molecules A, $p_{A,I}$ and $p_{A,o}$ are the total pressure at the inlet and exit of the pore. The total pressure on either side in these cases is the same, but the partial pressures of the molecules may be different.

3.3.1 Knudsen Diffusion

As shown in Figure 3.4a, if the mean free path is very large compared to the average pore diameter, the molecule collides with the pore walls frequently. This type of diffusion is called Knudsen diffusion. The Knudsen diffusion coefficient is given as follows, [16]

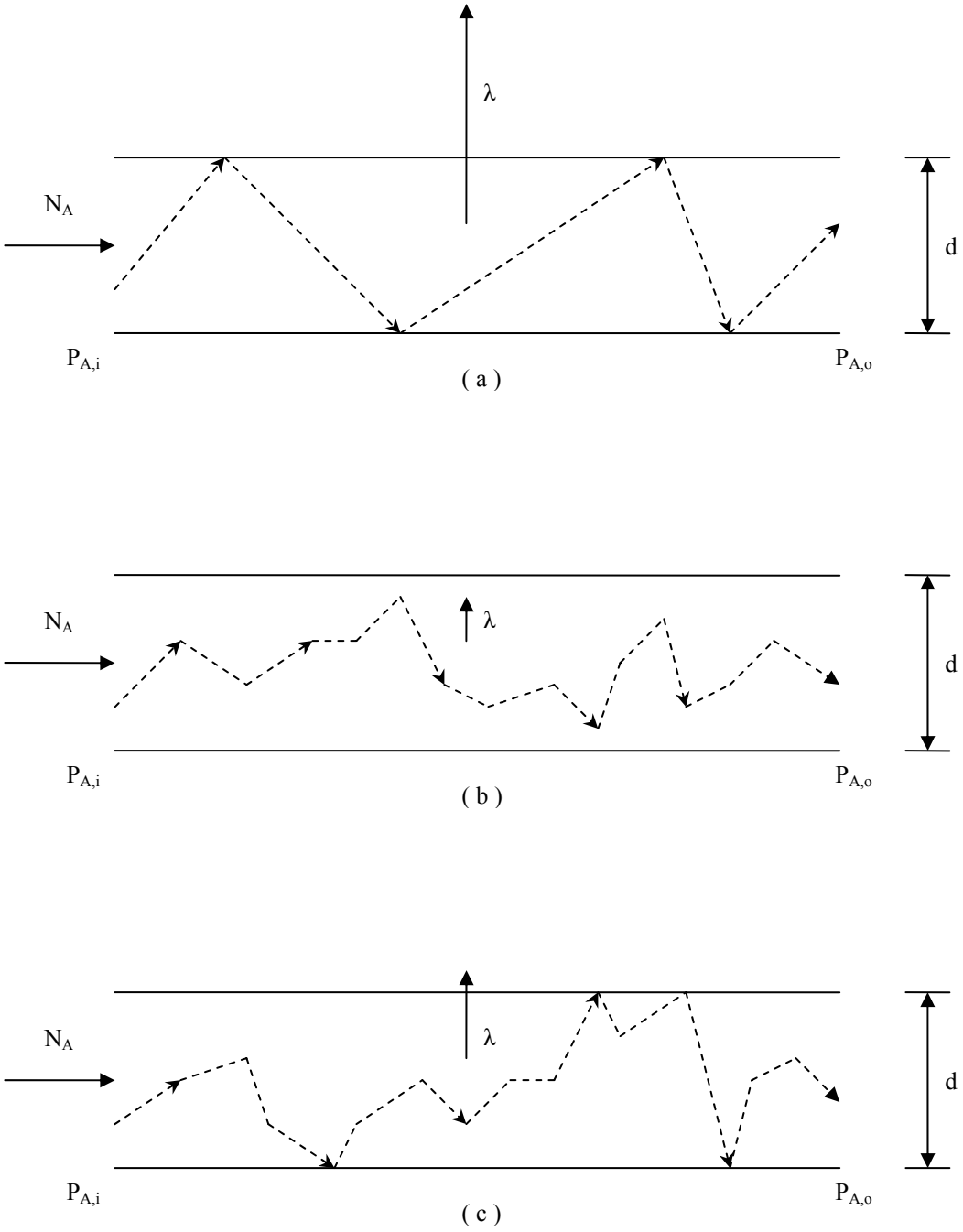

Figure 3.4: Types of diffusion through the pores: (a) Knudsen diffusion, (b) molecular diffusion, (c) transition diffusion. [16]

$$D_{KA} = 9.7 \cdot 10^{-3} \cdot \bar{r} \cdot \sqrt{\frac{T}{M_A}} \tag{3.29}$$

D_{KA} is the Knudsen diffusion coefficient of A, $\bar{r}$ is the average pore radius.

3.3.2 Molecular Diffusion

Figure 3.4b shows the mechanism of molecular diffusion. If the average pore diameter is very large compared to the mean free path, then molecular diffusion, where molecules collide with each other frequently, occurs. Due to this collision of molecules, the molecular diffusion coefficient of a binary gas pair A-B, using the Chapman – Enskog theory of prediction, can be given as, [16]

$$D_{AB} = 0.0018583\left(\frac{1}{M_A} + \frac{1}{M_B}\right)^{1/2} \frac{T^{3/2} f_D}{P\sigma_{AB}^2 \Omega_{D,AB}} \tag{3.30}$$

D_{AB} is the diffusion coefficient of gas A diffusing in gas B, σ_{AB} is the collision diameter, $\Omega_{D,AB}$ is the collision integral based on the Lennard-Jones potential, which is obtained from the energy of molecular interaction, e_{AB}, and f_D is a small second order correction factor, which is close to 1 and may be dropped.†

3.3.3 Transition Region Diffusion

If neither the mean free path, nor the average pore diameter is very large compared to the other, then transition or mixed type diffusion occurs, as shown in Figure 3.4c. In this diffusion regime, both molecule to molecule collisions and molecule to wall collisions become significant, and they both must be taken into account. Since both molecular diffusion and Knudsen diffusion may occur simultaneously, diffusion coefficient for the transition region may be written as,

† $\sigma_{AB} = \frac{\sigma_A + \sigma_B}{2}$ and $\frac{e_{AB}}{k} = \sqrt{\frac{e_A}{k} \cdot \frac{e_B}{k}}$ are calculated from the relational tables.

$$\frac{1}{D_{tA}} = \frac{1}{D_{AB}} + \frac{1}{D_{KA}} \tag{3.31}$$

D_{tA} is the diffusion coefficient of gas A in transition region.

Since the diffusion of molecules will be through tortuous path in the pores of the electrodes, the two factors "porosity" and "tortuosity" are taken into account and therefore the effective diffusion coefficients for each diffusion type is given as follows,

$$D_{KA\ (eff)} = \frac{\beta}{\xi} D_{KA} \tag{3.32a}$$

$$D_{AB\ (eff)} = \frac{\beta}{\xi} D_{AB} \tag{3.32b}$$

$$\frac{1}{D_{tA\ (eff)}} = \frac{\xi}{\beta}\left(\frac{1}{D_{AB}} + \frac{1}{D_{KA}}\right) = \frac{1}{D_{AB\ (eff)}} + \frac{1}{D_{KA\ (eff)}} \tag{3.32c}$$

In the Eqs.3.32a – c, β is the porosity, and ξ is the tortuosity.

Now the anode and cathode electrode reactions can be examined. By using the diffusion coefficients, the concentration polarization can be calculated for both parts.

On the anode side, counter-current equimolar diffusion of the reactant (H_2 for this case) and the product (H_2O for this case) occur. Therefore, the molar flux for the anode side can be written as [17],

$$J_A = -D_{A\ (eff)} \frac{dC_A}{dx} \tag{3.33}$$

The subscript A is H_2 or H_2O (i.e., reactant or product), and D represents the suitable diffusion type occurring in the anode.

For the reactant, H_2, using Eq.3.20, with n = 2, since 1 mole of H_2 reacts with 2 electrons, and from the knowledge of the ideal gas equation of state, the following equations can be obtained.

$$J_{H_2} = -\left(\frac{i}{2F}\right) \tag{3.34}$$

$$dC_{H_2} = \left(\frac{dp_{H_2}}{RT} \right) \tag{3.35}$$

Substituting Eqs.3.34 and 3.35 into Eq.3.33 and solving for the pressure, for the hydrogen the pressure change can be written as,

$$dp_{H_2} = \frac{RTi}{2FD_{H_2\ (eff)}} dx \tag{3.36}$$

Integrating this equation gives,

$$p^{I}_{H_2} - p_{H_2} = \frac{RTi}{2FD_{H_2\ (eff)}} l_a \tag{3.37}$$

The superscript "I" is used to denote initial values of the pressure of the hydrogen, l_a is the thickness of the anode.

For the product, H_2O, using the same equations as for the hydrogen, the following reaction is obtained.

$$p_{H_2O} - p^{I}_{H_2O} = \frac{RTi}{2FD_{H_2O\ (eff)}} l_a \tag{3.38}$$

Rearranging the Eqs.3.37 and 3.38, partial pressures of hydrogen and water vapor in terms of current density are obtained as follows,

$$p_{H_2} = p^{I}_{H_2} - \frac{RTl_a}{2FD_{H_2\ (eff)}} i \tag{3.39}$$

$$p_{H_2O} = p^{I}_{H_2O} + \frac{RTl_a}{2FD_{H_2O\ (eff)}} i \tag{3.40}$$

At the cathode side, on the other hand, there are two gases, and diffusion is nonequimolar. The molar flux for this case can be written as,

$$J_A = -D_{A\ (eff)} \left(\frac{dC_A}{dx} \right) + X_A J \tag{3.41}$$

$J = J_A + J_B$ is the total flux, where subscripts A and B are the two diffusing components, X_A is the molar ratio of component A. In terms of the molecular diffusion coefficient, Eq.3.41 becomes,

$$J_A = -D_{MA\ (eff)}\left(\frac{dC_A}{dx}\right) + X_A J \tag{3.42}$$

Subscript "MA" is used to indicate molecular diffusion coefficient of gas A, in order not to confuse with D_A. The flux at the cathode in terms of Knudsen diffusion coefficient is given as,

$$J_A = -D_{KA\ (eff)}\left(\frac{dC_A}{dx}\right) \tag{3.43}$$

Solving Eqs.3.42 and 3.43 for the concentration drop terms gives,

$$\left(\frac{dC_A}{dx}\right) = \left(\frac{1}{D_{MA\ (eff)}} + \frac{1}{D_{KA\ (eff)}}\right) J_A - \frac{X_A}{D_{MA\ (eff)}} J \tag{3.44}$$

Thus, flux becomes,

$$J_A = -\left[\frac{1}{\left(\frac{1}{D_{MA\ (eff)}} + \frac{1}{D_{KA\ (eff)}}\right)}\right]\frac{dC_A}{dx} + X_A J\left[\frac{1}{D_{MA\ (eff)}\left(\frac{1}{D_{MA\ (eff)}} + \frac{1}{D_{KA\ (eff)}}\right)}\right] \tag{3.45}$$

The flux can be written in a simpler equation as follows,

$$J_A = -D_{A\ (eff)}\frac{dC_A}{dx} + X_A J\delta_A \tag{3.46}$$

δ is defined as,

$$\delta_A = \frac{D_{KA\ (eff)}}{D_{KA\ (eff)} + D_{MA\ (eff)}} \tag{3.47}$$

If the molecular diffusion coefficient is very large compared to the Knudsen diffusion coefficient, then $D_{A\ (eff)} = D_{KA\ (eff)}$, and δ approaches zero. If the Knudsen diffusion

coefficient is very large compared to the molecular diffusion coefficient, then $D_{A\,(eff)} = D_{KA\,(eff)}$, and $\delta = 1$.

At the cathode, since the flux of nitrogen is zero, using the Eq.3.46, the flux of oxygen is given as,

$$J_{O_2} = -D_{O_2\ \ (eff)} \frac{dC_{O_2}}{dx} + X_{O_2} J_{O_2} \delta_{O_2} \tag{3.48}$$

$$\delta_{O_2} = \frac{D_{KO_2\ \ (eff)}}{D_{KO_2\ \ (eff)} + D_{MO_2\ \ (eff)}} \tag{3.49}$$

For oxygen, using Eq.3.20, with n = 4, since one mole of oxygen produces 4 electrons, and from the knowledge of the ideal gas equation of state, the following equations can be obtained.

$$J_{O_2} = -\frac{i}{4F} \tag{3.50}$$

$$dC_{O_2} = \frac{dp_{O_2}}{RT} \tag{3.51}$$

Substituting Eqs.3.50 and 3.51 into Eq.3.48 gives,

$$\frac{dp_{O_2}}{\left(1 - X_{O_2}\delta_{O_2}\right)} = \frac{RTi}{4FD_{O_2\ \ (eff)}} dx \tag{3.52}$$

Since the partial pressure of oxygen is equal to its molar ratio at the cathode part, each terms in the Eq.3.52 can be divided by the cathode pressure, p_c. Hence,

$$\frac{dp_{O_2}}{\left(p_c - p_{O_2}\delta_{O_2}\right)} = \frac{RTi}{4FD_{O_2\ \ (eff)} p_c} dx \tag{3.53}$$

Integrating Eq.3.53 gives,

$$\ln\left[\frac{\left(\frac{p_c}{\delta_{O_2}}\right) - p_{O_2}}{\left(\frac{p_c}{\delta_{O_2}}\right) - p^I_{O_2}}\right] = \frac{\delta_{O_2} RTi}{4FD_{O_2\ \ (eff)} p_c} l_c \tag{3.54}$$

The partial pressure of the oxygen at the cathode, therefore, will be,

$$p_{O_2} = \frac{p_c}{\delta_{O_2}} - \left(\frac{p_c}{\delta_{O_2}} - p_{O_2}^I \right) \exp\left(\frac{\delta_{O_2} RTil_c}{4FD_{O_2\ (eff)} p_c} \right) \tag{3.55}$$

The partial pressures of the gases at both the anode and cathode sides are obtained. Substituting the obtained partial pressures (i.e. Eqs.3.39 , 3.40, and 3.55) into Eq.3.27, the concentration polarization at the anode is given by,

$$\eta_{Conc,a} = -\frac{RT}{2F} \ln \left[\frac{\left(\frac{p_{H_2}}{p_{H_2}^I} \right)}{\left(\frac{p_{H_2O}}{p_{H_2O}^I} \right)} \right] \tag{3.56a}$$

Hence, the concentration polarization at the anode side is obtained as follows.

$$\eta_{Conc,a} = -\frac{RT}{2F} \ln \left[\frac{1 - \left(\frac{RTl_a}{2FD_{H_2\ (eff)} p_{H_2}^I} \right) i}{1 + \left(\frac{RTl_a}{2FD_{H_2O\ (eff)} p_{H_2O}^I} \right) i} \right] \tag{3.56b}$$

Concentration polarization at the cathode, using the same way, is given,

$$\eta_{Conc,c} = -\frac{RT}{4F} \ln \left(\frac{p_{O_2}}{p_{O_2}^I} \right) \tag{3.57a}$$

Therefore, the concentration polarization at the cathode is,

$$\eta_{Conc,c} = -\frac{RT}{4F} \ln \left[\frac{\frac{p_c}{\delta_{O_2}} - \left(\frac{p_c}{\delta_{O_2}} - p_{O_2}^I \right) \exp\left(\frac{\delta_{O_2} RTl_c}{4FD_{O_2\ (eff)} p_c} i \right)}{p_{O_2}^I} \right] \tag{3.57b}$$

CHAPTER 4

MODELING AND CALCULATION

4.1 Fuel Cell Type Selection

As a first step, the type of fuel cell that will be studied on throughout the study must be selected. Solid oxide fuel cell with external reformer is selected for the calculations. Solid oxide type fuel cell has the following advantages:

- SOFC unit sizes can be as small as 2.5 kW, and as large as 100 kW.
- Its ability to be used for power production applications.
- SOFC is simple in concept than the other types of fuel cell systems, since it is a completely solid state device that uses an oxide ion conducting ceramic electrolyte, whereas the other types require solid and gas phases.
- The solid state character of the SOFC components means that there is no restiriction on the cell configuration, in principle. SOFC can be designed as tubular or as flat plate.

The material data of the SOFC type selected referencing from [18], and is given in Table 4.1.

Table 4.1: Properties of SOFC materials

	Component			
	Anode	**Cathode**	**Electrolyte**	**Interconnector**
Material	Ni/ZrO_2	*LSC*	*YSZ*	$LaCrO_3$
Thickness (μm)	*150*	*1000*	*100*	*100*
Resistivity (Ω cm)				
at 1073 K	*0.0003*	*0.001*	*17.24*	*0.033*
at 1273 K	*0.0003*	*0.0011*	*10*	*0.033*

4.2 Environment and Air Composition

As mentioned in chapter 2, the second law analysis requires that the environment is defined. For the study, we assume the environment to be in standard state (i.e. T_o = 298.25 K, P_o = 1 atm).

The air is assumed to be consist of oxygen and nitrogen only. The molar ratios of oxygen and nitrogen are 20% and 80% respectively.

4.3 Chemical Reactions and Components of SOFC System

Methane is used as the fuel for the SOFC system. Direct oxidation of methane has not been successful in calculations so far, because carbon that is a product of oxidized methane is an unwanted element at the anode part since it causes carbonization. Current technology of electrodes are not sufficient to produce such an anode to avoid this problem.

For the simulation, SOFC system with external reformer will be used. Hydrogen will be produced by reforming methane with water vapor. Therefore, the stoichiometric reaction of methane with water vapor will be as follows,

$$CH_4 + 2H_2O \rightarrow 4H_2 + CO_2 \qquad (4.1)$$

As mentioned earlier, carbon is an unwanted element, since it causes carbonization at the anode. To avoid this problem, additional moles of water vapor are used to prevent possible thermal decomposition of the methane that would otherwise form solid carbon which would deactivate the catalytic reaction of the reformer [12]. From literature survey, water – methane mole ratios of 3.0 and 2.2 seem to be conservative values [11]. Selecting water – methane mole ratio to be 2.2, the stoichiometric reaction in Eq.4.1 can be given as,

$$CH_4 + 2.2H_2O \rightarrow 4H_2 + CO_2 + 0.2H_2O \qquad (4.2)$$

The water vapor that is required to reform methane to produce hydrogen is supplied to the system after vaporized. This reaction in the vaporizer is simply given as

$$H_2O(l) \rightarrow H_2O(g) \qquad (4.3)$$

Temperature is kept constant. This reaction, since it is endothermic (i.e. requires heat) is heated by the afterburner.

After vaporizer, water vapor is mixed with methane in the mixer and then before reformer reaction, they are heated by the pre-heater. This is because SOFC unit requires high operating temperature.

In the SOFC, the reactions at the anode and cathode will be as follows;

$$½O_2 + 2e^- \rightarrow O^{2-} \quad (cathode) \qquad (4.4a)$$

$$O^{2-} \quad (cathode) \rightarrow O^{2-} \quad (anode) \qquad (4.4b)$$

$$H_2 + O^{2-} \rightarrow H_2O + 2e^- \quad (anode) \qquad (4.4c)$$

Hence, the overall reaction in the cell is,

$$H_2 + ½O_2 \rightarrow H_2O \qquad (4.4d)$$

The degree of fuel utilization in the cell unit has a very strong effect on the efficiency of the system. From the literature survey, it is found that if the supplied fuel is hydrogen then it may have a high fuel utilization rate almost very close to the ideal case

(i.e. 100%). If the supplied fuel is a gas mixture, fuel utilization rate may change between 0.7 – 0.85.

Conversion rates of hydrogen and oxygen are interrelated. Oxygen ions (O^{2-}) are assumed to be always available at the anode for hydrogen to react to produce water vapor.

The reformer reaction is endothermic. The required heat is supplied by the afterburner, where the unreformed methane and surplus hydrogen are burnt. The reactions in the afterburner are assumed to be complete. Afterburner is also assumed to be isothermal (i.e. temperature is the same at the inlet and exit of the afterburner). The reactions in the afterburner are as follows;

$$aCH_4 + 2aO_2 \rightarrow 2aH_2O + aCO_2 \quad (4.5a)$$

$$bH_2 + ½bO_2 \rightarrow bH_2O \quad (4.5b)$$

The variables “a” and “b” are used to indicate the unreformed methane and unreacted hydrogen mole numbers.

In the foregoing discussion, the composition of air is defined. Regarding to the fuel cell unit and the afterburner reactions, the amount of oxygen, therefore the amount of air, required can be calculated. This amount of air, before entering the SOFC unit, is heated by the pre-heater, since SOFC requires high operating temperature.

The pre-heaters that have been discussed use the waste heat of the products to heat the fuel and air inlet parts. For the design of the pre-heaters, heat exchanger method is explained using the ε-NTU method. The counter flow type heat exchangers are selected, and the total heat transfer coefficients are set equal to 0.05 kW/m².

4.4 Simulation Models

4.4.1 Simulation Model 1: SOFC Unit Analysis

The first model is used to investigate the fuel cell and reformer reactions, and their effects on the SOFC second law efficiency. Besides, the effects of polarizations on fuel cell voltage and power density are also examined. Each polarization type effects and their change with current density are examined and are presented in graphs. This model is limited to the calculation of a unit cell, operating at constant temperature and pressure only. Operating the fuel cell unit with different temperature and pressure values, its second law efficiency change and polarization changes are examined. The schematic of this model is given in Figure 4.1.

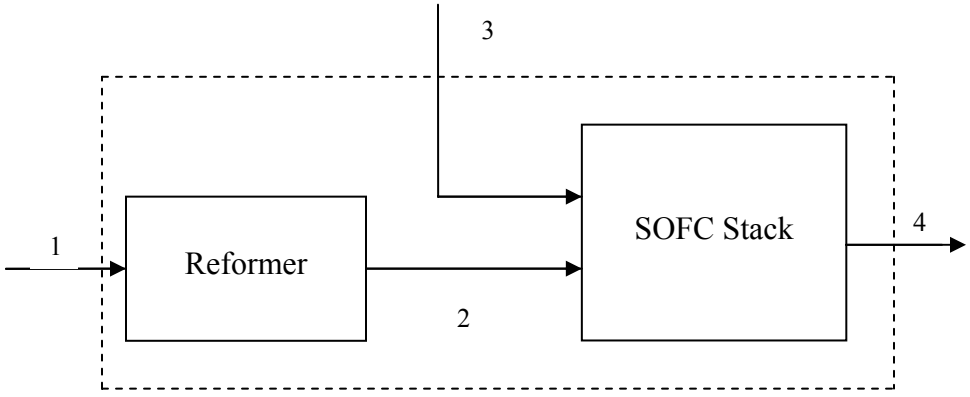

Figure 4.1: Schematic of simulation model 1.

4.4.2 Simulation Model 2: SOFC System Analysis

The second model is more complex than the first one. The components: afterburner, two preheaters, mixer and a vaporizer, are added in addition to the basic system requirements described for the first model. The model of the system is given in Figure 4.2.

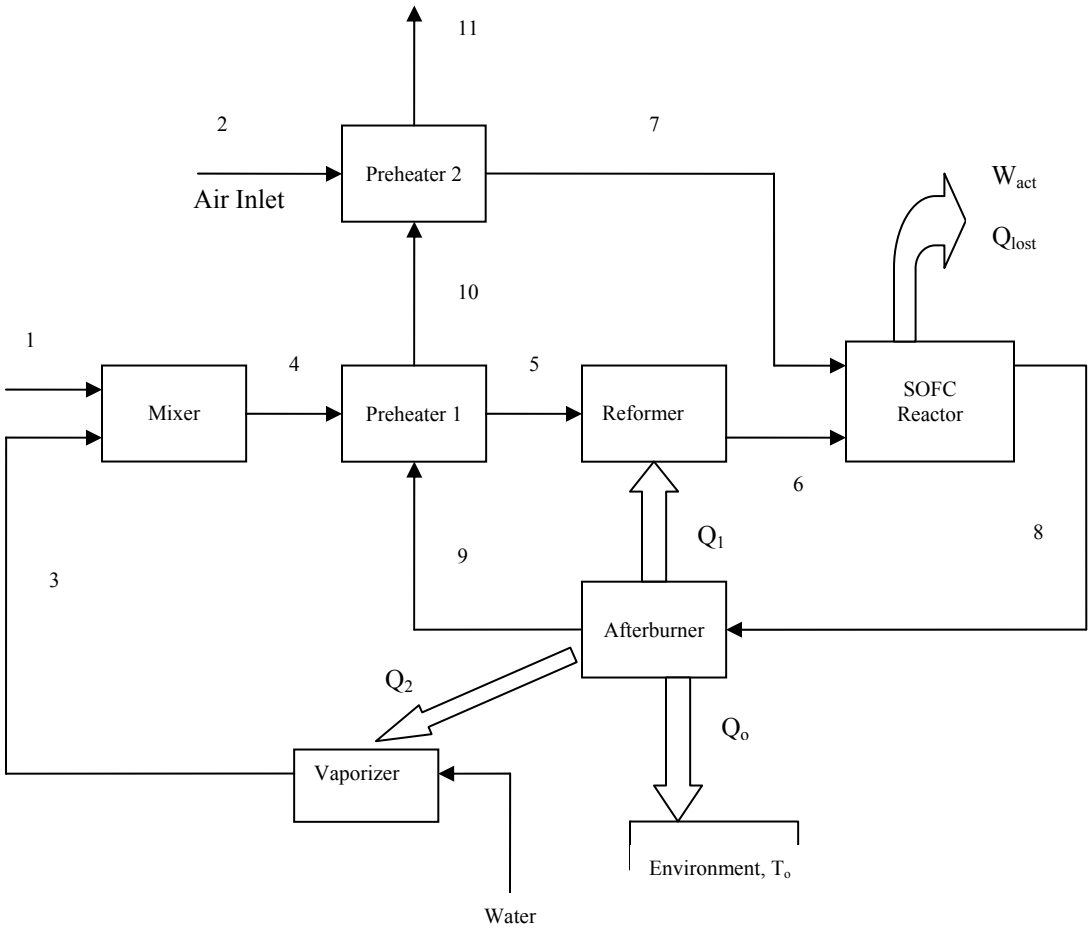

Figure 4.2: Schematic of simulation model 2.

Fuel, water vapor and air inlet conditions are taken to be at standard temperature and pressure conditions. Water vapor, being vaporized in the vaporizer and methane enter the mixer and after mixing, they are heated in preheater, before entering the reformer (the mixer component is not shown in Figure 4.1. The fuel and water vapor entering the reformer are mixed). The heat required for the vaporizer and the reformer is supplied by the afterburner. Some heat is also lost to environment from the afterburner.

The fuel cell fuel inlet temperature, and hence the reformer exit temperature will be assumed to be known initially, and so will the fuel cell air inlet temperature be. The SOFC requires high operating temperature. Because of this reason, the assumed temperatures will be high (around 800 – 1000°C.). Theoretical percentage of the air, fuel utilization rate and the reformer efficiency are also assumed to be known. The variables to be assumed will be discussed later.

4.5 Electrochemical Model

As mentioned earlier, three types of polarization occur in the cell. Activation and concentration polarizations take place in the anode and cathode sides, while the ohmic polarization takes place in all of the components of the fuel cell (i.e. electrolyte, anode, cathode, and interconnector). Using the relative equations derived in sections 3.2 and 3.3, the polarization values can be calculated. As a summary, the polarization equations needed to calculate the voltage drop in the cell are given below.

$$\eta_{Act,a} = \frac{2RT}{n_e F} \sinh^{-1}\left(\frac{i}{2i_{o,a}}\right) \tag{3.16b}$$

$$\eta_{Act,c} = \frac{2RT}{n_e F} \sinh^{-1}\left(\frac{i}{2i_{o,c}}\right) \tag{3.16a}$$

$$\eta_{Ohm} = i \cdot R \tag{3.17}$$

$$\eta_{Conc,a} = -\frac{RT}{2F}\ln\left[\frac{1-\left(\frac{RTl_a}{2FD_{H_2\ (eff)}p^I_{H_2}}\right)i}{1+\left(\frac{RTl_a}{2FD_{H_2O\ (eff)}p^I_{H_2O}}\right)i}\right] \tag{3.55b}$$

$$\eta_{Conc,c} = -\frac{RT}{4F}\ln\left[\frac{\frac{p_c}{\delta_{O_2}}-\left(\frac{p_c}{\delta_{O_2}}-p^I_{O_2}\right)\exp\left(\frac{\delta_{O_2}RTl_c}{4FD_{O_2\ (eff)}p_c}i\right)}{p^I_{O_2}}\right] \tag{3.56b}$$

After each of the polarizations is calculated, using Eq.3.1, the actual electric voltage can be determined.

$$E = E_o - \left(\eta_{Act,a} + \eta_{Act,c} + \eta_{Ohm} + \eta_{Conc,a} + \eta_{Conc,c}\right) \tag{4.6}$$

E_o is the Nernst potential and is given by the Eq.2.68a and 2.68b.

Let us consider the following reaction.

$$H_2 + ½O_2 \rightarrow H_2O \tag{4.7}$$

The Nernst potential for the Eq.4.7 is given as follows.

$$E_o = \frac{RT}{2F}\ln K + \frac{RT}{2F}\ln\left(\frac{\left(p^I_{H_2}\right)\left(p^I_{O_2}\right)^{½}}{\left(p_{H_2O}\right)}\right) \tag{4.8}$$

Once the polarizations and the Nernst potential are determined, the actual cell voltage can be calculated. The electrical power density produced by the fuel cell is calculated by the following equation.

$$P = E \cdot I \tag{4.9}$$

For the fuel cell reaction of the control volume in Figure 2.1, assuming steady state steady flow and negligible changes in kinetic and potential energies, the energy balance in terms of molar properties and molar flow rates can be written as,

$$\dot{Q} - \dot{W} = \sum_i \left(\dot{n}_i \bar{h}_i\right)_P - \sum_i \left(\dot{n}_i \bar{h}_i\right)_R \tag{4.10}$$

For the same reaction, the entropy balance can be written as,

$$\frac{\dot{Q}}{T} = \sum_i \left(\dot{n}_i \bar{s}_i\right)_P - \sum_i \left(\dot{n}_i \bar{s}_i\right)_R - \dot{S}_{gen} \tag{4.11}$$

Combining Eqs.4.10 and 4.11, the exergy balance can be obtained.

$$-\dot{W} = \sum_i \left(\dot{n}_i \bar{h}_i - T\dot{n}_i \bar{s}_i\right)_P - \sum_i \left(\dot{n}_i \bar{h}_i - T\dot{n}_i \bar{s}_i\right)_R + T\dot{S}_{gen} \tag{4.12}$$

The work done by the cell is the electrical work. Hence, from Eq.2.61, Eq.4.12 can be rearranged as follows.

$$nFE = -\sum_i \left(\dot{n}_i \bar{g}_i\right)_P + \sum_i \left(\dot{n}_i \bar{g}_i\right)_R - T\dot{S}_{gen} \tag{4.13}$$

Substituting Eqs.2.64 and 2.65 into Eq.4.13 gives,

$$nFE = -\Delta G^o - \sum_i \left(\dot{n}_i RT \ln \frac{p_i}{p_o} \right)_P + \sum_i \left(\dot{n}_i RT \ln \frac{p_i^I}{p_o} \right)_R - T\dot{S}_{gen} \tag{4.14}$$

Substituting Eq.2.62 into Eq.4.14, and solving for the cell voltage yields,

$$E = \frac{RT}{nF} \ln K - \frac{RT}{nF} \ln \left(\frac{\left(p_{H_2O}\right)\left(p_o\right)^{1/2}}{\left(p_{H_2}^I\right)\left(p_{O_2}^I\right)^{1/2}} \right) - \frac{T\dot{S}_{gen}}{nF} \tag{4.15}$$

The first term on the right hand side of the Eq.4.15 shows the effect of temperature on the cell voltage, the second term shows the effect of the pressures on the cell voltage. The third term shows the irreversibility drop (i.e. polarization) in the cell voltage.

The heat lost to the environment from the fuel cell can be calculated from,

$$\dot{Q} = T\left(\Delta S - \dot{S}_{gen}\right) \tag{4.16}$$

The terms ΔS and $\dot{S}_{gen}$ are defined as follows.

$$\Delta S = \left(S_{H_2O}{}^{o} - S_{H_2}{}^{o} - \tfrac{1}{2}S_{O_2}{}^{o}\right) - R\ln\left(\frac{p_{H_2O}}{p_{H_2}\left(p_{O_2}\right)^{1/2}}\right) \tag{4.17}$$

$$\dot{S}_{gen} = \frac{nF}{T}\left(\eta_{Act,a} + \eta_{Act,c} + \eta_{Ohm} + \eta_{Conc,a} + \eta_{Conc,c}\right) \tag{4.18}$$

4.6 Heat Exchanger Model

To model the preheaters of the SOFC system (i.e. simulation model 1), effectiveness-NTU method (ε-NTU) is used. The counter flow type heat exchangers are selected as the preheaters. The heat transfer coefficients are set equal to 0.05 kW/m²K. The areas of the heat exchangers must be determined before the calculation steps, in order to use the effectiveness-NTU method. Because of this reason, the preheaters are first sized according to the assumed operating conditions. After sizing, the performance analysis can be carried out.

The outlet temperatures of the preheaters depend on the inlet conditions. To define the effectiveness of the heat exchanger, the maximum possible heat transfer rate, q_{max} must be determined. This maximum possible heat transfer rate depends on the minimum heat capacity rate. [19] To determine the minimum heat capacity rate, the heat capacity rates of the cold and hot gas streams are calculated from the following equations.

$$C_c = \sum \dot{m}_c c_{p,c} \tag{4.19a}$$

$$C_h = \sum \dot{m}_h c_{p,h} \tag{4.19b}$$

The subscripts “c” and “h” indicate cold and hot gas streams respectively. Comparing the heat capacity rates of the cold and hot gas streams, one with the lower value is determined as the minimum heat capacity rate, while the other is determined as the maximum heat capacity rate. Following this, the heat capacity rates ratio is given as,

$$C_r = \frac{C_{\min}}{C_{\max}} \tag{4.20}$$

Hence, the maximum possible heat transfer rate can be calculated by,

$$q_{\max} = C_{\min}\left(T_{h,i} - T_{c,i}\right) \tag{4.21}$$

$T_{h,i}$ is the inlet temperature of the hot gas stream, and $T_{c,i}$ is the inlet temperature of the cold gas stream.

The number of transfer units (NTU) is a dimensionless parameter that is used for heat exchanger analysis and is defined as,

$$NTU = \frac{UA}{C_{\min}} \tag{4.22}$$

U is the heat transfer coefficient; A is the area of the heat exchanger.

The effectiveness of the counter flow type heat exchangers can be calculated from the following equation.

$$\varepsilon = \frac{1 - \exp\left[-NTU\left(1 - C_r\right)\right]}{1 - C_r \exp\left[-NTU\left(1 - C_r\right)\right]} \tag{4.23}$$

The effectiveness, ε, is defined as the ratio of the actual heat transfer rate to the maximum possible heat transfer rate. Therefore, with known effectiveness and maximum possible heat transfer rate, the actual heat transfer rate can be calculated.

$$q = \varepsilon \cdot q_{\max} \tag{4.24}$$

The energy balance for the cold and hot gas streams can be written as follows.

$$q = C_c\left(T_{c,o} - T_{c,i}\right) \tag{4.25a}$$

$$q = C_h\left(T_{h,i} - T_{h,o}\right) \tag{4.25b}$$

$T_{c,o}$ and $T_{h,o}$ represents the outlet temperature of the cold gas stream and the outlet temperature of the hot gas stream respectively. As a result, the cold and hot gas streams' outlet temperatures can be found by rearranging Eqs.4.25a – b, as follows.

$$T_{c,o} = T_{c,i} + \frac{q}{C_c} \tag{4.26a}$$

$$T_{h,o} = T_{h,i} - \frac{q}{C_h} \tag{4.26b}$$

The hot gas stream inlet temperature is also the SOFC outlet temperature. Because of this, the hot gas inlet temperatures of both of the preheaters are affected by the SOFC outlet temperature. For this reason, the calculation steps for the heat exchanger model are repeated until the outlet temperatures of the gas streams from the preheaters converge.

4.7 Calculation Procedure

In the calculations, two different models are simulated as mentioned. The reason for this is first of all to investigate the effects on the fuel cell unit and the changes of effects with different conditions. After this study, using a simple model, a general thermodynamic analysis for every component of the fuel cell system is made.

The model 1 is simulated in order to examine

- The effect of reformer efficiency and fuel utilization rate on the fuel cell second law efficiency,
- The effect of pressure on the fuel cell second law efficiency,
- The comparison of the results obtained with different temperatures,
- The polarization effects on fuel cell voltage,
- The effect of temperature on fuel cell voltage and power density.

On the other hand, the more complex system, model 2, is simulated in order to make a full thermodynamic analysis on each component of a simple SOFC system. The first model deals with the SOFC unit with external reformer only. But the second model examines the use of the waste heat at the exit of the SOFC unit to heat the reformer and

vaporizer for the reactions to take place, and to heat the fuel and air inlet nodes to the required temperatures. For these purposes afterburner and two preheaters are added to the system. The preheaters are designed using the heat exchanger model.

4.7.1 General Assumptions

Before the calculation steps, the general assumptions and conditions for the simulation models are listed as follows;

- Steady flow throughout the nodes,
- Kinetic and potential energy changes are neglected,
- Frictional effects are assumed to be negligible,
- Fuel supplying rate is 1 kg/s,
- Operating temperature is constant throughout the fuel cell unit (i.e. fuel cell unit inlet, exit and reformer inlet temperatures are all the same) (for model 1 only),
- Afterburner is assumed to be isothermal, i.e. the inlet and outlet temperatures are the same (for model 2 only),
- The reactions in the afterburner are assumed to be complete (for model 2 only),
- The environment is at standard temperature and pressure conditions, i.e. 298 K, and 1 atm.

The calculations are carried out under the given assumptions. Since simulation model 1 will investigate the effects of the reformer efficiency, fuel utilization rate, the operating pressure on the fuel cell efficiency and the effects of polarizations on fuel cell voltage and power density with changing current density, there is no need to make additional assumptions for these variables for model 1. Hence, the general assumptions are applied to the simulation model 1 directly. For simulation model 2, the following variables will be assumed to be known initially, and the values will be given for these variables.

- The operating pressure of the fuel cell system,

- Percentage of theoretical air,
- Reformer efficiency,
- Fuel utilization rate,
- Fuel cell fuel inlet and air inlet temperatures.

4.7.2 Calculation Steps for Simulation Model 1

Before thermodynamic analysis of the fuel cell unit, using the electrochemical model, the voltage drops in fuel cell unit due to polarizations, their effect on fuel cell voltage and power density are calculated.

The model is first assumed to be at T = 1273 K , and then at T = 1073 K. The electrochemical model to calculate the polarizations is used for both temperature values. By this way, the effect of temperature on fuel cell power density, voltage and polarizations can be considered. The anode and cathode exchange current densities are taken as $I_{o,a}$ = 70000 A / m² , $I_{o,c}$ = 24000 A / m² for T = 1273 K, and $I_{o,a}$ = 5000 A / m², $I_{o,c}$ = 2000 A / m² for T = 1073 K [12].

After the calculation of the polarization effects using the electrochemical model, thermodynamic analysis of the fuel cell unit is made.

Exergy efficiency is defined as the ratio of the work output to the maximum work output of the system. Hence, it can be written as follows,

$$\eta_{II} = \frac{W_{\max} - W_{lost}}{W_{\max}} \tag{4.27}$$

The maximum work available for the system is given by the Eq.2.45. Writing Eq.2.45 in terms of molar properties,

$$W_{\max} = \Delta G = \Delta \overline{H} - T_o \Delta \overline{S} \tag{4.28}$$

The work losses are due to incomplete reactions in the reformer and fuel cell unit, and polarizations occurring in the fuel cell unit. Since hydrogen is reformed from methane

gas, the moles of hydrogen depend on reformed methane, and so do the moles of oxygen. The reactions occurring in reformer and at the anode and cathode of the fuel cell are written assuming methane is completely reformed and the fuel cell reactions are ideal.

$$CH_4 + 2.2H_2O \rightarrow 4H_2 + CO_2 + 0.2H_2O \quad (reformer) \tag{4.29a}$$

$$4H_2 + 4O^{2-} \rightarrow 4H_2O + 8e^- \quad (anode) \tag{4.29b}$$

$$2O_2 + 8e^- \rightarrow 4O^{2-} \quad (cathode) \tag{4.29c}$$

The overall reaction of the system is the sum of reactions 4.17a – c.

$$CH_4 + 2O_2 \rightarrow 2H_2O + CO_2 \tag{4.30}$$

The maximum work of the system is calculated using complete conversion ratios (i.e. $\eta_{CH_4} = 1$, $\eta_{H_2} = 1$, and $\eta_{O_2} = 1$).[§] In reality, maximum values of the conversion ratios will not be unity, but smaller. These differences cause incomplete reactions and hence work loss.

The reformer reaction, since it is an irreversible combustion process, is a complete loss of work. Hence work loss can be calculated using the Gibbs function.

$$W_{loss,ref} = \Delta G = \Delta H - T\Delta S \tag{2.45}$$

The work loss for the incomplete reactions can be calculated the same way, since the conversion ratio decreases the available work output of the reaction.

$$W_{loss,inc.} = \Delta G = \Delta H - T\Delta S \tag{2.45}$$

In the electrolyte cracks may occur. This means that the cell is short circuited, some fuel reacts irreversible with oxygen and this produces hot spots. [20] An assumption of 1 % of the hydrogen react in this way, the work loss due to cracks is given by the following equation.

[§] $\eta_{CH_4}, \eta_{H_2}, \eta_{O_2}$ are the conversion ratios of CH_4, H_2, and O_2, respectively. This value indicates how much of CH_4 is reformed and how much of H_2, and O_2 is reacted in the reaction. Since maximum work is the reversible work, the ideal conversion ratios are assumed, which is not the case realistically.

$$W_{loss,crack} = 0.01 \cdot \Delta G_{H_2-reaction} = 0.01(\Delta H - T\Delta S)_{H_2-reaction} \quad (4.31)$$

The polarizations occurring in the fuel cell causes work loss. From the electrochemical model, the polarizations are calculated with current density. Hence, operating fuel cell with an assumed current density, the work loss due to polarizations can be calculated. The work loss caused by polarizations is,

$$W_{loss,irr} = n \cdot F \cdot (\eta_{Act} + \eta_{Conc} + \eta_{Ohm}) \quad (4.32)$$

The number of electrons, n, is 8 in ideal case. But, that depends on the conversion ratios of methane, hydrogen, and oxygen, and is calculated according to the given conversion ratios.

As seen from Figure 4.1, there are four nodes in model 1. At each node of the system, there is a mixture of gases, and since partial pressures apply, the composition of the mixtures is to be figured out. For this reason, before analyzing the system thermodynamically, the mixture compositions at each node of the system regarding to the conversion ratios of each reaction are determined. With the mixture components known at each node, the related properties of the gases can be calculated.

After thermodynamic analysis is accomplished, the heat release in the fuel cell will also be examined.

4.7.3 Calculation Steps for Simulation Model 2

The complete reforming of methane in the reformer and complete reaction of hydrogen in the fuel cell stack are not realistic.

Reforming of methane is an endothermic reaction and requires heat input to the system for the reaction to take place. The vaporizing of liquid water to water vapor is also an endothermic reaction and requires heat input. Because of these heat requirements of the reformer and vaporizer reactions, there must be some fuel left at the exit of the fuel cell. The afterburner is added to the exit of the fuel cell stack in order to burn the remaining fuel and release heat required for the reformer and vaporizer reactions.

Before calculations, the heat requirements of the components are investigated. Regarding to these results, the conversion ratios for the reformer and the fuel cell unit reactions are determined.

Before stepping into calculations, using the heat exchanger model, the heat areas of the two preheaters are calculated. The system is modeled stoichiometrically, that is the air supplied to the system is 100% theoretical (i.e. there is no extent of air).

With the calculations explained above, the reformer efficiency due to the conversion ratio of methane, the fuel utilization rate due to the conversion ratio of hydrogen are determined, and the heat transfer area needed in the two preheaters are calculated. Modeling the inlet conditions at standard temperature and pressure (i.e. T = 298 K, P = 1 atm), under the general assumptions and the assumed and calculated values for the reformer efficiency, fuel utilization rate and heat transfer area, the simulation model 2 can be analyzed. The calculation steps for this model are numbered and listed in order as follows:

1. Since the methane and hydrogen conversion ratios are determined, and there is a complete combustion in the afterburner, the required air amount by the SOFC stack and the afterburner to sustain the system operation is calculated.
2. The molar chemical compositions of the flow streams at each node of the system are determined.
3. Using the known molar chemical compositions of the flow streams at each node and the fuel supplying rate, the mass flow rates at each node are determined.
4. The temperature values of the fuel and air inlet must be assumed. With known fuel and air inlet temperatures, the electrochemical model can be used in order to determine the electrical work output, the exit temperature, and the heat rejection of the SOFC stack. The first law and second law efficiencies of the SOFC stack are also calculated.
5. Heat exchanger model is used to determine the exit temperatures of the heat exchangers. The reformer inlet temperature is calculated at this step. The cold gas stream outlet temperature of the preheater 2, which is also the assumed air

inlet temperature of the SOFC, is compared with the calculated result. Since the exit temperatures of the preheaters depend on the exit temperature of the SOFC stack, the iteration is continued until the outlet temperature of the preheater 2 converges.

6. Since temperatures and molar chemical compositions at each node are known, applying the energy and exergy balance at each component, the enthalpy and exergy at each node are calculated.

The exergy balance for a component is derived in Eq.2.74 and is used to calculate the exergy destruction in the component. The exergy of a mixture at a node, where the temperature and molar chemical compositions are known, is calculated by using Eqs.2.76 and 2.77.

CHAPTER 5

RESULTS AND DISCUSSION

5.1 Results of Simulation Model 1

5.1.1 Electrochemical Model Analysis

The first electrochemical results for the simulation model 1 are calculated at T = 1273 K.

The changes in activation, ohmic, and concentration polarizations with current density are given in Figures 5.1, 5.2, and 5.3, respectively. The change in cell voltage and power density due to the polarizations is given in Figure 5.4. The change in all kinds of polarizations with current density is grouped and shown in a single graph in Figure 5.5. The calculated power density, cell voltage, and polarizations versus current density is given in Figure 5.6.

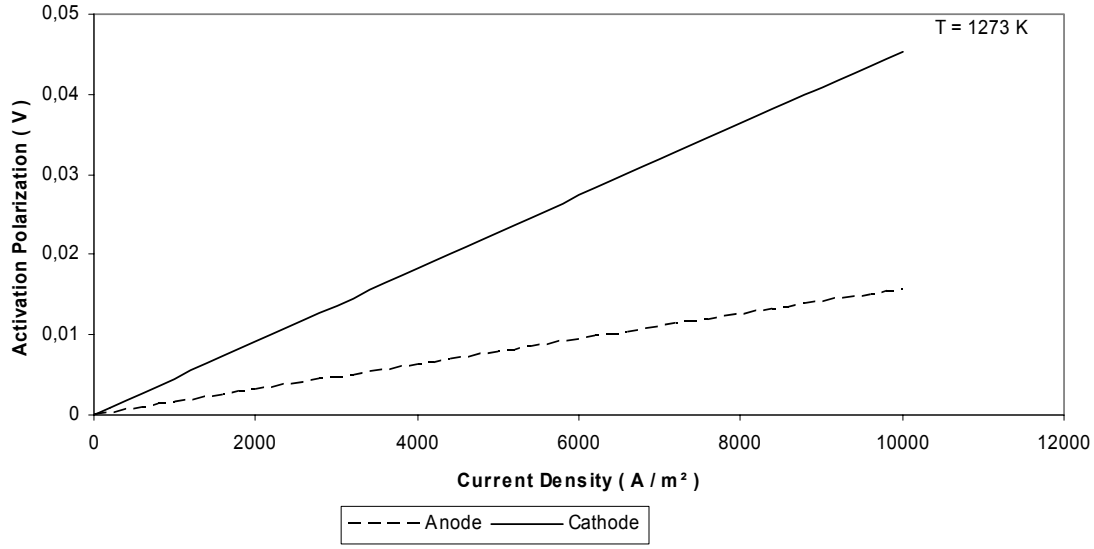

Figure 5.1: Activation polarization change with current density (T = 1273 K).

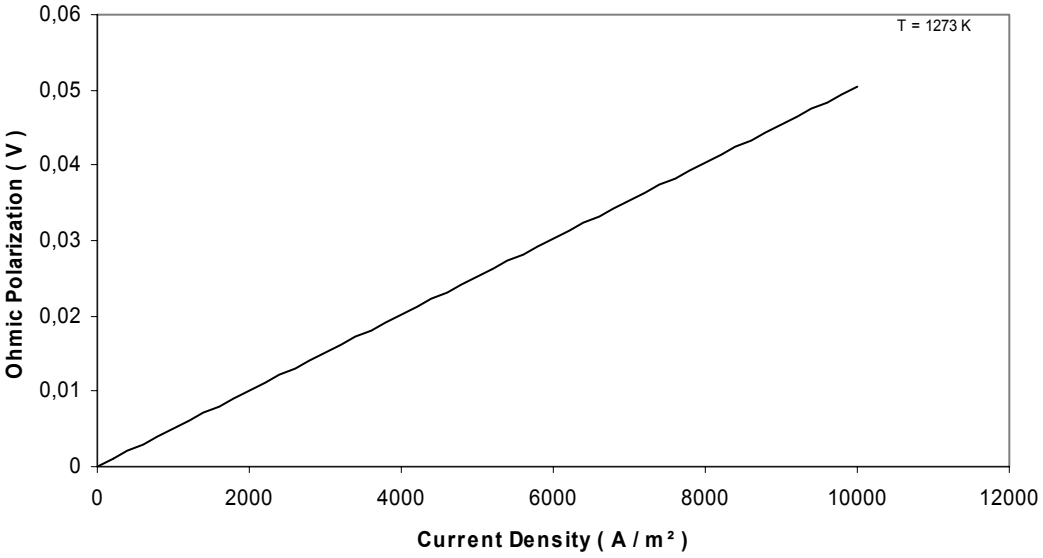

Figure 5.2: Ohmic polarization change with current density (T = 1273 K).

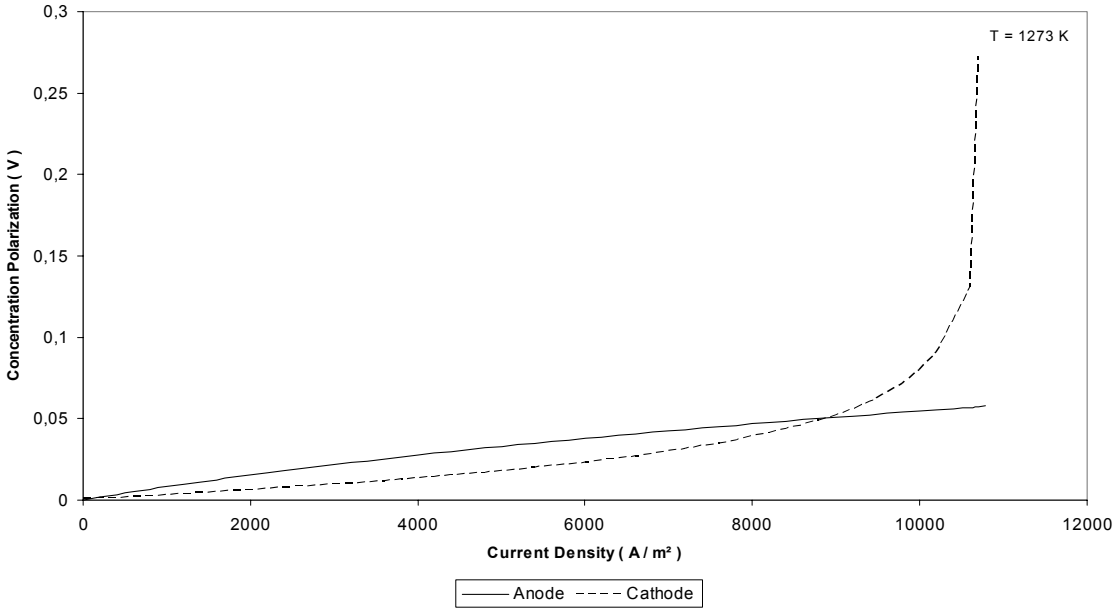

Figure 5.3: Concentration polarization change with current density (T = 1273 K).

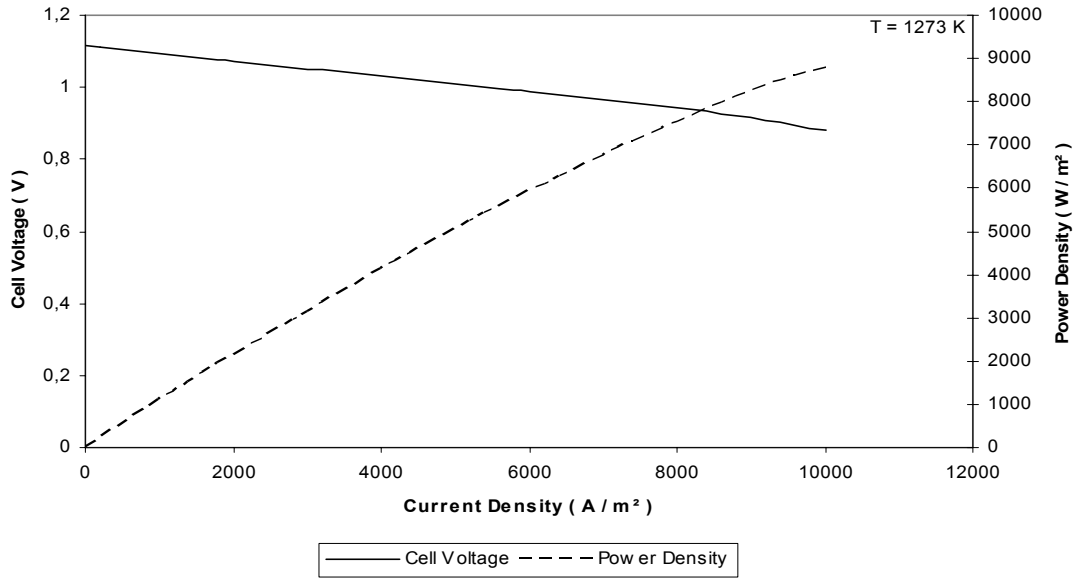

Figure 5.4: Change in the cell voltage and the power density with current density (T = 1273 K).

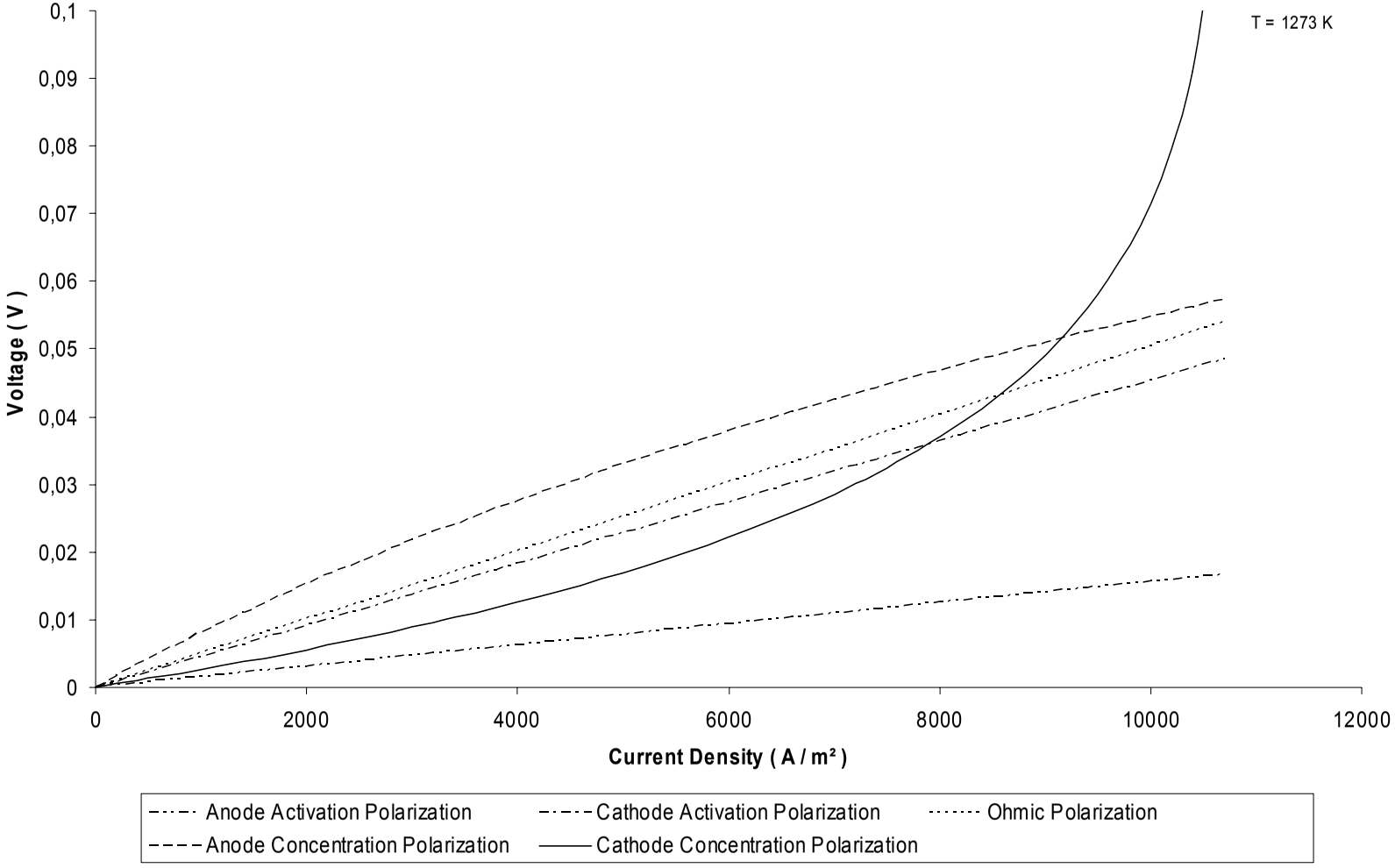

Figure 5.5: Calculated polarization effects with current density (T = 1273 K).

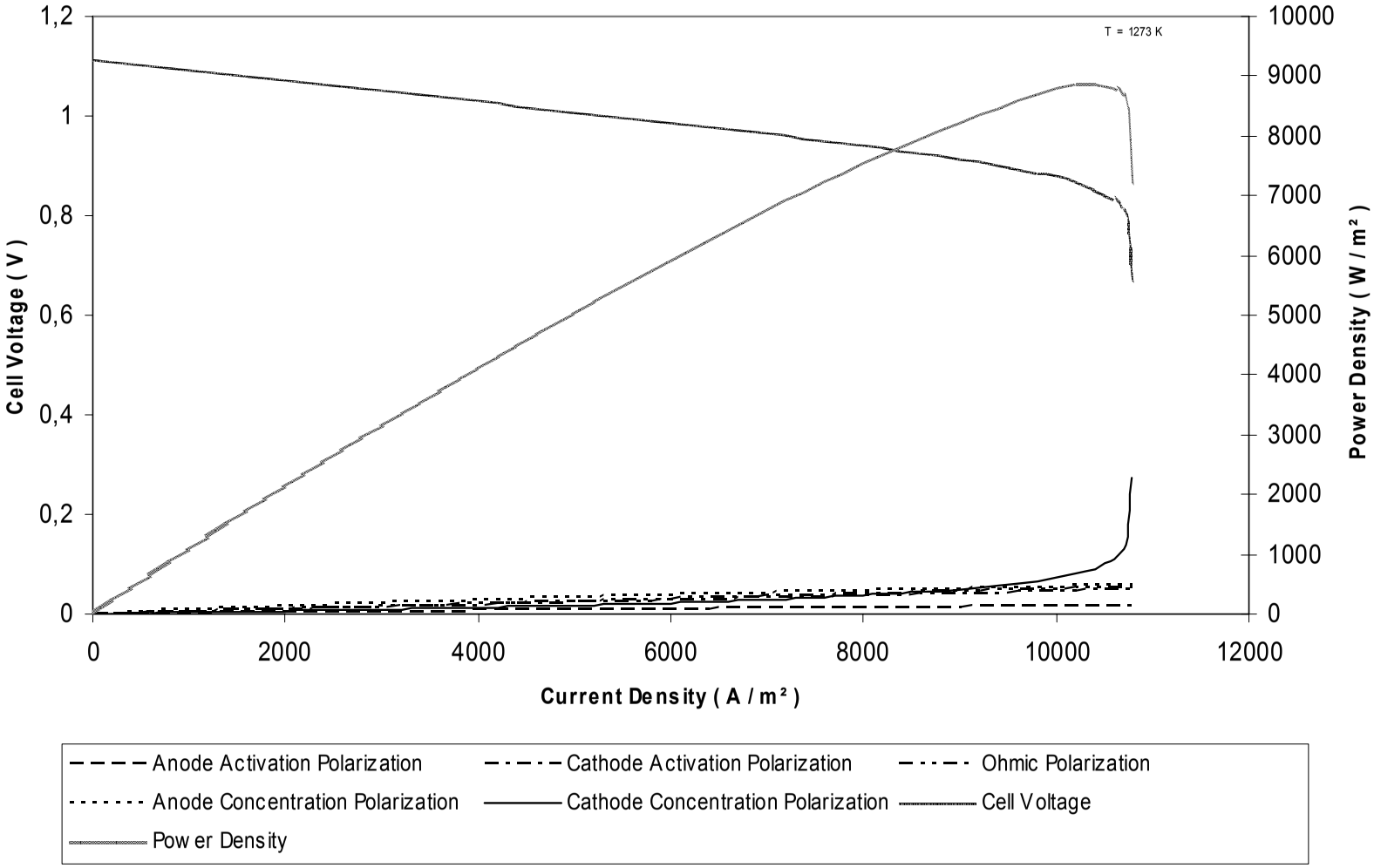

Figure 5.6: Calculated power density, cell voltage, and polarizations with current density (T = 1273 K).

For a second condition, temperature is decreased to T = 1073 K. The same results graphed for T = 1073 this time.

The changes in activation, ohmic, and concentration polarizations with current density are given in Figures 5.7, 5.8, and 5.9. The change in cell voltage and the power density due to the polarizations is given in Figure 5.10. The change in all kinds of polarizations with current density is grouped and shown in a single graph in Figure 5.11. The calculated power density, cell voltage, and polarizations versus current density is shown in Figure 5.12.

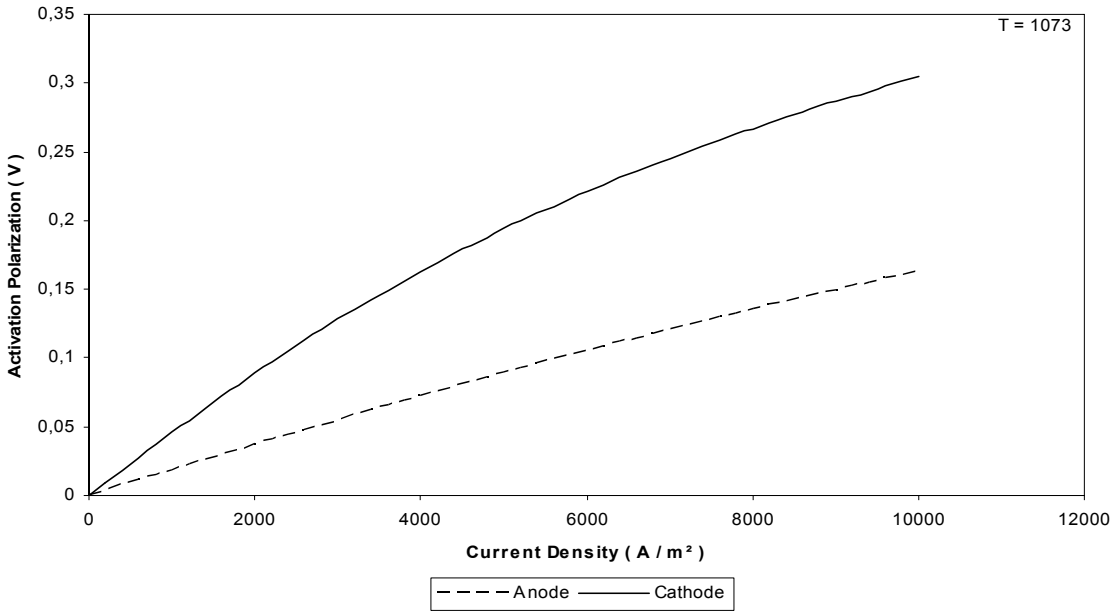

Figure 5.7: Activation polarization change with current density (T = 1073 K).

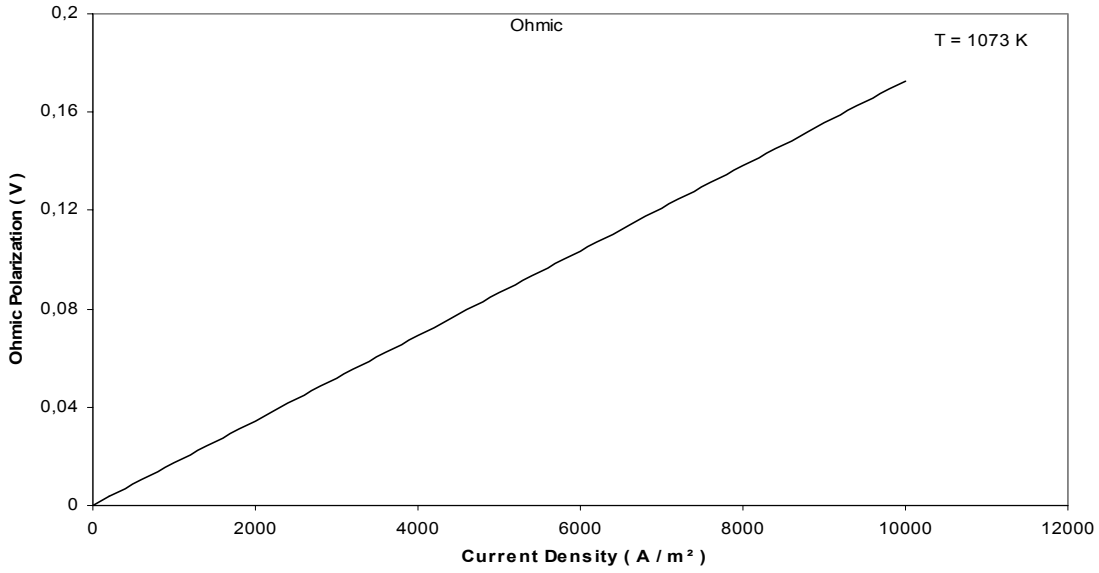

Figure 5.8: Ohmic polarization change with current density (T = 1073 K).

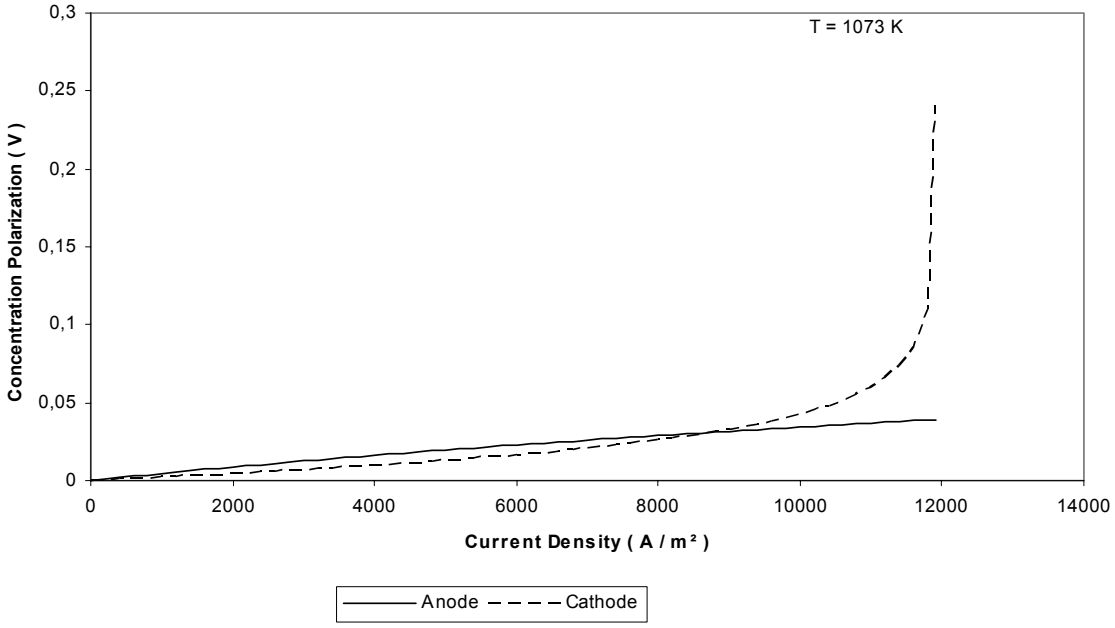

Figure 5.9: Concentration polarization change with current density (T = 1073 K).

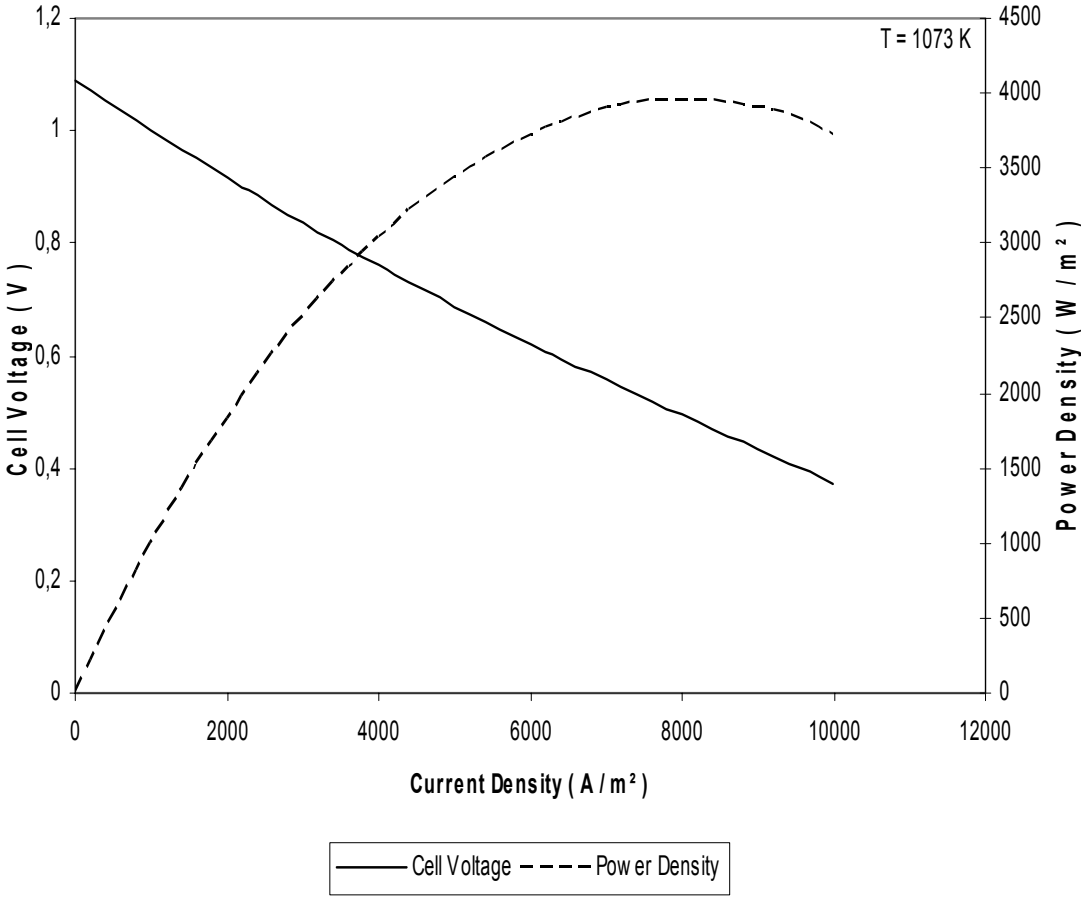

Figure 5.10: Change in the cell voltage and the power density with current density (T = 1073 K).

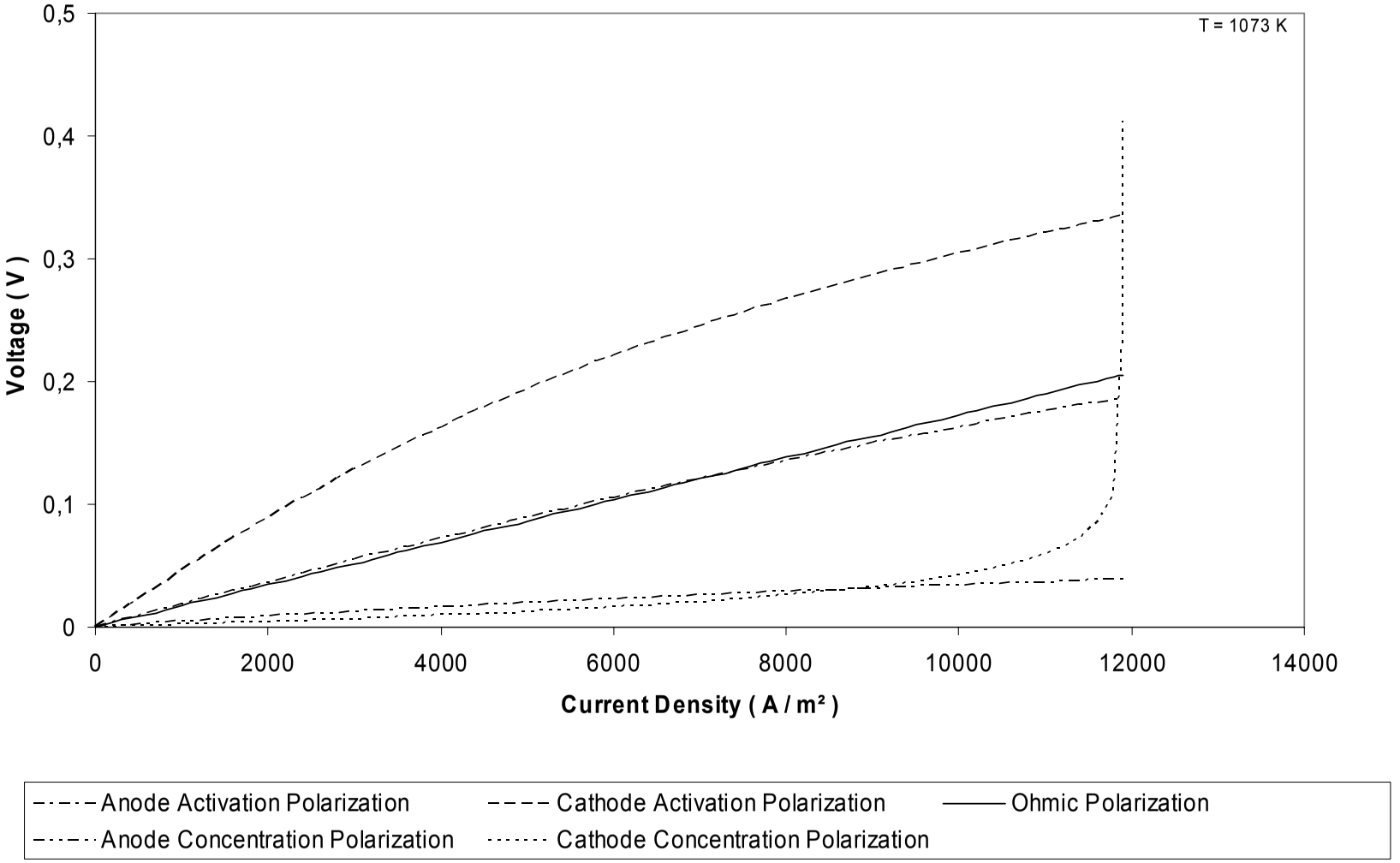

Figure 5.11: Calculated polarization effects with current density (T = 1073 K).

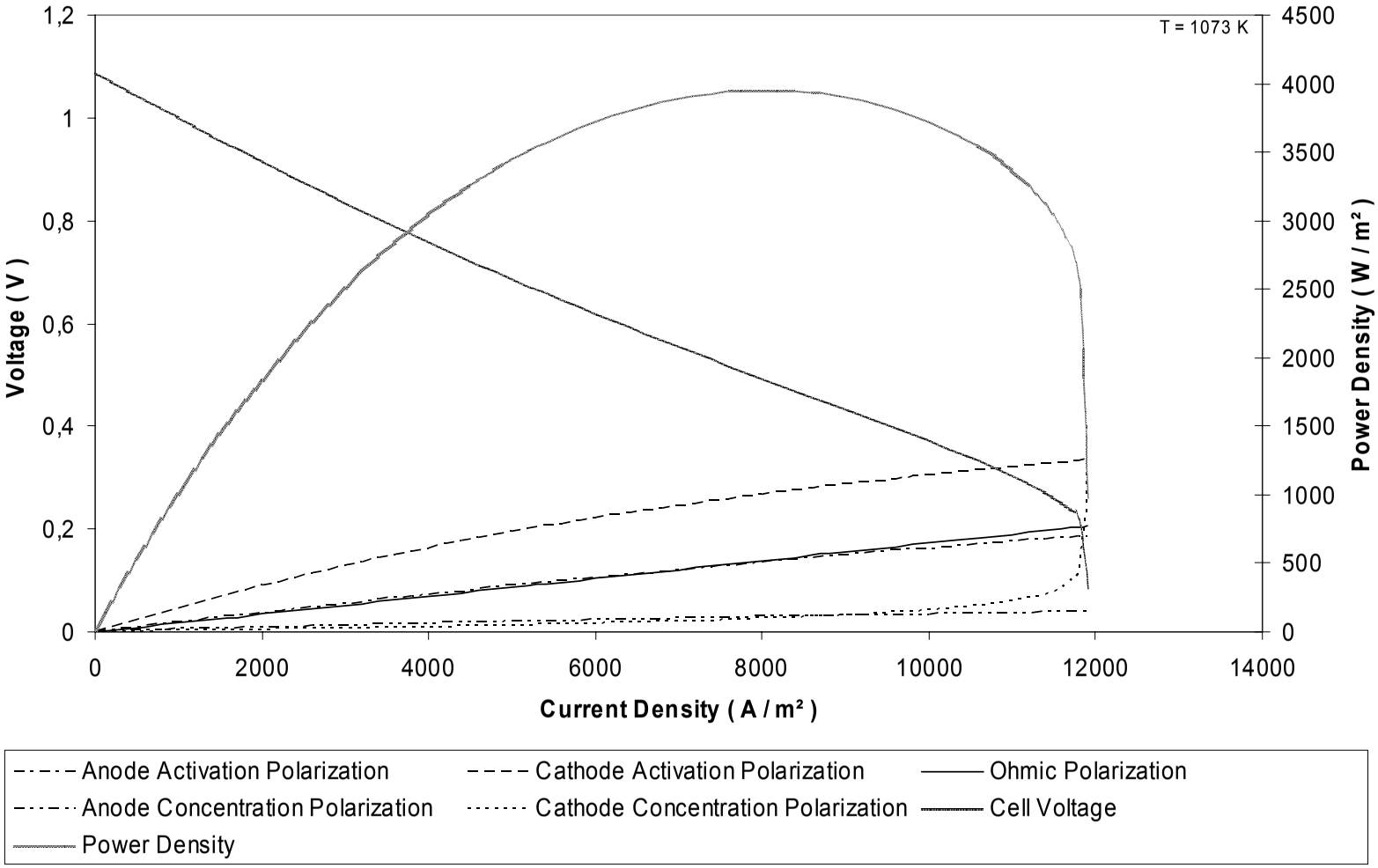

Figure 5.12: Calculated power density, cell voltage and polarizations with current density (T = 1073 K).

The cathode activation polarization is obviously higher than the anode activation polarization. This is because of the cathode's lower exchange current density. Both the cathode and anode activation polarizations increase almost linearly at T = 1273 K.

Ohmic polarization changes linearly with increasing current, since it is related to the material thickness. Electrolyte section has the main effect on ohmic polarization due to its material's high resistivity. The effect of ohmic polarization can be changed by changing the thickness of materials or by using another material instead.

Anode concentration polarization is higher than the cathode concentration polarization at low current densities. But after a critical region, cathode concentration polarization increases exponentially and goes to infinity as can be seen from the graphs. Regarding to Figures 5.3 and 5.9, for the cell working at T = 1273 K, I_L = 10788 A / m², and for the one working at T = 1073 K, I_L = 11900 A / m² are the limiting current densities.

Figures 5.4 and 5.10 give the change of the cell voltage and the power densities with current density. The lower the temperature, the more the cell voltage drops, and the less the power density is. This result is just as expected. In chapter 3, it was explained that the efficiency of fuel cells decreases with increasing temperature, but on the other hand, as it can be observed from the results, as the temperature increases, the drop in cell voltage decreases, and power density increases.

Figures 5.5 and 5.11 show the polarization effects in a single graph for both temperatures. The results show that at lower temperatures, the cathode activation polarization becomes significant and has the most effect on voltage drop. The ohmic and anode activation polarizations behave similarly at lower temperatures. The anode concentration polarization, on the other hand, becomes significant at high temperature values, while cathode concentration polarization has very little effect at low temperatures and low current densities. At high temperature, cathode concentration polarization increases exponentially. Anode and cathode activation polarizations depend on temperature much more than the other types of polarizations. The increase in

activation polarization with decreasing temperature is the highest in all types of polarizations.

Figures 5.6 and 5.12 give a better understanding of the effect of temperature on the fuel cell voltage and the power density. For the cell operating at T = 1273 K, at I ≈ 10400 A / m², the power density reaches its peak point P ≈ 8889 W / m². For the cell operating at T = 1073 K, at I ≈ 8000 A / m², the power density reaches its peak point P ≈ 3955 W / m².

At I = 6000 A / m², for the cell working at T = 1273, cell voltage is, E = 0.989 V, while for the cell working at T = 1073 K, cell voltage is, E = 0.621 V. There is a significant difference between the two cell voltages.

As a conclusion, as the fuel cell operating temperature increases, the polarizations decrease and this results higher cell voltages and high power densities

5.1.2 Thermodynamic Analysis

The system is assumed to be at following conditions:

- T = 1273 K., P = 1 atm.
- The air consists of 20 % O_2 and 80 % N_2 in molar ratios.

In order to calculate the entropies at each node of the system, the partial pressures of the molecules must be determined. For this reason, mixture compositions at each node of the system for ideal case (i.e. conversion ratios are unity) is given in Table 5.1. Mixture compositions for different conversion ratios at each node of the system are given in Tables 5.2 – 7.

Table 5.1: Mixture compositions for ideal case (i.e. $\eta_{CH_4}=1$, $\eta_{H_2}=1$, $\eta_{O_2}=1$).

	Mole Numbers **Nodes**				***Mole Ratios*** **Nodes**			
	1	**2**	**3**	**4**	**1**	**2**	**3**	**4**
CH_4	*1*	*0*	*0*	*0*	*0,3125*	*0*	*0*	*0*
H_2O	*2,2*	*0,2*	*0*	*4,2*	*0,6875*	*0,03846*	*0*	*0,31818*
H_2	*0*	*4*	*0*	*0*	*0*	*0,76923*	*0*	*0*
O_2	*0*	*0*	*2*	*0*	*0*	*0*	*0,2*	*0*
CO_2	*0*	*1*	*0*	*1*	*0*	*0,19231*	*0*	*0,07576*
N_2	*0*	*0*	*8*	*8*	*0*	*0*	*0,8*	*0,60606*

Table 5.2: Mixture compositions for $\eta_{CH_4}=0.9$, $\eta_{H_2}=0.9$, $\eta_{O_2}=0.9$.

	Mole Numbers **Nodes**				***Mole Ratios*** **Nodes**			
	1	**2**	**3**	**4**	**1**	**2**	**3**	**4**
CH_4	*1*	*0,1*	*0*	*0,1*	*0,3125*	*0,02*	*0*	*0,00747*
H_2O	*2,2*	*0,4*	*0*	*3,64*	*0,6875*	*0,08*	*0*	*0,27205*
H_2	*0*	*3,6*	*0*	*0,36*	*0*	*0,72*	*0*	*0,02691*
O_2	*0*	*0*	*2*	*0,38*	*0*	*0*	*0,2*	*0,02840*
CO_2	*0*	*0,9*	*0*	*0,9*	*0*	*0,18*	*0*	*0,06727*
N_2	*0*	*0*	*8*	*8*	*0*	*0*	*0,8*	*0,59791*

Table 5.3: Mixture compositions for $\eta_{CH_4}=0.9$, $\eta_{H_2}=0.9$, $\eta_{O_2}=0.8$.

	Mole Numbers **Nodes**				***Mole Ratios*** **Nodes**			
	1	**2**	**3**	**4**	**1**	**2**	**3**	**4**
CH_4	*1*	*0,1*	*0*	*0,1*	*0,3125*	*0,02*	*0*	*0,00746*
H_2O	*2,2*	*0,4*	*0*	*3,6*	*0,6875*	*0,08*	*0*	*0,26866*
H_2	*0*	*3,6*	*0*	*0,4*	*0*	*0,72*	*0*	*0,02985*

O_2	*0*	*0*	*2*	*0,4*	*0*	*0*	*0,2*	*0,02985*
CO_2	*0*	*0,9*	*0*	*0,9*	*0*	*0,18*	*0*	*0,06716*
N_2	*0*	*0*	*8*	*8*	*0*	*0*	*0,8*	*0,59701*

Table 5.4: Mixture compositions for $\eta_{CH_4} = 0.9$, $\eta_{H_2} = 0.9$, $\eta_{O_2} = 0.7$.

	Mole Numbers **Nodes**				***Mole Ratios*** **Nodes**			
	1	**2**	**3**	**4**	**1**	**2**	**3**	**4**
CH_4	*1*	*0,1*	*0*	*0,1*	*0,3125*	*0,02*	*0*	*0,007353*
H_2O	*2,2*	*0,4*	*0*	*3,2*	*0,6875*	*0,08*	*0*	*0,235294*
H_2	*0*	*3,6*	*0*	*0,8*	*0*	*0,72*	*0*	*0,058824*
O_2	*0*	*0*	*2*	*0,6*	*0*	*0*	*0,2*	*0,044118*
CO_2	*0*	*0,9*	*0*	*0,9*	*0*	*0,18*	*0*	*0,066176*
N_2	*0*	*0*	*8*	*8*	*0*	*0*	*0,8*	*0,588235*

Table 5.5: Mixture compositions for $\eta_{CH_4} = 0.9$, $\eta_{H_2} = 0.8$, $\eta_{O_2} = 0.8$.

	Mole Numbers **Nodes**				***Mole Ratios*** **Nodes**			
	1	**2**	**3**	**4**	**1**	**2**	**3**	**4**
CH_4	*1*	*0,1*	*0*	*0,1*	*0,3125*	*0,02*	*0*	*0,007375*
H_2O	*2,2*	*0,4*	*0*	*3,28*	*0,6875*	*0,08*	*0*	*0,241888*
H_2	*0*	*3,6*	*0*	*0,72*	*0*	*0,72*	*0*	*0,053097*
O_2	*0*	*0*	*2*	*0,56*	*0*	*0*	*0,2*	*0,041298*
CO_2	*0*	*0,9*	*0*	*0,9*	*0*	*0,18*	*0*	*0,066372*
N_2	*0*	*0*	*8*	*8*	*0*	*0*	*0,8*	*0,589971*

Table 5.6: Mixture compositions for $\eta_{CH_4} = 0.9$, $\eta_{H_2} = 0.8$, $\eta_{O_2} = 0.7$.

	Mole Numbers **Nodes**				***Mole Ratios*** **Nodes**			
	1	**2**	**3**	**4**	**1**	**2**	**3**	**4**
CH_4	*1*	*0,1*	*0*	*0,1*	*0,3125*	*0,02*	*0*	*0,007353*
H_2O	*2,2*	*0,4*	*0*	*3,2*	*0,6875*	*0,08*	*0*	*0,235294*
H_2	*0*	*3,6*	*0*	*0,8*	*0*	*0,72*	*0*	*0,058824*
O_2	*0*	*0*	*2*	*0,6*	*0*		*0,2*	*0,044118*

CO_2	0	0,9	0	0,9	0	0,18	0	0,066176
N_2	0	0	8	8	0	0	0,8	0,588235

Table 5.7: Mixture compositions for $\eta_{CH_4} = 0.9$, $\eta_{H_2} = 0.7$, $\eta_{O_2} = 0.7$.

	Mole Numbers **Nodes**				***Mole Ratios*** **Nodes**			
	1	**2**	**3**	**4**	**1**	**2**	**3**	**4**
CH_4	1	0,1	0	0,1	0,3125	0,02	0	0,007278
H_2O	2,2	0,4	0	2,92	0,6875	0,08	0	0,212518
H_2	0	3,6	0	1,08	0	0,72	0	0,078603
O_2	0	0	2	0,74	0		0,2	0,053857
CO_2	0	0,9	0	0,9	0	0,18	0	0,065502
N_2	0	0	8	8	0	0	0,8	0,582242

The maximum work calculated for the fuel cell unit working at T = 1273 K is, W_{max} = 805.6 kJ, and for the fuel cell unit working at T = 1073 K is, W_{max} = 808.8 kJ,. The losses in work due to reformer reaction, incomplete reactions, cracks and polarizations are calculated as a function of the conversion ratios. For each conversion ratio, the obtainable works are calculated. Using Eq.4.15, the second law efficiencies are calculated as functions of the conversion ratios. These calculations are repeated for each temperature value.

For the calculations, as a first step, the pressure is assumed to be, P = 1 atm. Keeping the pressure constant, the second law efficiencies of the fuel cell unit as functions of different conversion ratios are calculated with different current densities. These results are obtained for each temperature value. As a result, under constant pressure, the effects of both the temperature and the current density on the fuel cell unit are investigated. The results obtained are presented in Tables 5.8 – 5.15.

As a second step, in order to investigate the pressure effect on the second law efficiency of the fuel cell unit, the calculation steps are repeated at P = 5 atm. For different current density values, the second law efficiencies are calculated as functions of conversion

ratios, for both T = 1073 K, and T = 1273 K. The results obtained are presented in Tables 5.16 – 5.23.

Table 5.8: Calculated second law efficiencies as functions of conversion ratios (T = 1273 K, P = 1 atm, I = 8000 A / m²).

Conversion ratios								
	methane	**1**	**0,9**	**0,9**	**0,9**	**0,9**	**0,9**	**0,9**
	hydrogen	**1**	**0,9**	**0,9**	**0,9**	**0,8**	**0,8**	**0,7**
	oxygen	**1**	**0,9**	**0,8**	**0,7**	**0,8**	**0,7**	**0,7**
Maximum energy available (kJ)		***805,6***	***805,6***	***805,6***	***805,6***	***805,6***	***805,6***	***805,6***
Irreversible losses (kJ)								
	due to reformer reaction	*105,6*	*104,7*	*104,7*	*104,7*	*104,7*	*104,7*	*104,7*
	due to incomplete reactions	*0*	*110,7*	*116,3*	*175,0*	*162,9*	*175,0*	*218,2*
	due to cracks	*7*	*6*	*6*	*5*	*5*	*5*	*4*
	due to polarizations	*133,5*	*108,2*	*106,8*	*93,5*	*96,1*	*93,5*	*84,1*
Obtainable work (kJ)		*559,445*	*476,001*	*471,737*	*427,390*	*436,820*	*427,390*	*394,538*
Second law efficiency		***0,694***	***0,591***	***0,586***	***0,531***	***0,542***	***0,531***	***0,490***

Table 5.9: Calculated second law efficiencies as functions of conversion ratios (T = 1073 K, P = 1 atm, I = 8000 A / m²).

Conversion ratios								
	methane	**1**	**0,9**	**0,9**	**0,9**	**0,9**	**0,9**	**0,9**
	hydrogen	**1**	**0,9**	**0,9**	**0,9**	**0,8**	**0,8**	**0,7**
	oxygen	**1**	**0,9**	**0,8**	**0,7**	**0,8**	**0,7**	**0,7**
Maximum energy available (kJ)		***808,8***	***808,8***	***808,8***	***808,8***	***808,8***	***808,8***	***808,8***
Irreversible losses (kJ)								
	due to reformer reaction	*69,5*	*70,7*	*70,7*	*70,7*	*70,7*	*70,7*	*70,7*
	due to incomplete reactions	*0*	*122,9*	*129,2*	*194,3*	*181,0*	*194,3*	*241,7*
	due to cracks	*7*	*6*	*6*	*5*	*5*	*5*	*4*
	due to polarizations	*459,3*	*372,0*	*367,4*	*321,5*	*330,7*	*321,5*	*289,3*
Obtainable work (kJ)		*273,022*	*237,185*	*235,478*	*217,305*	*221,420*	*217,305*	*203,055*
Second law efficiency		***0,338***	***0,293***	***0,291***	***0,269***	***0,274***	***0,269***	***0,251***

Table 5.10: Calculated second law efficiencies as functions of conversion ratios (T = 1273 K, P = 1 atm, I = 6000 A / m²).

Conversion ratios								
	methane	1	0,9	0,9	0,9	0,9	0,9	0,9
	hydrogen	1	0,9	0,9	0,9	0,8	0,8	0,7
	oxygen	1	0,9	0,8	0,7	0,8	0,7	0,7
Maximum energy available (kJ)		***805,6***	***805,6***	***805,6***	***805,6***	***805,6***	***805,6***	***805,6***
Irreversible losses (kJ)								
	due to reformer reaction	*105,6*	*104,7*	*104,7*	*104,7*	*104,7*	*104,7*	*104,7*
	due to incomplete reactions	*0*	*110,7*	*116,3*	*175,0*	*162,9*	*175,0*	*218,2*
	due to cracks	*7*	*6*	*6*	*5*	*5*	*5*	*4*
	due to polarizations	*98,0*	*79,4*	*78,4*	*68,6*	*70,6*	*68,6*	*61,8*
Obtainable work (kJ)		*594,952*	*504,762*	*500,142*	*452,245*	*462,385*	*452,245*	*416,908*
Second law efficiency		***0,739***	***0,627***	***0,621***	***0,561***	***0,574***	***0,561***	***0,518***

Table 5.11: Calculated second law efficiencies as functions of conversion ratios (T = 1073 K, P = 1 atm, I = 6000 A / m²).

Conversion ratios								
	methane	1	0,9	0,9	0,9	0,9	0,9	0,9
	hydrogen	1	0,9	0,9	0,9	0,8	0,8	0,7
	oxygen	1	0,9	0,8	0,7	0,8	0,7	0,7
Maximum energy available (kJ)		***808,8***	***808,8***	***808,8***	***808,8***	***808,8***	***808,8***	***808,8***
Irreversible losses (kJ)								
	due to reformer reaction	*69,5*	*70,7*	*70,7*	*70,7*	*70,7*	*70,7*	*70,7*
	due to incomplete reactions	*0*	*122,9*	*129,2*	*194,3*	*181,0*	*194,3*	*241,7*
	due to cracks	*7*	*6*	*6*	*5*	*5*	*5*	*4*
	due to polarizations	*362,0*	*293,2*	*289,6*	*253,4*	*260,7*	*253,4*	*228,1*
Obtainable work (kJ)		*370,281*	*315,964*	*313,285*	*285,387*	*291,446*	*285,387*	*264,328*
Second law efficiency		***0,458***	***0,391***	***0,387***	***0,353***	***0,360***	***0,353***	***0,327***

Table 5.12: Calculated second law efficiencies as functions of conversion ratios (T = 1273 K, P = 1 atm, I = 4000 A / m²).

Conversion ratios	***methane***	**1**	**0,9**	**0,9**	**0,9**	**0,9**	**0,9**	**0,9**
	hydrogen	**1**	**0,9**	**0,9**	**0,9**	**0,8**	**0,8**	**0,7**
	oxygen	**1**	**0,9**	**0,8**	**0,7**	**0,8**	**0,7**	**0,7**
Maximum energy available (kJ)		***805,6***	***805,6***	***805,6***	***805,6***	***805,6***	***805,6***	***805,6***
Irreversible losses (kJ)								
	due to reformer reaction	*105,6*	*104,7*	*104,7*	*104,7*	*104,7*	*104,7*	*104,7*
	due to incomplete reactions	*0*	*110,7*	*116,3*	*175,0*	*162,9*	*175,0*	*218,2*
	due to cracks	*7*	*6*	*6*	*5*	*5*	*5*	*4*
	due to polarizations	*65,6*	*53,1*	*52,5*	*45,9*	*47,2*	*45,9*	*41,3*
Obtainable work (kJ)		*627,372*	*531,022*	*526,078*	*474,939*	*485,727*	*474,939*	*437,332*
Second law efficiency		***0,779***	***0,659***	***0,653***	***0,590***	***0,603***	***0,590***	***0,543***

Table 5.13: Calculated second law efficiencies as functions of conversion ratios (T = 1073 K, P = 1 atm, I = 4000 A / m²).

Conversion ratios	***methane***	**1**	**0,9**	**0,9**	**0,9**	**0,9**	**0,9**	**0,9**
	hydrogen	**1**	**0,9**	**0,9**	**0,9**	**0,8**	**0,8**	**0,7**
	oxygen	**1**	**0,9**	**0,8**	**0,7**	**0,8**	**0,7**	**0,7**
Maximum energy available (kJ)		***808,8***	***808,8***	***808,8***	***808,8***	***808,8***	***808,8***	***808,8***
Irreversible losses (kJ)								
	due to reformer reaction	*69,5*	*70,7*	*70,7*	*70,7*	*70,7*	*70,7*	*70,7*
	due to incomplete reactions	*0*	*122,9*	*129,2*	*194,3*	*181,0*	*194,3*	*241,7*
	due to cracks	*7*	*6*	*6*	*5*	*5*	*5*	*4*
	due to polarizations	*254,7*	*206,3*	*203,8*	*178,3*	*183,4*	*178,3*	*160,5*
Obtainable work (kJ)		*477,574*	*402,872*	*399,119*	*360,492*	*368,698*	*360,492*	*331,923*
Second law efficiency		***0,590***	***0,498***	***0,493***	***0,446***	***0,456***	***0,446***	***0,410***

Table 5.14: Calculated second law efficiencies as functions of conversion ratios (T = 1273 K, P = 1 atm, I = 2000 A / m²).

Conversion ratios								
	methane	1	0,9	0,9	0,9	0,9	0,9	0,9
	hydrogen	1	0,9	0,9	0,9	0,8	0,8	0,7
	oxygen	1	0,9	0,8	0,7	0,8	0,7	0,7
Maximum energy available (kJ)		***805,6***	***805,6***	***805,6***	***805,6***	***805,6***	***805,6***	***805,6***
Irreversible losses (kJ)								
	due to reformer reaction	*105,6*	*104,7*	*104,7*	*104,7*	*104,7*	*104,7*	*104,7*
	due to incomplete reactions	*0*	*110,7*	*116,3*	*175,0*	*162,9*	*175,0*	*218,2*
	due to cracks	*7*	*6*	*6*	*5*	*5*	*5*	*4*
	due to polarizations	*33,2*	*26,9*	*26,6*	*23,2*	*23,9*	*23,2*	*20,9*
Obtainable work (kJ)		*659,791*	*557,282*	*552,014*	*497,633*	*509,069*	*497,633*	*457,756*
Second law efficiency		***0,819***	***0,692***	***0,685***	***0,618***	***0,632***	***0,618***	***0,568***

Table 5.15: Calculated second law efficiencies as functions of conversion ratios (T = 1073 K, P = 1 atm, I = 2000 A / m²).

Conversion ratios								
	methane	1	0,9	0,9	0,9	0,9	0,9	0,9
	hydrogen	1	0,9	0,9	0,9	0,8	0,8	0,7
	oxygen	1	0,9	0,8	0,7	0,8	0,7	0,7
Maximum energy available (kJ)		***808,8***	***808,8***	***808,8***	***808,8***	***808,8***	***808,8***	***808,8***
Irreversible losses (kJ)								
	due to reformer reaction	*69,5*	*70,7*	*70,7*	*70,7*	*70,7*	*70,7*	*70,7*
	due to incomplete reactions	*0*	*122,9*	*129,2*	*194,3*	*181,0*	*194,3*	*241,7*
	due to cracks	*7*	*6*	*6*	*5*	*5*	*5*	*4*
	due to polarizations	*146,7*	*118,8*	*117,3*	*102,7*	*105,6*	*102,7*	*92,4*
Obtainable work (kJ)		*585,640*	*490,405*	*485,572*	*436,138*	*446,505*	*436,138*	*400,004*
Second law efficiency		***0,724***	***0,606***	***0,600***	***0,539***	***0,552***	***0,539***	***0,495***

Table 5.16: Calculated second law efficiencies as functions of conversion ratios (T = 1273 K, P = 5 atm, I = 8000 A / m²).

Conversion ratios								
	methane	1	0,9	0,9	0,9	0,9	0,9	0,9
	hydrogen	1	0,9	0,9	0,9	0,8	0,8	0,7
	oxygen	1	0,9	0,8	0,7	0,8	0,7	0,7
Maximum energy available (kJ)		***805,6***	***805,6***	***805,6***	***805,6***	***805,6***	***805,6***	***805,6***
Irreversible losses (kJ)								
	due to reformer reaction	*63,6*	*66,9*	*66,9*	*66,9*	*66,9*	*66,9*	*66,9*
	due to incomplete reactions	*0*	*125,6*	*132,0*	*198,6*	*185,0*	*198,6*	*247,4*
	due to cracks	*7*	*6*	*6*	*5*	*5*	*5*	*4*
	due to polarizations	*133,5*	*108,2*	*106,8*	*93,5*	*96,1*	*93,5*	*84,1*
Obtainable work (kJ)		*591,627*	*500,099*	*495,135*	*443,988*	*454,718*	*443,988*	*406,336*
Second law efficiency		***0,747***	***0,619***	***0,613***	***0,548***	***0,562***	***0,548***	***0,500***

Table 5.17: Calculated second law efficiencies as functions of conversion ratios (T = 1073 K, P = 5 atm, I = 8000 A / m²).

Conversion ratios								
	methane	1	0,9	0,9	0,9	0,9	0,9	0,9
	hydrogen	1	0,9	0,9	0,9	0,8	0,8	0,7
	oxygen	1	0,9	0,8	0,7	0,8	0,7	0,7
Maximum energy available (kJ)		***808,8***	***808,8***	***808,8***	***808,8***	***808,8***	***808,8***	***808,8***
Irreversible losses (kJ)								
	due to reformer reaction	*33,5*	*38,3*	*38,3*	*38,3*	*38,3*	*38,3*	*38,3*
	due to incomplete reactions	*0*	*134,7*	*141,6*	*212,9*	*198,3*	*212,9*	*264,6*
	due to cracks	*7*	*6*	*6*	*5*	*5*	*5*	*4*
	due to polarizations	*459,3*	*372,0*	*367,4*	*321,5*	*330,7*	*321,5*	*289,3*
Obtainable work (kJ)		*309,022*	*264,985*	*262,678*	*238,405*	*243,720*	*238,405*	*219,855*
Second law efficiency		***0,382***	***0,319***	***0,316***	***0,286***	***0,292***	***0,286***	***0,263***

Table 5.18: Calculated second law efficiencies as functions of conversion ratios (T = 1273 K, P = 5 atm, I = 6000 A / m²).

Conversion ratios	*methane*	1	0,9	0,9	0,9	0,9	0,9	0,9
	hydrogen	1	0,9	0,9	0,9	0,8	0,8	0,7
	oxygen	1	0,9	0,8	0,7	0,8	0,7	0,7
Maximum energy available (kJ)		***805,6***	***805,6***	***805,6***	***805,6***	***805,6***	***805,6***	***805,6***
Irreversible losses (kJ)								
	due to reformer reaction	*63,6*	*66,9*	*66,9*	*66,9*	*66,9*	*66,9*	*66,9*
	due to incomplete reactions	*0*	*125,6*	*132,0*	*198,6*	*185,0*	*198,6*	*247,4*
	due to cracks	*7*	*6*	*6*	*5*	*5*	*5*	*4*
	due to polarizations	*98,0*	*79,4*	*78,4*	*68,6*	*70,6*	*68,6*	*61,8*
Obtainable work (kJ)		*627,134*	*528,860*	*523,540*	*468,843*	*480,283*	*468,843*	*428,706*
Second law efficiency		***0,791***	***0,655***	***0,648***	***0,579***	***0,593***	***0,579***	***0,528***

Table 5.19: Calculated second law efficiencies as functions of conversion ratios (T = 1073 K, P = 5 atm, I = 6000 A / m²).

Conversion ratios	*methane*	1	0,9	0,9	0,9	0,9	0,9	0,9
	hydrogen	1	0,9	0,9	0,9	0,8	0,8	0,7
	oxygen	1	0,9	0,8	0,7	0,8	0,7	0,7
Maximum energy available (kJ)		***808,8***	***808,8***	***808,8***	***808,8***	***808,8***	***808,8***	***808,8***
Irreversible losses (kJ)								
	due to reformer reaction	*33,5*	*38,3*	*38,3*	*38,3*	*38,3*	*38,3*	*38,3*
	due to incomplete reactions	*0*	*134,7*	*141,6*	*212,9*	*198,3*	*212,9*	*264,6*
	due to cracks	*7*	*6*	*6*	*5*	*5*	*5*	*4*
	due to polarizations	*362,0*	*293,2*	*289,6*	*253,4*	*260,7*	*253,4*	*228,1*
Obtainable work (kJ)		*406,281*	*343,764*	*340,485*	*306,487*	*313,746*	*306,487*	*281,128*
Second law efficiency		***0,502***	***0,416***	***0,412***	***0,370***	***0,379***	***0,370***	***0,339***

Table 5.20: Calculated second law efficiencies as functions of conversion ratios (T = 1273 K, P = 5 atm, I = 4000 A / m²).

Conversion ratios								
	methane	1	0,9	0,9	0,9	0,9	0,9	0,9
	hydrogen	1	0,9	0,9	0,9	0,8	0,8	0,7
	oxygen	1	0,9	0,8	0,7	0,8	0,7	0,7
Maximum energy available (kJ)		***805,6***	***805,6***	***805,6***	***805,6***	***805,6***	***805,6***	***805,6***
Irreversible losses (kJ)								
	due to reformer reaction	*63,6*	*66,9*	*66,9*	*66,9*	*66,9*	*66,9*	*66,9*
	due to incomplete reactions	*0*	*125,6*	*132,0*	*198,6*	*185,0*	*198,6*	*247,4*
	due to cracks	*7*	*6*	*6*	*5*	*5*	*5*	*4*
	due to polarizations	*65,6*	*53,1*	*52,5*	*45,9*	*47,2*	*45,9*	*41,3*
Obtainable work (kJ)		*659,554*	*555,120*	*549,476*	*491,537*	*503,625*	*491,537*	*449,130*
Second law efficiency		***0,831***	***0,688***	***0,680***	***0,607***	***0,622***	***0,607***	***0,554***

Table 5.21: Calculated second law efficiencies as functions of conversion ratios (T = 1073 K, P = 5 atm, I = 4000 A / m²).

Conversion ratios								
	methane	1	0,9	0,9	0,9	0,9	0,9	0,9
	hydrogen	1	0,9	0,9	0,9	0,8	0,8	0,7
	oxygen	1	0,9	0,8	0,7	0,8	0,7	0,7
Maximum energy available (kJ)		***808,8***	***808,8***	***808,8***	***808,8***	***808,8***	***808,8***	***808,8***
Irreversible losses (kJ)								
	due to reformer reaction	*33,5*	*38,3*	*38,3*	*38,3*	*38,3*	*38,3*	*38,3*
	due to incomplete reactions	*0*	*134,7*	*141,6*	*212,9*	*198,3*	*212,9*	*264,6*
	due to cracks	*7*	*6*	*6*	*5*	*5*	*5*	*4*
	due to polarizations	*254,7*	*206,3*	*203,8*	*178,3*	*183,4*	*178,3*	*160,5*
Obtainable work (kJ)		*513,574*	*430,672*	*426,319*	*381,592*	*390,998*	*381,592*	*348,723*
Second law efficiency		***0,635***	***0,524***	***0,518***	***0,463***	***0,475***	***0,463***	***0,422***

Table 5.22: Calculated second law efficiencies as functions of conversion ratios (T = 1273 K, P = 5 atm, I = 2000 A / m²).

Conversion ratios	***methane***	**1**	**0,9**	**0,9**	**0,9**	**0,9**	**0,9**	**0,9**
	hydrogen	**1**	**0,9**	**0,9**	**0,9**	**0,8**	**0,8**	**0,7**
	oxygen	**1**	**0,9**	**0,8**	**0,7**	**0,8**	**0,7**	**0,7**
Maximum energy available (kJ)		***805,6***	***805,6***	***805,6***	***805,6***	***805,6***	***805,6***	***805,6***
Irreversible losses (kJ)								
	due to reformer reaction	*63,6*	*66,9*	*66,9*	*66,9*	*66,9*	*66,9*	*66,9*
	due to incomplete reactions	*0*	*125,6*	*132,0*	*198,6*	*185,0*	*198,6*	*247,4*
	due to cracks	*7*	*6*	*6*	*5*	*5*	*5*	*4*
	due to polarizations	*33,2*	*26,9*	*26,6*	*23,2*	*23,9*	*23,2*	*20,9*
Obtainable work (kJ)		*691,973*	*581,380*	*575,412*	*514,231*	*526,967*	*514,231*	*469,554*
Second law efficiency		***0,871***	***0,720***	***0,713***	***0,635***	***0,651***	***0,635***	***0,579***

Table 5.23: Calculated second law efficiencies as functions of conversion ratios (T = 1073 K, P = 5 atm, I = 2000 A / m²).

Conversion ratios	***methane***	**1**	**0,9**	**0,9**	**0,9**	**0,9**	**0,9**	**0,9**
	hydrogen	**1**	**0,9**	**0,9**	**0,9**	**0,8**	**0,8**	**0,7**
	oxygen	**1**	**0,9**	**0,8**	**0,7**	**0,8**	**0,7**	**0,7**
Maximum energy available (kJ)		***808,8***	***808,8***	***808,8***	***808,8***	***808,8***	***808,8***	***808,8***
Irreversible losses (kJ)								
	due to reformer reaction	*33,5*	*38,3*	*38,3*	*38,3*	*38,3*	*38,3*	*38,3*
	due to incomplete reactions	*0*	*134,7*	*141,6*	*212,9*	*198,3*	*212,9*	*264,6*
	due to cracks	*7*	*6*	*6*	*5*	*5*	*5*	*4*
	due to polarizations	*146,7*	*118,8*	*117,3*	*102,7*	*105,6*	*102,7*	*92,4*
Obtainable work (kJ)		*621,640*	*518,205*	*512,772*	*457,238*	*468,805*	*457,238*	*416,804*
Second law efficiency		***0,769***	***0,632***	***0,625***	***0,556***	***0,571***	***0,556***	***0,506***

For both T = 1273 K, and T = 1073 K, the change in second law efficiencies with current densities are calculated as functions of conversion ratios. To make it clear, the results obtained at different temperature and pressure values for 100% and 90% conversion ratios are graphed, first by keeping temperature constant in order to investigate the pressure effect on the second law efficiency, and secondly by keeping pressure constant in order to investigate the effect of temperature on the second law efficiency. The graphs are presented in Figures 5.13 – 15.6.

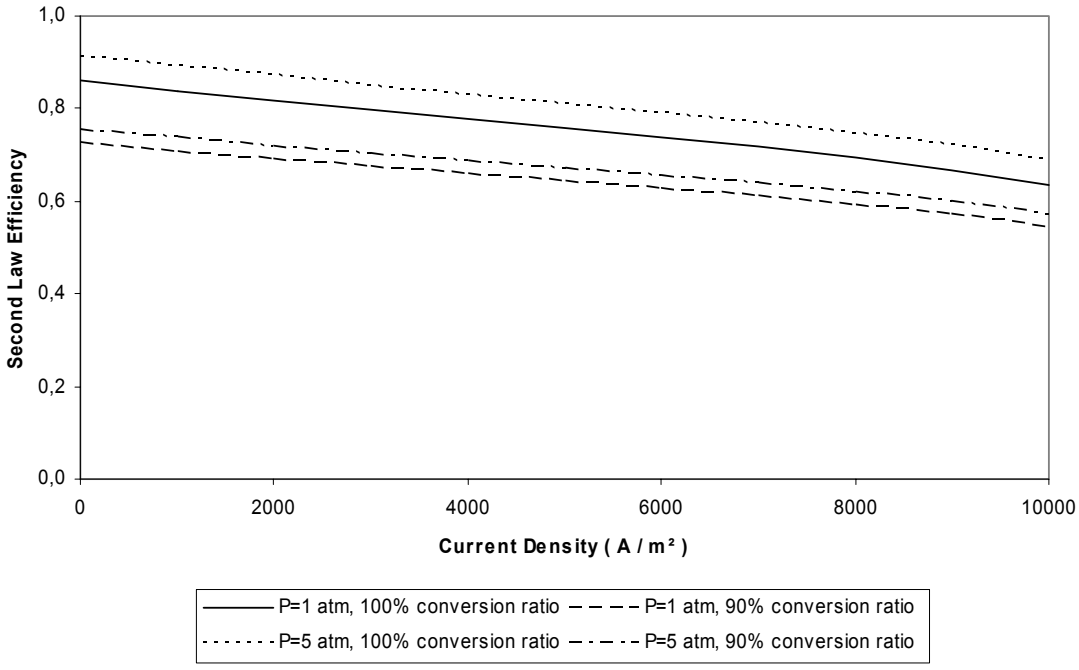

Figure 5.13: Second law efficiency with current density at P = 1 atm, and P = 5 atm, conversion ratios are 100% and 90% respectively, T = 1273 K.

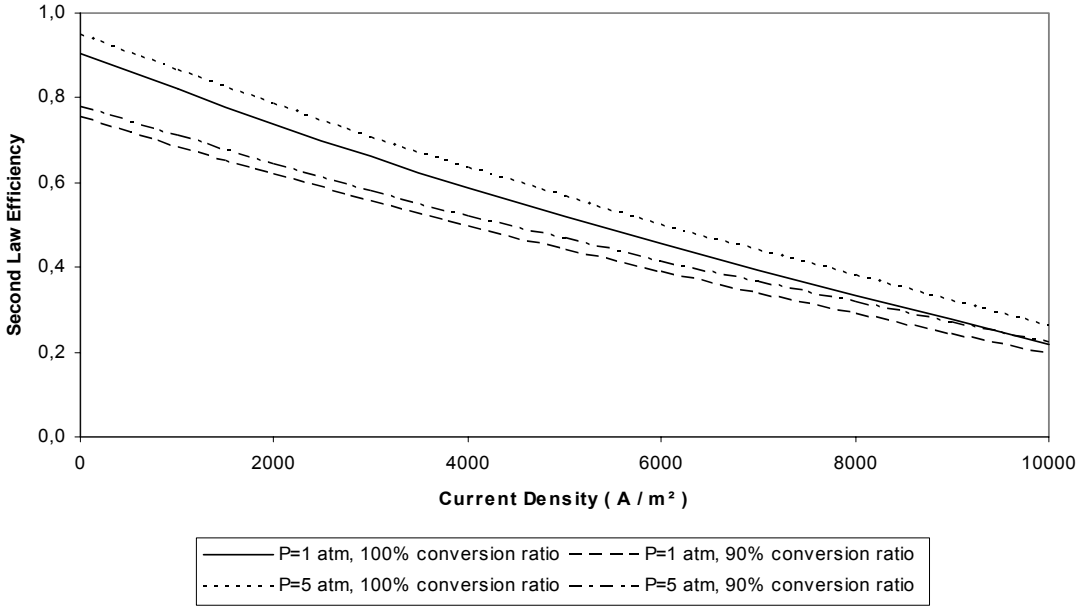

Figure 5.14: Second law efficiency with current density at P = 1 atm, and P = 5 atm, conversion ratios are 100% and 90% respectively, T = 1073 K.

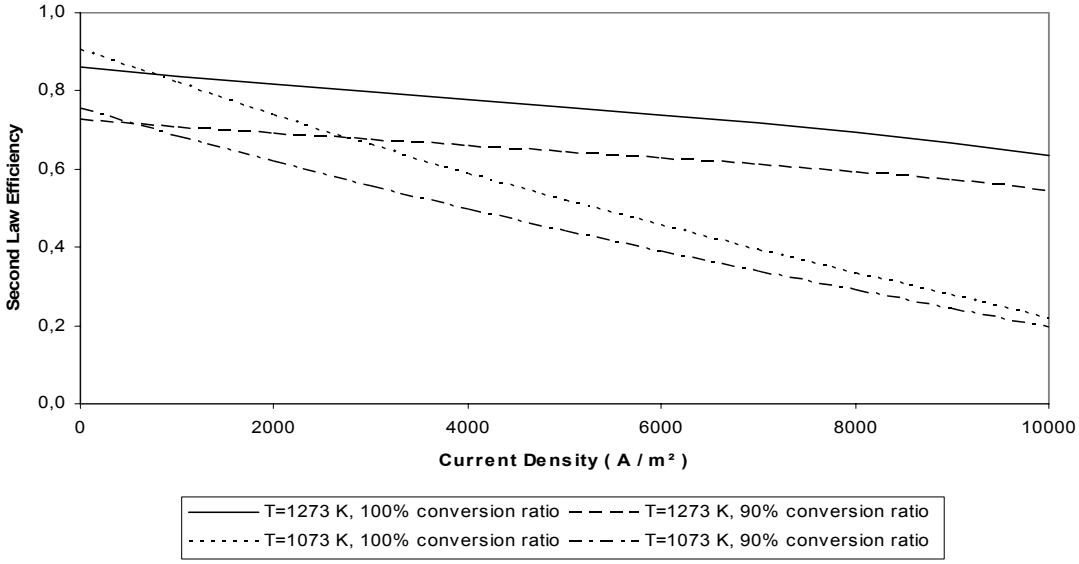

Figure 5.15: Second law efficiency with current density at T = 1273 K, and T = 1073 K, conversion ratios are 100% and 90% respectively, P = 1 atm.

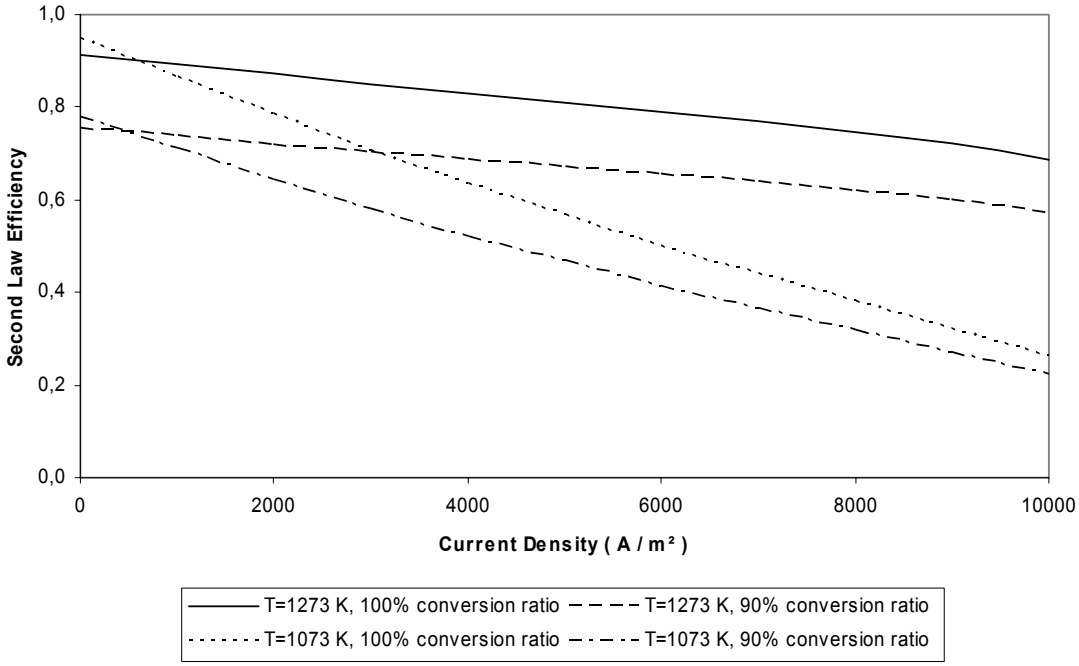

Figure 5.16: Second law efficiency with current density at T = 1273 K, and T = 1073 K, conversion ratios are 100% and 90% respectively, P = 5 atm.

At constant temperature, it can be observed from the graphs that the second law efficiency of the system increases with increasing pressure. The difference in second law efficiency between a high pressure system and a low pressure one remains almost constant (i.e. the same) as the current density increases.

At constant pressure, on the other hand, the second law efficiency of a low temperature system is greater at very low current densities. But as the current density increases, the second law efficiency of a low temperature system decreases much more than the second law efficiency of a higher temperature system does. For current density values of $I > 4000$ A / m², the second law efficiency of a high temperature system becomes much greater than the second law efficiency of a low temperature system. Hence, if the cell is

operated at low current densities, the low temperature gives a better second law efficiency, while for the cell operated at high current densities, the high temperature gives a better second law efficiency.

As a conclusion, it can be stated that, for a system operating at a constant current density value, keeping the temperature constant, the second law efficiency increases as the pressure is increased, and keeping the pressure constant, the second law efficiency increases as the temperature is increased, unless it is operated at very low current density.

5.2 Results of Simulation Model 2

5.2.1 The Heat Required by The Reformer and Vaporizer

In order to determine how much fuel must be left to be burnt in the afterburner, the heat requirement of the reformer and vaporizer must be determined, as a first step. The heat requirement of the reformer and vaporizer reactions with percentage of methane reforming (or the reformer efficiency) is presented in Figure 5.17. The fuel left at the exit of the fuel cell stack is burnt in the afterburner, and the heat released by the combustion process is used in reformer and vaporizer reactions. The remaining heat is lost to the environment. The heat release by the combustion of the fuel in the afterburner is given in Figure 5.18. The temperatures are assumed to be $T_{r,i}$ = 1100 K for the reformer reaction and T = 1200 K for the afterburner reaction, while T=298 K is the exact temperature value for the vaporizer reaction. $T_{r,i}$ is used to indicate the reformer inlet temperature. These temperatures will differ with the calculated temperatures of the reformer inlet and afterburner temperatures, but they are assumed so, in order to make conservative assumptions for the reformer efficiency and the fuel utilization rate.

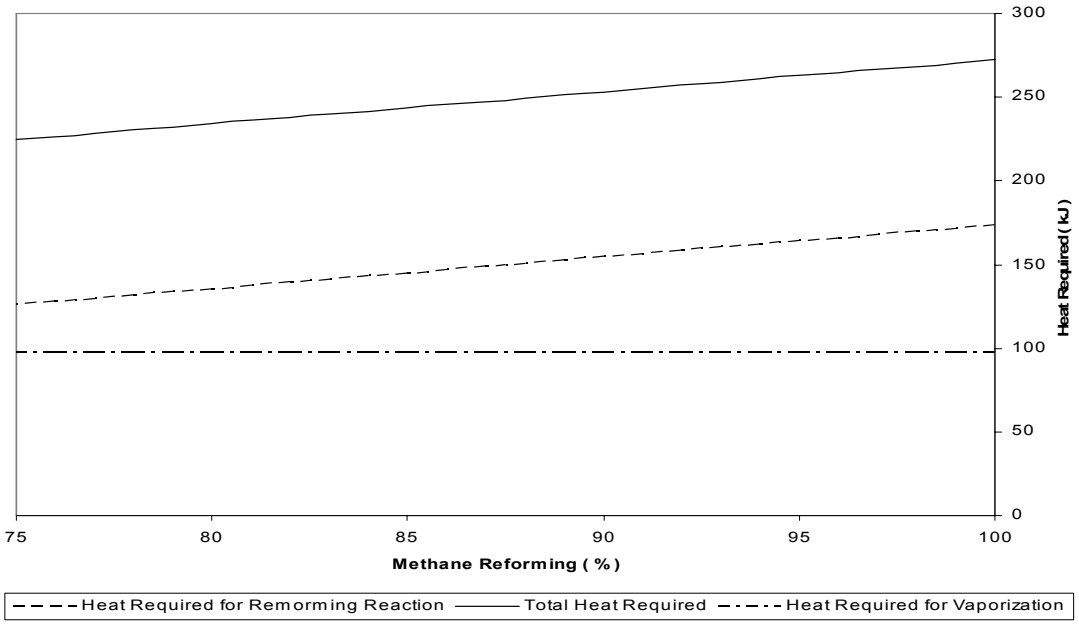

Figure 5.17: Heat requirement of the components of the SOFC system with methane reforming rate ($T_{r,i}$ = 1100 K).

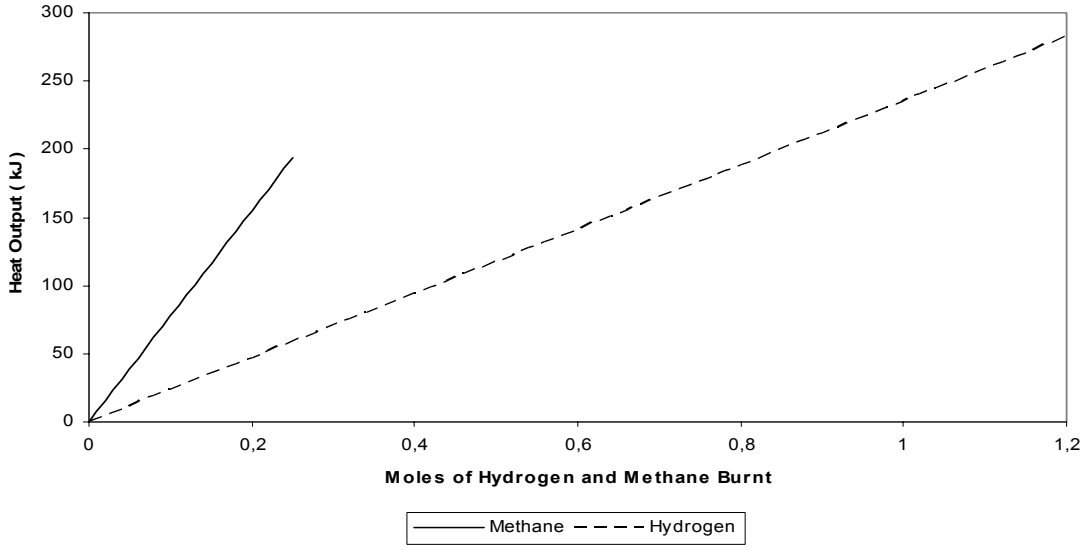

Figure 5.18: Heat release of the combustion processes in the afterburner with respect to the mole number of the fuel that is burnt.

The reformer efficiency and fuel utilization rate directly affect the second law efficiency of the cell. The unreacted methane and hydrogen are burnt in the afterburner as mentioned. As the reformer efficiency and fuel utilization rate change, the heat release due to these unreacted fuel changes as well. The comparison of the heat release of the methane and hydrogen with decreasing reformer efficiency is given in Figure 5.19. Following this, the change in fuel utilization rate with reformer efficiency is given in Figure 5.20.

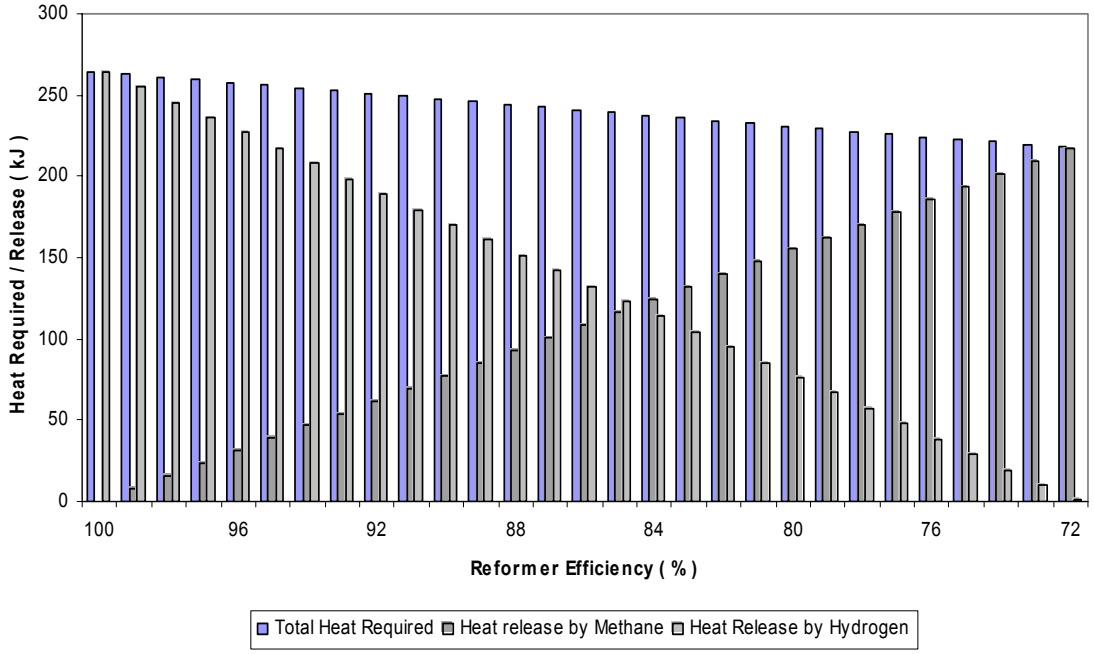

Figure 5.19: Comparison of heat release by methane and hydrogen with reformer efficiency.

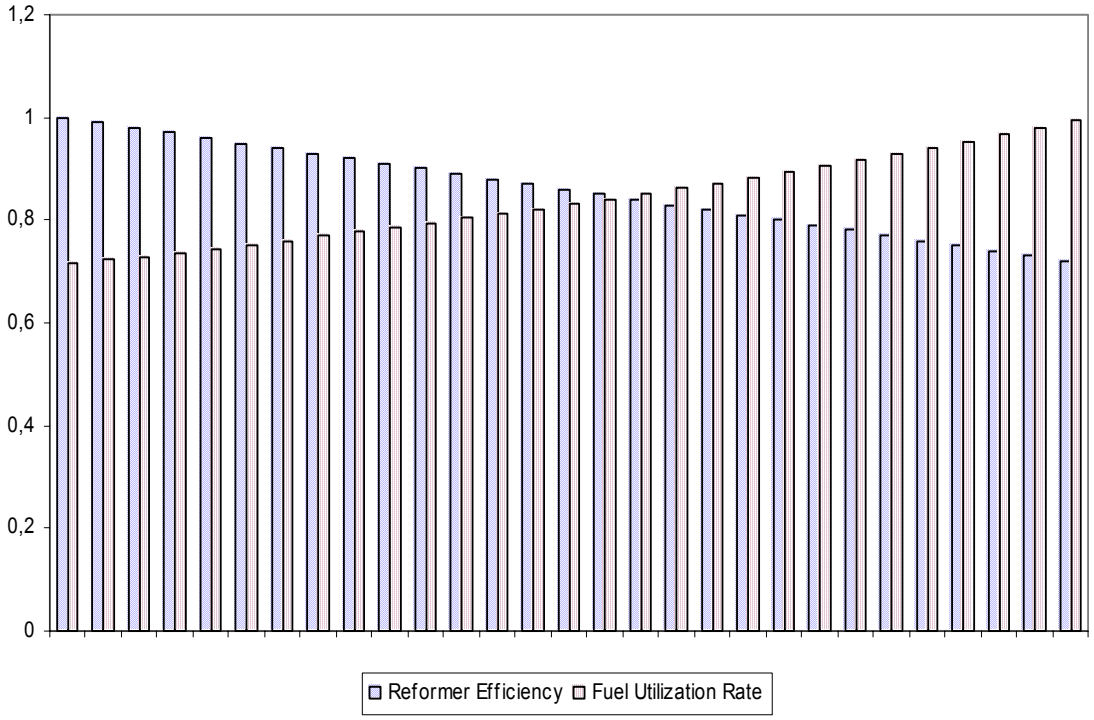

Figure 5.20: Change in fuel utilization rate with reformer efficiency.

Referring to Figures 5.19 and 5.20, the reformer efficiency of 0.9 and fuel utilization rate of 0.75 seem to be conservative values. With a higher fuel utilization rate value, there was not sufficient fuel left to satisfy the heating requirements in the reformer and vaporizer reactions.

5.2.2 Heat Exchanger Design

Keeping the overall heat transfer coefficient constant for both preheaters, U = 0.05 kW / m²K, the areas of heat exchangers are calculated according to the given conditions in Table 5.24. The results are also given in Table 5.24.

Table 5.24: Heat exchanger design conditions and results.

Preheater Number	*Cold Gas Stream Inlet Temperature (K)*	*Cold Gas Stream Outlet Temperature (K)*	*Hot Gas Stream Inlet Temperature (K)*	*Hot Gas Stream Outlet Temperature (K)*	*Calculated Preheater Area (m²)*
1	**298**	**1133**	**1200**	**959**	**566**
2	**298**	**900**	**1010**	**560**	**1657**

5.2.3 Thermodynamic Analysis

The 90% of methane conversion ratio (i.e. reformer efficiency) yields the reformer reaction as follows.

$$CH_4 + 2.2H_2O \rightarrow 3.6H_2 + 0.9CO_2 + 0.1CH_4 + 0.4H_2O$$

The fuel utilization of 75% means that 75% of hydrogen will react with oxygen. Hence, the fuel cell reaction will be,

$$3.6H_2 + 1.35O_2 \rightarrow 2.7H_2O + 0.9H_2$$

The unreacted methane and hydrogen are burnt in the afterburner. Since complete combustion is assumed, the combustion reactions are as follows.

$$0.1CH_4 + 0.2O_2 \rightarrow 0.2H_2O + 0.1CO_2$$

$$0.9H_2 + 0.45O_2 \rightarrow 0.9H_2O$$

As seen from the reactions above, the required oxygen to sustain the system operations, is 2 moles. Hence, 2 moles of oxygen must be supplied to the system. Since air is assumed to be consisting of 20% O_2 and 80% N_2, a total of 10 moles of air is to be supplied into the system.

Since the number of moles of air supplied into the system is determined, the molar chemical compositions of the gas streams at each node can be calculated. After determining the molar chemical compositions at each node of the system, the mass flow rates at each node, referring to fuel supply rate of 1 kg/s, can be calculated as well. The results are presented in table 5.25. In the table, n_i and y_i indicates the mole number and molar composition of each element.

Table 5.25: Calculated molar chemical compositions of gas streams at each node.

Node	CH4		H2O		O2		N2		H2		CO2		$\dot{m}$
	n_i	y_i	n_i	y_i	n_i	y_i	n_i	y_i	n_i	y_i	n_i	y_i	(kg/s)
1	*1*	*1*	*0*	*0*	*0*	*0*	*0*	*0*	*0*	*0*	*0*	*0*	1
2	*0*	*0*	*0*	*0*	*2*	*0,2*	*8*	*0,8*	*0*	*0*	*0*	*0*	17,5
3	*0*	*0*	*2,2*	*1*	*0*	*0*	*0*	*0*	*0*	*0*	*0*	*0*	2,5
4	*1*	*0,3125*	*2,2*	*0,6875*	*0*	*0*	*0*	*0*	*0*	*0*	*0*	*0*	3,5
5	*1*	*0,3125*	*2,2*	*0,6875*	*0*	*0*	*0*	*0*	*0*	*0*	*0*	*0*	3,5
6	*0,1*	*0,02*	*0,4*	*0,08*	*0*	*0*	*0*	*0*	*3,6*	*0,72*	*0,9*	*0,18*	3,5
7	*0*	*0*	*0*	*0*	*2*	*0,2*	*8*	*0,8*	*0*	*0*	*0*	*0*	3,5
8	*0,1*	*0,0074*	*3,1*	*0,2305*	*0,45*	*0,0335*	*8*	*0,5948*	*0,9*	*0,0669*	*0,9*	*0,0669*	21
9	*0*	*0*	*4,2*	*0,3182*	*0*	*0*	*8*	*0,6061*	*0*	*0*	*1*	*0,0758*	21
10	*0*	*0*	*4,2*	*0,3182*	*0*	*0*	*8*	*0,6061*	*0*	*0*	*1*	*0,0758*	21
11	*0*	*0*	*4,2*	*0,3182*	*0*	*0*	*8*	*0,6061*	*0*	*0*	*1*	*0,0758*	21

To determine the electrical work output of the system, the fuel inlet and the air inlet temperatures must be assumed. The fuel inlet temperature is assumed to be, T_a = 1000 K and the air inlet temperature is assumed to be, T_c = 900 K. The SOFC stack is assumed to work under I = 1000 A / m² current density.

First of all, regarding to electrochemical model, the Nernst potential is calculated. With known anode and cathode operating temperatures, the activation and concentration polarizations at both anode and cathode, and the ohmic polarization in the SOFC stack

are calculated. The cell voltage is obtained by subtracting the irreversibilities due to polarizations from the Nernst potential. Hence, the electrical work output is obtained. This net work output, i.e. the actual work, is compared with the heat input to the system and the chemical exergy of methane to determine the first and second law efficiencies. The results obtained are given in Table 5.26 and 5.27. Table 5.27 also gives the heat released by the SOFC stack.

Table 5.26: Net work output of the SOFC operating at T_a = 1000 K, T_c = 900 K, I = 1000 A/m².

E_o (V)	$\eta_{Act,a}$ (V)	$\eta_{Act,c}$ (V)	$\eta_{Conc,a}$ (V)	$\eta_{Conc,c}$ (V)	η_{Ohm} (V)	E_{Act} (V)	W_e (kJ/s)
1,09	*0,0172*	*0,0384*	*0,0039*	*0,0014*	*0,0173*	*1,0118*	***32866,456***

Table 5.27: The first and second law efficiencies of model 2.

W_e (kJ/s)	Q_{lost} (kJ/s)	LHV (kJ/s)	Exergy Input (kJ/s)	η_I (%)	η_{II} (%)
32866.456	*2892.613*	*50018.703*	*52177.681*	***65.71***	***62.99***

The enthalpy and exergy values are calculated for each node by applying the energy balance and the exergy balance at each component. The calculated enthalpy and exergy values and temperatures of each node are given in Figure 5.21. The comparison of input, output and loss of energy and exergy in the system is given in Table 5.28.

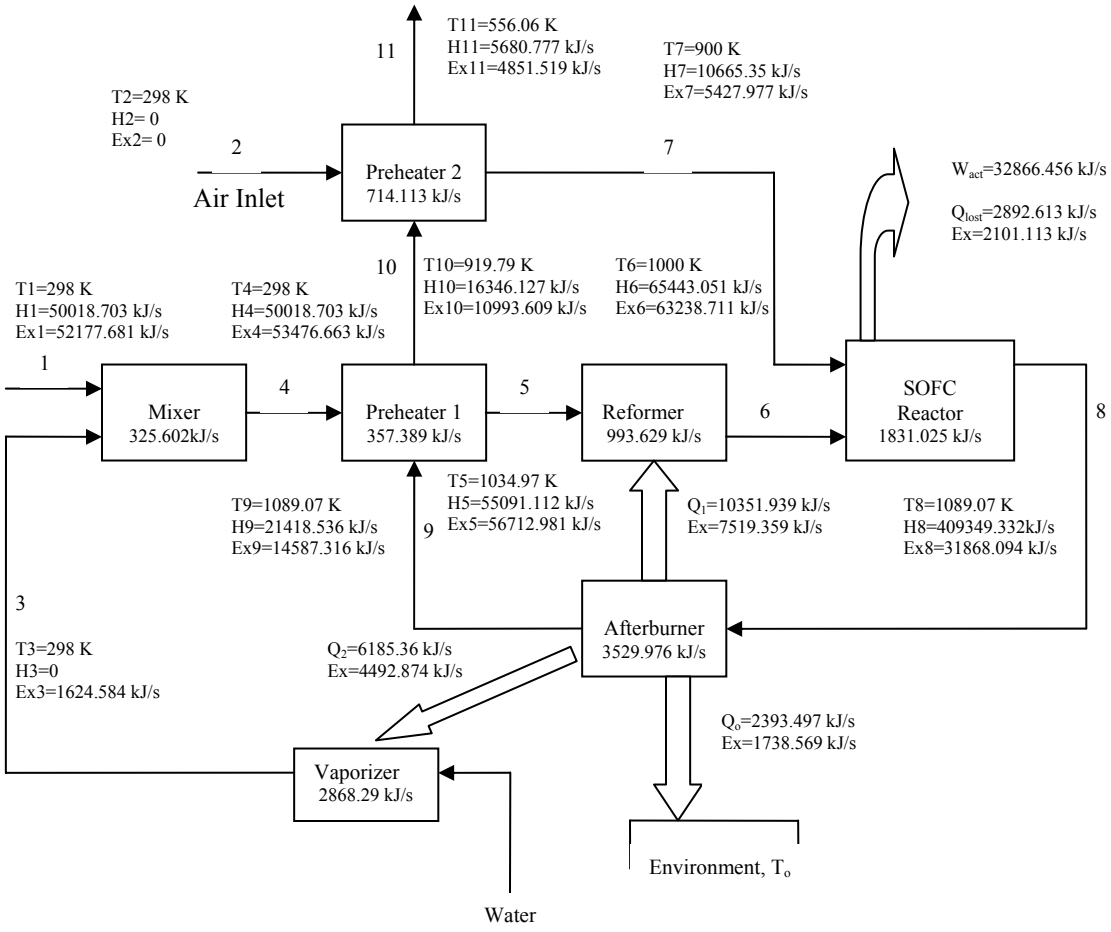

Figure 5.21: System 2 operating at 1 atm, 90% reformer efficiency, 75% fuel utilization rate, fuel inlet temperature is 1000 K, air inlet temperature is 900 K.

Table 5.28: The comparison of input, output, and loss of energy and exergy in the system. Energy and exergy values are normalized relative to the lower heating value and chemical exergy of the fuel, respectively.

	Energy	Exergy
Fuel Input	**100**	**100**
Work Output	65,709	62,99
Heat to the Environment	10,568	7,359
Vaporization Process	12,366	5,497
Exhaust Gas (Node 11)	11,357	9,298
Irreversibility in System Units		14,856
	100	100

The results obtained show that the first law and second law efficiencies for the model simulated are 65.71% and 62.99%, respectively. The second law efficiency of the model is lower than the first law efficiency, because of the higher chemical exergy of the fuel than its lower heating value.

The system is modeled with the assumption that the fuel cell is supplied 100% theoretical air. In practice, in order to maintain a relatively high oxygen concentration at the cathode, a high air – fuel ratio is required. This high ratio of air – fuel will increase the irreversibility.

The exhaust gas (node 11) has a high temperature. This high temperature value causes more exergy destruction. Reducing the fuel utilization rate or methane reforming rate can decrease this high temperature value, provided that the required heat is produced in the afterburner to sustain the system operations. The exhaust gas of the fuel cell system being supplied with high extent of air will have a lower temperature value, since preheater 1 in that case will destroy more exergy.

Mixer destroyed little exergy since the inlet and outlet temperatures are the same and irreversibility is only due to mixing of methane and water vapor.

The most irreversible process is the combustion in the afterburner. The system with a high fuel cell exit temperature value would have less irreversibility in the afterburner. The irreversibility in the SOFC stack would be decreased with a low fuel cell exit temperature value.

Vaporization process requires heat input. This irreversibility can be eliminated by developing a recycling fuel cell system which can be used to eliminate the need for the vaporizer.

Methane reforming causes more exergy destruction within the system. Reducing the combustion of fuel while reforming as much methane as possible (hence producing as much fuel as possible) would increase the second law efficiency.

CHAPTER 6

CONCLUSION

The results obtained for the simulation models show that solid oxide fuel cells have high second law efficiencies. As discussed before, this high efficiency values are one of the benefits of fuel cell systems. Solid oxide fuel cell's high operating temperature caused less voltage drop, and therefore the irreversibilities occuring inside the fuel cell were less.

Different configurations for the system might be studied, such as assuming different methane – water vapor ratio, supplying some extent air, or trying different reformer efficiency and fuel utilization rate values. Results obtained from these configurations can be compared with the results obtained in this study to give a more general discussion to the subject.

High operating temperature of the solid oxide fuel cell system gives the advantage to be combined with a gas turbine system for higher efficiencies. Studies on this combined system show that high efficiency values can be obtained this way.

The exhaust gas stream of the solid oxide fuel cell system has high exergy value. This exhaust gas may be used for local area heating.

The vaporizer and afterburner components of the system destroyed more exergy when compared with the other components of the system. Hence, different alternatives should be tried in order to increase the second law efficiency of the system.

One of the alternatives can be the elimination of vaporizer. Since water vapor is produced at the exit of the fuel cell stack, addition of a splitter at the outlet of the fuel cell stack might be used to recycle the required water vapor to the reformer. The required water vapor can be recycled from the splitter to the reformer. This arrangement would eliminate the need for the vaporizer while increasing the system's second law efficiency.

Another alternative should consider the heating requirement of the reformer. Since this heat requirement is supplied by combustion of methane and hydgoren, the fuel utilization rate and the reformer efficiency are lower. Instead of using hydrogen, some of the methane entering the system might directly be used to heat the reformer, hence the reformer efficiency would be higher and system would be modeled in order to reform as much methane as possible. This way, more methane would be reformed and more fuel would be produced. Combustion of the fuel should therefore be reduced as much as possible. Such a model with higher reformer efficiency and fuel utilization rate would have high second law efficiency.

These alternatives can increase the second law efficiency, and hence offers much better results. The future works should consider these alternative configurations.

REFERENCES

1. "Fuel Cell Handbook (Fifth Edition)", EG&G Services Parsons, Inc. Science Applications International Corporation, 2000.

2. Robert H. Perry, Don W. Green, James O. Maloney, "Perry's Chemical Engineers' Handbook (Seventh Edition)", McGraw-Hill, 1999.

3. J.R. Will Mitchell, "Fuel Cells", Academic Press, 1963.

4. James Larminie, Andrew Dicks, "Fuel Cell Systems Explained", John Wiley & Sons, 2000.

5. Reinhold Wurster, "PEM Fuel Cells in Stationary and Mobile Applications: infrastructural requirements, environmental benefits, efficiency advantages and economical implications", Ludwig-Bölkow-Systemtechnik GmbH, 1997.

6. Michael J. Moran, Howard N. Shapiro, "Fundamentals of Engineering Thermodynamics (Third Edition)", John Wiley & Sons, 1998.

7. Jr. Kenneth Wark, "Advanced Thermodynamics For Engineers", Mc-Graw-Hill, 1995.

8. J.O'M. Bockris, S. Srinivasan, "Fuel Cells: Their Electrochemistry", McGraw-Hill, 1969.

9. T.J.Kotas, "The Exergy Method of Thermal Plant Analysis", Butterworths, 1985.

10. Adrian Bejan, “Advanced Engineering Thermodynamics”, John Wiley & Sons, 1988.

11. Kai W. Bedringås, Ivar S. Ertesvåg, Ståle Byggstøyl, Bjørn F. Magnussen, “Exergy Analysis of Solid Oxide Fuel cell (SOFC) Systems”, Energy, 4, 1997, 403 – 412.

12. S.H. Chan, C.F. Low, O.L. Ding, “Energy and Exergy Analysis of Simple Solid-Oxide Fuel-Cell Power Systems”, Journal of Power Sources, 103, 2002, 188 – 200.

13. Keith R. Williams, “An Introduction to Fuel Cells”, Elsevier Pub. Co., 1966.

14. Stanley W. Angrist, “Direct Energy Conversion (Third Edition)”, Allyn and Bacon, Boston, 1976.

15. S.H. Chan, K.A. Khor, Z.T. Xia, “A Complete Polarization Model of a Solid Oxide Fuel Cell and Its Sensitivity to the Change of Cell Component Thickness”, Journal of Power Sources, 93, 2001, 130 – 140.

16. Christie J. Geankoplis, “Mass Transport Phenomena”, Holt, Rinehart and Winston, Inc., 1972.

17. Carl Berger, “Handbook of Fuel Cell Technology”, Prentice-Hall, 1968.

18. Karl Kordesch, Günter Simader, “Fuel Cells and Their Applications”, VCH, 1996.

19. Frank P. Incropera, David P. De Witt, “Fundamentals of Heat and Mass Transfer (Third Edition)”, John Wiley & Sons, 1990.

20. Signe Kjelstrup Ratkje, Steffen Møller-Holst, “Exergy Efficiency and Local Heat Production in Solid Oxide Fuel Cells”, Electrochimiza Acta, 38, 2/3, 1993, 447 – 453.